Title
Mathematical models of stress disorders: Neuroendocrine dynamics and response

Author
Kim, Lae Un

Publication Date
2017

Peer reviewed|Thesis/dissertation

UNIVERSITY OF CALIFORNIA
Los Angeles

Mathematical models of stress disorders: Neuroendocrine dynamics and response

A dissertation submitted in partial satisfaction
of the requirements for the degree
Doctor of Philosophy in Biomathematics

by

Lae Kim

2017

ABSTRACT OF THE DISSERTATION

Mathematical models of stress disorders:
Neuroendocrine dynamics and response

by

Lae Kim
Doctor of Philosophy in Biomathematics
University of California, Los Angeles, 2017
Professor Tom Chou, Chair

The hypothalamic-pituitary-adrenal (HPA) axis is a neuroendocrine system that regulates numerous physiological processes. Disruptions in the activity of the HPA axis are correlated with many stress-related diseases such as post-traumatic stress disorder (PTSD) and major depressive disorder. In this dissertation, we characterize "normal" and "diseased" states of the HPA axis as basins of attraction of a dynamical system describing the inhibition of peptide hormones such as corticotropin-releasing hormone (CRH) and adrenocorticotropic hormone (ACTH) by circulating glucocorticoids such as cortisol. In addition to including key physiological features such as circadian and ultradian oscillations in cortisol levels and self-upregulation of CRH neuron activity, our model distinguishes the relatively slow process of cortisol-mediated CRH biosynthesis from rapid trans-synaptic effects that regulate the CRH secretion process.

We use the developed dynamical systems model of the HPA axis to understand the mechanisms underlying clinical protocols used to probe patient stress response. Specifically, we address dexamethasone and ACTH challenge tests, which probe pituitary and adrenal gland responses, respectively. We show that some previously observed features and experimental observations can arise from the dynamics intrinsic to our bistable model, rather than relying on specific and permanent parameter changes due to physiological disruption.

Importantly, we find that the slow regulation mechanism mediates external stress-driven

transitions between the stable states in intensity, duration, and timing-dependent ways. These results indicate that the timing of traumatic events may be a significant factor in determining if and how patients will exhibit hallmarks of stress disorders.

Motivated by the importance of the timing, we develop a preliminary model that includes the interaction between the HPA axis and the endocannabinoid system, which regulates the initiation and termination process of the stress response. The preliminary model exhibited habituation of the stress response to a repeated stressor. We investigate the general mechanism shared in different levels of the sensory system that establishes and stores the information of a repeating stimulus pattern and propose a possible form of basic elements of such systems.

The dissertation of Lae Kim is approved.

Elliot M. Landaw

Maria R. D'Orsogna

Van M. Savage

Tom Chou, Committee Chair

University of California, Los Angeles

2017

For Donghyun Min and his unfulfilled dreams.

TABLE OF CONTENTS

1 Introduction **1**

2 HPA axis dynamics **4**

2.1 Background 4

2.2 Mathematical Description 8

2.2.1 Ultradian rhythm and time delay 9

2.2.2 Synthesis of CRH 10

2.2.3 Secretion of CRH 11

2.2.4 Complete delay-differential equation model 13

2.2.5 Nondimensionalized model 14

2.3 Multiple Timescale Analysis 15

2.3.1 Fast-slow variable separation and bistability 15

2.3.2 Projected dynamics on the reduced system 19

2.4 Discussion 22

2.4.1 Three types of bistable nullcline structure 24

2.4.2 Bistable limit cycle attractors 27

2.4.3 Normal stress response 27

2.4.4 Timing of stress onset and transient response 28

2.5 Summary and Conclusions 30

2.6 Appendix 32

2.6.1 Nondimensionalization 32

2.6.2 Parameter estimates 32

3 The HPA axis and PTSD **34**

3.1 Introduction . . . 34
3.2 Parameters and long-term dynamics . . . 39
3.2.1 Parameter dependencies . . . 43
3.2.2 Nullcline analysis: c-nullcline . . . 43
3.2.3 Nullcline analysis: c_s-nullcline . . . 45
3.3 Pharmacological Challenge Tests . . . 48
3.3.1 Dexamethasone suppression test (DST) . . . 49
3.3.2 ACTH stimulation test . . . 53
3.4 Stress-driven Transitions . . . 56
3.4.1 External stress induces transition from normal to diseased state . . . 56
3.4.2 Transition to diseased state depends on stress timing . . . 59
3.4.3 Stress of intermediate duration can induce "reverse" transitions . . . 61
3.5 Proposal and Predictions for a new two-stage challenge tests . . . 62
3.6 Summary and Conclusions . . . 65
3.7 Appendix . . . 69
3.7.1 Nondimensionalization . . . 69
3.7.2 Comparison of new and previous model . . . 71

4 Circadian rhythms in the HPA axis . . . 73
4.1 Introduction . . . 73
4.2 Suprachiasmatic nucleus and the HPA axis . . . 74
4.3 Projected dynamics on the reduced system . . . 77
4.4 Circadian rhythm and Stress-driven transitions . . . 80
4.5 Conclusion . . . 83

5 Prospective works . . . 84

5.1 Endocannabinoid system and the HPA axis 84
5.1.1 A preliminary model of the eCB + HPA axis 85
5.1.2 Decay of AEA at stress response initiation 86
5.1.3 Synthesis of 2-AG during stress response 86
5.1.4 Preliminary results: Habituation in stress response 87
5.2 Novelty detection in retina-tectum neural network 89
5.2.1 Background 89
5.2.2 Model development 91
5.2.3 Novelty detecting ganglion cells 92
5.2.4 A toy model 97
5.2.5 The building block model 107
5.2.6 Conclusion 112

References **115**

LIST OF FIGURES

2.1 Schematic of the HPA axis. 5

2.2 Nonlinear $g_c(c)$ and bistability of fast variables. 17

2.3 Dynamics of the oscillating PA-subsystem as a function of fixed c. 18

2.4 Classification of variables. 18

2.5 Slow and fast nullclines and overall flow field. 20

2.6 Equilibria at the intersections of nullclines. 21

2.7 The possible number of equilibria of the reduced (c_s, c) system. 24

2.8 Phase diagram in (μ_c, q_0, q_1)-space. 26

2.9 Normal stress response. 28

2.10 Stress timing and cortisol response. 29

2.11 Fitting $c_\infty(o)$ to rat data. 33

3.1 (Modified) Schematic of the HPA axis. 36

3.2 Effects of changing parameters on the c-nullcline 46

3.3 Effect of changing parameters on c_s-nullcline 48

3.4 Numerical simulation of DEX challenge test on normal and PTSD subjects. . . 53

3.5 Numerical solutions of ACTH stimulation test. 57

3.6 Stress-induced transitions into an oscillating low-cortisol diseased state. 58

3.7 Stress timing and transition to low-cortisol oscillating state. 60

3.8 Stress-induced transitions to high-cortisol oscillating state. 62

3.9 Numerical solutions of a combined two-step challenge test. 64

3.10 Effects of changing parameters on the c-nullcline 72

4.1 Modulation of adrenal sensitivity by the SCN. 76

4.2 Response of the HPA axis to circadian adrenal sensitivity. 77
4.3 Long-term behavior under periodic c_s-nullcline. 79
4.4 Long-term dynamics under stress 80
4.5 Stress-induced transition under circadian rhythm during phase I and IV 81
4.6 Stress-induced transition under circadian rhythm during phase I and III 82

5.1 Habituation of HPA response to a repeated stress. 88
5.2 A schematic diagram of the retina-tectum network. 91
5.3 A schematic diagram of the building block. 93
5.4 Establishing the expectation of regularity and the effect of an extra stimulus. . . 100
5.5 Extra stimulus detection of the toy model. 102
5.6 Stimulus frequency and extra stimulus detection. 103
5.7 Extended decay over an omitted stimulus induces negative response. 104
5.8 Negaitve response of the toy model to an omitted stimulus. 105
5.9 Positive response of the toy model to an omitted stimulus. 106
5.10 A building block with slow direct and fast indirect OFF-bipolar cells. 109
5.11 Linear filtering process of a periodic stimulus in bipolar cells. 111
5.12 A building block with fast direct and slow indirect OFF-bipolar cells. 113

LIST OF TABLES

2.1 Dimensionless parameter values of our full model. 23

3.1 Parameters and their effects on nullcline structure 44

ACKNOWLEDGMENTS

First, I would like to acknowledge my advisor, Professor Tom Chou, for the support and guidance he has provided me over my years at UCLA. He has broadened the scope of my research interest throughout those years and given me the audacity to delve into a new field or area of research. I am grateful especially for his patience in dealing with my weak writing. I wish to pay him back someday by becoming a decent writer and a scientist.

I also thank Professor Maria R. D'Orsogna for helping me with my research and giving me opportunities to present my work to different audiences. I have realized how crucial those experiences were in my developing as a researcher. She has also given me many valuable pieces of advice on how to become successful in academia. I will always keep them in mind.

Professor Elliot M. Landaw also has helped me improve my work by asking insightful questions that were overlooked by me. I thank him for giving me grammar lessons that were more than merely correcting the spotted errors. I am also grateful to Professor Van M. Savage for his encouragement and advice about the academic job search, in addition to discussions on research.

There are many others whose encouragement, companionship, and trust has kept me going: fellow Biomathematics graduate students and visiting scholars, including Bhaven Mistry, for always willing to discuss and provide constructive criticisms; Stephanie Lewkiewicz, for checking my mathematics; Song Xu for always encouraging to stay fit and healthy; Yao-li Chuang, for answering my endless questions. I also thank the Biomathematics department's faculty and staff for helping me through all the bureaucracies at UCLA.

I am grateful to my family and many dear friends. This journey would have been a tedious one without their presence. Claire Hwang, who has helped me settle in the new city and given me countless rides around the city. Kevin Young Lee, for all the genuine conversations and adventures. Joe Reyes, for all the good music. Kate Gayoung Lee, for being next to me when I was in despair and lifting my spirits up. My father and Julie Kim, for their generosity and sending care packages. Last but not the least, I thank God for answering my mother's prayers, which have protected and guided me in ways I do not even

understand.

Parts of this dissertation have appeared elsewhere or accepted. Chapter 2 and elements of Chapter 3 have been published by BioMed Central on Biology Direct [KDC16]. Also, a paper relating to a few sections of Chapter 3 has been accepted by the Journal of Computational Psychiatry (in press). They are joint work with Maria R. D'Orsogna and Tom Chou.

VITA

2008	B.A. (Applied Mathematics), University of California, Berkeley.
2010	M.S. (Mathematics), New York University, New York
2010–2011	Teaching Assistant, New York University, New York.
2012	M.S. (Biomathematics), University of California, Los Angeles.
2015–2016	Teaching Associate, Life Sciences, UCLA.
2014–2017	Graduate Student Researcher, Biomathematics, UCLA.

PUBLICATIONS

Lae U. Kim, Maria R. D'Orsogna, and Tom Chou. Perturbing the hypothalamic-pituitary-adrenal stress response system: A mathematical model to mechanistically reinterpret PTSD assessment tests. Computational Psychiatry, (in press).

Lae U. Kim, Maria R. D'Orsogna, and Tom Chou. Onset, timing, and exposure therapy of stress disorders: mechanistic insight from a mathematical model of oscillating neuroendocrine dynamics. Biology Direct (2016), 11(13).

CHAPTER 1

Introduction

The topic of this dissertation was motivated by a neuroendocrine problem found in the research pertaining to post-traumatic stress disorder (PTSD). This psychiatric disorder was first brought into public attention as a recognized medical diagnosis by Vietnamese War veterans and has gradually become one of the most well-known and actively researched stress-related disorders. As is common in the case of mental disorders, the diagnostic criteria for PTSD relies heavily on self-reports and questionnaires that are subjective in nature. The lack of objective measures with which to examine the disease has been a huge challenge in this field. Cortisol, a steroid hormone also known as the "stress hormone," was measured in PTSD patients as a measure for monitoring stress level under PTSD and its progress. As the level of cortisol typically increases during a stress response, cortisol levels were expected to be higher among PTSD patients. For this reason, the first study that showed lower cortisol levels among PTSD patients was initially met with a lot of resistance from the field. Despite a few conflicting results in the literature, lower cortisol levels under PTSD is now accepted as one of the features of the dysfunction.

Cortisol levels show birhythmic behavior, in which the hourly and daily rhythms are superimposed. The regulation of the steroid hormone is a very dynamic process that involves an interplay between the group of endocrine glands and a part of the brain, which communicate with each other by secreting peptide hormones that also exhibit the oscillating behavior observed in cortisol levels. The fundamental mechanism of the cortisol regulation is well-described, and a handful of mathematical models have been developed in the past to shed light on the same. Most of these models attempted to explain the ultradian (hourly) oscillations seen in cortisol levels, and attributed the dysregulations in cortisol dynamics to

the changes in the parameters of the system. The general assumption ascribed the enhanced negative feedback sensitivity of the negative feedback effect of cortisol at the pituitary as the cause for the decreased basal cortisol level, based on some pharmacological challenge test results.

The most distinctive feature of post-traumatic stress disorder that separates it from other mental disorders is that it requires exposure to a traumatic experience. The experience can be direct or indirect like witnessing an event taking place or even learning about a traumatic incident that happened to a close friend or a relative. One of the most common symptoms of the illness is recurrent, involuntary, and intrusive memories of the trauma and their accompanying physiological responses. In this sense, PTSD is truly a psychological disorder, originating from the dysfunctions in the memory consolidation and retrieval. On the other hand, cortisol secretion is regulated by the endocrine system which, in turn, is controlled by the central nervous system and the brain. Therefore, dysregulations in the cortisol dynamics can be viewed as a downstream effect that reflects the dysfunction in the "psychology" manifested by the changes in the parts of the brain.

If PTSD is caused by a psychological distress that is not accompanied by physical trauma, should the parameters representing the anatomical structure and biochemical rates change? This dissertation attempts to explore this question through a mathematical description of the known physiology of the neuroendocrine system, the interface that connects the endocrine aspects of the disease to its psychological realm. In Chapter 2, we develop a dynamical systems model of the neuroendocrine system based on the known physiology and analyze the model using methods from multiple timescale analysis. In particular, we look for bistability that can describe the lowered cortisol state as one of the stable states of the system.

Chapter 3 and 4 extends the analysis of the model to investigate the effects of each parameter on the nullcline structure and the long-term behavior of the model. In Chapter 3, previous pharmacological challenge tests result used to support the current view of the cortisol disruption (as altered negative feedback action) is replicated within our model and compared to the measurements. Moreover, the effects of trauma are incorporated as perturbations to the dynamical system, and the way in which they can induce transitions

between the healthy and diseased stable states are demonstrated and discussed. Chapter 4 includes the exogenous circadian rhythm drive into the model and explores the influence of the two rhythms on the transitions induced by trauma. The model preserved its bistability and the ultradian oscillations under the circadian drive. Interestingly, the model predicted that stress-induced transitions between the stable states may be dependent on the timing of the termination of the stressor in relation to the circadian rhythm.

This prediction motivated us to investigate the mechanisms responsible for the regulation of the initiation and termination of the stress response in the hypothalamic-pituitary-adrenal (HPA) axis, in Chapter 5. Recent studies have suggested that the endocannabinoid (eCB) system interacts with the HPA axis system to gate the synaptic input of the paraventricular nucleus (PVN). We develop a preliminary model of the eCB system and its interactions with the HPA axis. The model exhibits a habituation of the cortisol response to a repeated stressor. On the other hand, we initiated a study on the general mechanisms for establishing information on a repeated stimulus working at different levels of the sensory system. Based on the novelty detection in the retina-tectum network, we begin developing a model of a dynamic network that encodes the information of a repeated stimulus and registers violations in the expected stimulus pattern.

Parts of this dissertation have appeared in literature. Chapter 2 and elements of Chapter 3 have been published by BioMed Central on Biology Direct. Also, a paper relating to a few sections of Chapter 3 has been accepted by the Journal of Computational Psychiatry.

CHAPTER 2

HPA axis dynamics

2.1 Background

Stress is an essential component of an organism's attempt to adjust its internal state in response to environmental change. The experience, or even the perception of physical and/or environmental change, induces stress responses such as the secretion of glucocorticoids hormones (CORT) – cortisol in humans and corticosterone in rodents – by the adrenal gland. The adrenal gland is one component of the hypothalamic-pituitary-adrenal (HPA) axis, which is a collection of interacting neuroendocrine cells and endocrine glands that play a central role in stress response. The basic interactions involving the HPA axis are summarized in Fig. 2.1. The paraventricular nucleus (PVN) of the hypothalamus receives synaptic inputs from various neural pathways via the central nervous system that are activated by both cognitive and physical stressors. Once stimulated, CRH neurons in the PVN secrete corticotropin-releasing hormone (CRH), which then stimulates the anterior pituitary gland to release adrenocorticotropin hormone (ACTH) into the bloodstream. ACTH then activates a complex signaling cascade in the adrenal cortex, which ultimately releases glucocorticoids (Fig. 2.1B). In return, glucocorticoids exert a negative feedback on the hypothalamus and pituitary, suppressing CRH and ACTH release and synthesis in an effort to return them to baseline levels. Classic stress responses include transient increases in levels of CRH, ACTH, and cortisol. The basic components and organization of the vertebrate neuroendocrine stress axis arose early in evolution and the HPA axis, in particular, has been conserved across mammals [Den09].

Dysregulation in the HPA axis is known to correlate with a number of stress-related

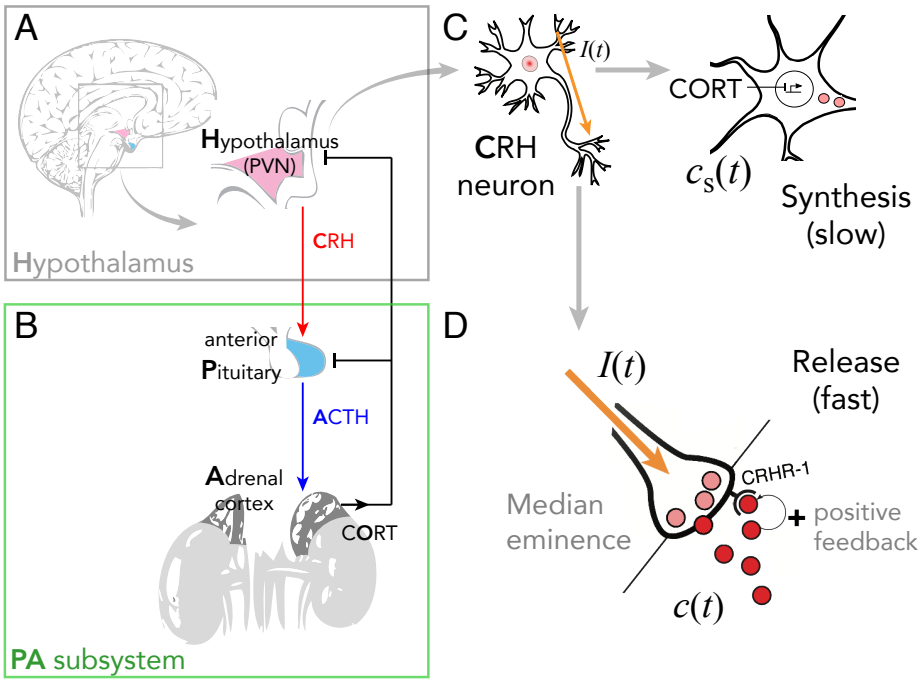

Figure 2.1: **Schematic of HPA axis.** (A) Stress is processed in the central nervous system (CNS) and a signal is relayed to the PVN in the hypothalamus to activate CRH secretion into the hypophyseal portal system. (B) CRH is carried to the pituitary gland by the hypophyseal portal system and activates ACTH secretion. ACTH travels to the adrenal cortex via the bloodstream to activate cortisol (CORT) release. Cortisol inhibits both CRH and ACTH secretion to down-regulate its own production, forming a closed loop. In the pituitary gland, cortisol binds to glucocorticoid receptors (GR) to inhibit ACTH and self-upregulate GR production. This part of the axis comprises the PA subsystem. (C) Negative feedback of cortisol affects the synthesis process in the hypothalamus, which indirectly suppresses the release of CRH. External inputs such as stressors and circadian inputs also directly affect the release rate of the CRH release rates. (D) Released CRH self-upregulates the secretion of CRH via binding to CRH-receptor 1 (CRHR-1) expressed on the PVN neurons. The self-upregulation of CRH is further addressed in Chapter 3.

disorders. Increased cortisol (hypercortisolism) is associated with major depressive disorder (MDD) [GC02, JCP04], while decreased cortisol (hypocortisolism) is a feature of post-traumatic stress disorder (PTSD), post infectious fatigue, and chronic fatigue syndrome (CFS) [RJW04, GHJ05, JPT06, CYC04]. Since PTSD develops in the aftermath of extreme levels of stress experienced during traumatic incidents like combat, sexual abuse, or life-threatening accidents, its progression may be strongly correlated with disruption of the HPA

axis caused by stress response. For example, lower peak and nadir cortisol levels were found in patients with combat-related PTSD [YTL94].

Mathematical models of the HPA axis have been previously formulated in terms of dynamical systems of ordinary differential equations (ODEs) [VAO11, JSC05, KSV05, SKO00] or delay differential equations (DDEs) [WTL10, RWW12, BCC08] that describe the time-evolution of the key regulating hormones of the HPA axis: CRH, ACTH, and cortisol. These models [WTL10, RWW12, SRD12] incorporate positive self-regulation of glucocorticoid receptor expression in the pituitary, which may generate bistability in the dynamical structure of the model [GAG07]. Of the two stable equilibrium states, one is characterized by higher levels of cortisol and is identified as the "normal" state. The other is characterized by lower levels of cortisol and can be interpreted as one of the "diseased" states associated with *hypocortisolism*. Stresses that affect the activity of neurons in the PVN are described as perturbations to endogenous CRH secretion activity. Depending on the length and magnitude of the stress input, the system may or may not shift from the basin of attraction of the normal steady state towards that of the diseased one. If such a transition does occur, it may be interpreted as the onset of disease. A later model [SRD12] describes the effect of stress on the HPA axis as a gradual change in the parameter values representing the maximum rate of CRH production and the strength of the negative feedback activity of cortisol. In this model, cortisol secretion patterns are assumed to depend solely on physiological changes arising from *e.g.,* anatomical or biochemical changes in cells or tissues. Such structural-level variations can be mathematically represented by changes in physiological parameter values.

These two classes of models imply qualitatively different time courses of disease progression [GAG07, SRD12]. The former suggests that the abnormal state is a pre-existing basin of attraction of a dynamical model that stays dormant until a sudden transition is triggered by exposure to trauma [GAG07]. In contrast, the latter assumes that the abnormal state is reached by the slow development of structural changes in physiology due to the traumatic experience [SRD12]. Although both models [GAG07, SRD12] describe changes in hormonal levels experienced by PTSD patients, they both fail to exhibit stable ultradian oscillations in cortisol, which is known to play a role in determining the responsiveness of the HPA axis

to stressors [WWL98].

In this chapter, we consider a number of distinctive physiological features of the HPA axis that give a more complete picture of the dynamics of stress disorders and that have not been considered in previous mathematical models. These include the effects of intrinsic ultradian oscillations on HPA dysregulation, stress response, distinct rapid and slow feedback actions of cortisol, and the correlation between HPA imbalance and disorders induced by external stress. As with the majority of hormones released by the body, cortisol levels undergo a circadian rhythm, starting low during night sleep, rapidly rising and reaching its peak in the early morning, then gradually falling throughout the day. Superposed on this slow diurnal cycle is an ultradian rhythm consisting of approximately hourly pulses. CRH, ACTH, and cortisol are all secreted episodically, with the pulses of ACTH slightly preceding those of cortisol [Chr98].

As for many other hormones such as gonadotropin-releasing hormone (GnRH), insulin, and growth hormone (GH), the ultradian release pattern of glucocorticoids is important in sustaining normal physiological functions, such as regulating gene expression in the hippocampus [CSM10]. It is as yet unclear what role ultradian oscillations of cortisol play in homeostasis, but the time of onset of a stressor in relation to the phase of the oscillation has been shown to influence the physiological response elicited by the stressor [WWS98].

To distinguish the rapid and slow actions of cortisol, we separate the dynamics of biosynthesis of CRH from its secretion process, which operate over very different timescales [Wat05]. While the two processes are mostly independent from each other, the rate of CRH secretion should depend on the synthesis process since CRH peptides must be synthesized first before being released (Fig. 2.1C). On the other hand, the rate of CRH peptide synthesis is influenced by cortisol levels, which in turn, are regulated by released CRH levels. We will investigate how the separation and coupling of these two processes can allow bistable limit cycle attractors.

2.2 Mathematical Description

Models of HPA dynamics [GAG07, WTL10, SRD12, RWW12, BVB09] are typically expressed in terms of ordinary differential equations (ODEs):

$$\frac{\mathrm{d}C}{\mathrm{d}T} = p_C I(T) f_C(O) - d_C(C), \tag{2.1}$$
$$\frac{\mathrm{d}A}{\mathrm{d}T} = p_A C f_A(OR, O) - d_A(A), \tag{2.2}$$
$$\frac{\mathrm{d}O}{\mathrm{d}T} = p_O A(T) - d_O(O), \tag{2.3}$$
$$\frac{\mathrm{d}R}{\mathrm{d}T} = p_R g_R(OR) - d_R(R), \tag{2.4}$$

where $C(T), A(T)$, and $O(T)$ denote the plasma concentrations of CRH, ACTH, and cortisol at time T, respectively. $R(T)$ represents the availability of glucocorticoid receptor (GR) in the anterior pituitary. The amount of cortisol-bound GR is typically in quasi-equilibrium so concentration of the ligand-receptor complex is approximately proportional to the product $O(T)R(T)$ [GAG07]. The parameters p_α ($\alpha \in \{C, A, O, R\}$) relate the production rate of each species α to specific factors that regulate its rate of release/synthesis. External stresses that drive CRH release by the PVN in the hypothalamus are represented by the input signal $I(T)$. The function $f_C(O)$ describes the negative feedback of cortisol on CRH levels in the PVN while $f_A(x)$ ($x \in O, OR$) describes the negative feedback of cortisol or cortisol-GR complex (at concentration $O(T)R(T)$) in the pituitary. Both are mathematically characterized as being positive, decreasing functions so that $f_{A,C}(\cdot) \geq 0$ and $f'_{A,C}(\cdot) < 0$. On the other hand, the function $g_R(OR)$ describes the self-upregulation effect of the cortisol-GR complex on GR production in the anterior pituitary [TCW88]. In contrast to $f_{A,C}(\cdot)$, $g_R(\cdot)$ is a positive but increasing function of OR so that $g_R(\cdot) \geq 0$ and $g'_R(\cdot) > 0$. Finally, the degradation functions $d_\alpha(\cdot)$ describe how each hormone and receptor is cleared and may be linear or nonlinear.

Without including the effects of the glucocorticoid receptor (neglecting Eq. 2.4 and assuming $f_A(OR, O) = f_A(O)$ in Eq. 2.2), Eqs. 2.1-2.3 form a rudimentary "minimal" model

of the HPA axis [VAO11, AVO13a]. If $f_{A,C}(\cdot)$ are Hill-type feedback functions dependent only on $O(T)$ and $d_\alpha(\cdot)$ are linear, a unique global stable point exists. This equilibrium point transitions to a limit cycle through a Hopf bifurcation but only within nonphysiological parameter regimes [VAO11]. The inclusion of GR and its self-upregulation in the anterior pituitary [GAG07] creates two stable equilibrium states of the system, but still does not generate oscillatory behavior. More recent studies extend the model (represented by Eq. 2.1-2.4) to include nonlinear degradation [SRD12] or constant delay to account for delivery of ACTH and synthesis of glucocorticoid in the adrenal gland [WTL10]. These two extended models exhibit only one intrinsic circadian [SRD12] or ultradian [WTL10] oscillating cycle for any given set of parameter values, precluding the interpretation of normal and diseased states as bistable oscillating modes of the model.

Here, we develop a new model of the HPA axis by first adapting previous work [WTL10] where a physiologically-motivated delay was introduced into Eq. 2.3, giving rise to the observed ultradian oscillations [WTL10]. We then improve the model by distinguishing the relatively slow mechanism underlying the cortisol-mediated CRH biosynthesis from the rapid trans-synaptic effects that regulate CRH secretion. This allows us to decompose the dynamics into slow and fast components. Finally, self-upregulation of CRH release is introduced which allows for bistability. These ingredients can be realistically combined in a way that leads to novel, clinically identifiable features and are systematically developed below

2.2.1 Ultradian rhythm and time delay

Experiments on rats show a 3-6 minute inherent delay in the response of the adrenal gland to ACTH [Pap77]. Moreover, in experiments performed on sheep [EPL90], persistent ultradian oscillations were observed even after surgically removing the hypothalamus, implying that oscillations are inherent to the pituitary-adrenal (PA) subsystem. Since oscillations can be induced by delays, we assume, as in Walker *et al.* [WTL10], a time delay T_d in the ACTH-mediated activation of cortisol production downstream of the hypothalamus. Eq. 2.3 is thus

modified to

$$\frac{\mathrm{d}O}{\mathrm{d}T} = p_O A(T - T_\mathrm{d}) - d_O O. \tag{2.5}$$

Walker *et al.* [WTL10] show that for fixed physiological levels of CRH, the solution to Eqs. 2.2, 2.5, and 2.4 leads to oscillatory $A(T), O(T)$, and $R(T)$. In order to describe the observed periodic cortisol levels in normal and diseased states, the model requires *two* oscillating stable states. We will see that dual oscillating states can arise within our model when the delay in ACTH-mediated activation of cortisol production is coupled with other known physiological processes that we describe below.

2.2.2 Synthesis of CRH

CRH synthesis involves various pathways, including CRH gene transcription and transport of packaged CRH from the cell body (soma) to their axonal terminals where they are stored prior to release. Changes in the steady state of the synthesis process typically occur on a timescale of minutes to hours. On the other hand, the secretory release process depends on changes in membrane potential at the axonal terminal of CRH neurons, which occur over millisecond to second timescales.

To model the synthesis and release process separately, we distinguish two compartments of CRH: the concentration of stored CRH within CRH neurons will be denoted $C_\mathrm{s}(T)$, while levels of released CRH in the portal vein outside the neurons will be labeled $C(T)$ (Fig. 2.1C). Newly synthesized CRH will first be stored, thus contributing to C_s. We assume that the stored CRH level C_s relaxes toward a target value set by the function $C_\infty(O)$:

$$\frac{\mathrm{d}C_\mathrm{s}}{\mathrm{d}T} = \frac{C_\infty(O) - C_\mathrm{s}}{T_C}. \tag{2.6}$$

Here, T_C is a characteristic time constant and $C_\infty(O)$ is the *cortisol-dependent* target level of stored CRH. Eq. 2.6 also assumes that the relatively small amounts of CRH released into the bloodstream do not significantly deplete the C_s pool. Note that the effects induced by changing cortisol levels are assumed to be immediate as the production term $C_\infty(O)/T_C$

adjusted relatively instantaneously to current cortisol levels. This assumption is supported by CRH hnRNA (precursor mRNA) measurements in [WOS11] that demonstrated the rapid effect of cortisol on the initial transcription activity. . On the other hand, the time required to reach the steady state for the completely synthesized CRH peptide will depend on the characteristic time scale constant T_C. Ideally, T_C should be estimated from measurements of the pool size of releasable CRH at the axonal terminals. To best of our knowledge, there are currently no such measurements available, so we base our estimation on mRNA level measurements. We believe this is a better representation of releasable CRH than hnRNA levels since mRNA synthesis is a further downstream process. Previous studies have shown that variations in CRH mRNA due to changes in cortisol levels take at least twelve hours to detect [MA99]. Therefore, we estimate $T_C \gtrsim 12\text{hrs} = 720\text{min}$. The negative feedback of cortisol on CRH levels thus acts through the production function $C_\infty(O)$ on the relatively slow timescale T_C. To motivate the functional form of $C_\infty(O)$, we invoke experiments on rats whose adrenal glands had been surgically removed and in which glucocorticoid levels were subsequently kept fixed (by injecting exogenous glucocorticoid) for 5-7 days [WS95, Wat05]. The measured CRH mRNA levels in the PVN were found to decrease exponentially with the level of administered glucocorticoid [WS95,Wat05]. Assuming the amount of releasable CRH is proportional to the amount of measured intracellular CRH mRNA, we can approximate $C_\infty(O)$ as a decreasing exponential function of cortisol level O.

2.2.3 Secretion of CRH

To describe CRH secretion, we consider the following three factors: synaptic inputs to CRH cells in the PVN, availability of releasable CRH peptide, and self-upregulation of CRH release.

CRH secretion activity is regulated by synaptic inputs received by the PVN from multiple brain regions including limbic structures such as the hippocampus and the amygdala, that are activated during stress. It has been reported that for certain types of stressors, these synaptic inputs are modulated by cortisol independent of, or parallel to, its regulatory function on

CRH synthesis activity [TDM06]. On the other hand, a series of studies [KY88b, KY88a, JHB77] showed that cortisol did not affect the basal spiking activity of the PVN. We model the overall synaptic input, denoted by $I(T)$ in Eq. 2.1, as follows

$$I(T) = I_{\text{base}} + I_{\text{ext}}(T), \tag{2.7}$$

where I_{base} and $I_{\text{ext}}(T)$ represent the basal firing rate and stress-dependent synaptic input of the PVN, respectively. As the effect of cortisol on the synaptic input during stress is specific to the type of stressor [GCD03, CHW91, IXS95], we assume $I_{\text{ext}}(T)$ to be independent of O for simplicity and generality.

The secretion of CRH will also depend upon the amount of stored *releasable* CRH, $C_{\text{s}}(T)$, within the neuron and inside the synaptic vesicles. Therefore, C_{s} can also be factored into Eq. 2.1 through a source term $h(C_{\text{s}})$ which describes the amount of CRH released per unit of action potential activity of CRH neurons. Finally, it has been hypothesized that CRH enhances its own release [OCM85], especially when external stressors are present. The enhancement of CRH release by CRH is mediated by activation of the membrane-bound G-protein-coupled receptor CRHR-1 whose downstream signaling pathways operate on timescales from milliseconds to seconds [PP09, MHG02]. Thus, self-upregulation of CRH release can be modeled by including a positive and increasing function $g_C(C)$ in the source term in Eq. 2.1. More details on the self-upregulation of CRH release will be addressed in Chapter 3.

Combining all these factors involved in regulating the secretion process, we can rewrite Eq. 2.1 by replacing $f_C(O)$ with $h(C_{\text{s}})g_C(C)$ as follows

$$\frac{\mathrm{d}C}{\mathrm{d}T} = p_C I(T) h(C_{\text{s}}) g_C(C) - d_C C. \tag{2.8}$$

In this model (represented by Eqs. 2.6,2.8,2.2,2.5, and 2.4), cortisol no longer *directly* suppresses CRH levels, rather, it decreases CRH synthesis through Eq. 2.6, in turn suppressing C_{s}. The combination $h(C_{\text{s}})g_C(C)$ in Eq. 2.8 indicates the release rate of stored CRH de-

creases when either C_s or C decrease. We assume that inputs into the CRH neurons modulate the overall release process with weight p_C.

2.2.4 Complete delay-differential equation model

We are now ready to incorporate the mechanisms described above into a new, more comprehensive mathematical model of the HPA axis, which, in summary, includes

(i) A delayed response of the adrenal cortex to cortisol (Eq. 2.5).

(ii) A slow time-scale negative feedback by cortisol on CRH synthesis (through the $C_\infty(O)$ production term in Eq. 2.6).

(iii) A fast-acting positive feedback of stored and circulating CRH on CRH release (through the $h(C_\mathrm{s})g_C(C)$ term in Eq. 2.8);

Our complete mathematical model thus consists of Eqs. 2.2, 2.4, 2.5, 2.6, and 2.8. We henceforth assume $f_A(OR, O) = f_A(OR)$ depends on only the cortisol-GR complex and use Hill-type functions for $f_A(OR)$ and $g_R(OR)$ [WTL10, RWW12, GAG07, SRD12]. Our full theory is characterized by the following system of delay differential equations:

$$\frac{\mathrm{d}C_\mathrm{s}}{\mathrm{d}T} = \frac{C_\infty(O) - C_\mathrm{s}}{T_C}, \tag{2.9}$$

$$\frac{\mathrm{d}C}{\mathrm{d}T} = p_C I(T) h(C_\mathrm{s}) g_C(C) - d_C C, \tag{2.10}$$

$$\frac{\mathrm{d}A}{\mathrm{d}T} = p_A C \left(\frac{K_A}{K_A + OR}\right) - d_A A, \tag{2.11}$$

$$\frac{\mathrm{d}O}{\mathrm{d}T} = p_O A(T - T_d) - d_O O, \tag{2.12}$$

$$\frac{\mathrm{d}R}{\mathrm{d}T} = p_R \left(1 - \frac{\mu_R K_R^2}{K_R^2 + (OR)^2}\right) - d_R R. \tag{2.13}$$

The parameters $K_{A,R}$ represent the level of A and R at which the negative or positive effect are at their half maximum and $1 - \mu_R$ represents the basal production rate for GR when $OR = 0$.

Of all the processes modeled, we will see that the slow negative feedback described in Eq. 2.9 will be crucial in mediating transitions between stable states of the system. The slow dynamics will allow state variables to cross basins of attraction associated with each of the stable states.

2.2.5 Nondimensionalized model

To simplify the further development and analysis of our model, we nondimensionalize Eqs. 2.9-2.13 by rescaling all variables and parameters in a manner similar to that of Walker *et al.* [WTL10], as explicitly shown in the Appendix. We find

$$\frac{\mathrm{d}c_\mathrm{s}}{\mathrm{d}t} = \frac{c_\infty(o) - c_\mathrm{s}}{t_c}, \tag{2.14}$$

$$\frac{\mathrm{d}c}{\mathrm{d}t} = q_0 I(t) h(c_\mathrm{s}) g_c(c) - q_2 c, \tag{2.15}$$

$$\frac{\mathrm{d}a}{\mathrm{d}t} = \frac{c}{1 + p_2(or)} - p_3 a, \tag{2.16}$$

$$\frac{\mathrm{d}o}{\mathrm{d}t} = a(t - t_\mathrm{d}) - o, \tag{2.17}$$

$$\frac{\mathrm{d}r}{\mathrm{d}t} = \frac{(or)^2}{p_4 + (or)^2} + p_5 - p_6 a, \tag{2.18}$$

where c_s, c, a, r, o are the dimensionless versions of the original concentrations C_s, C, A, R, O, respectively. The dimensionless delay in activation of cortisol production by ACTH is now denoted t_d. All dimensionless parameters q_i, p_i, t_d, and t_c are combinations of the physical parameters and are explicitly given in Appendix 2.6.1. The functions $c_\infty(o)$, $h(c_\mathrm{s})$, and $g_c(c)$ are dimensionless versions of $C_\infty(O)$, $h(C_\mathrm{s})$, and $g_C(C)$, respectively, and will be chosen phenomenologically to be

$$\begin{aligned} c_\infty(o) =& \bar{c}_\infty + e^{-bo}, \\ h(c_\mathrm{s}) =& 1 - e^{-kc_\mathrm{s}}, \\ g_c(c) =& 1 - \frac{\mu_\mathrm{c}}{1 + (q_1 c)^n}. \end{aligned} \tag{2.19}$$

The form of $c_\infty(o)$ is based on the above-mentioned exponential relation observed in adrenalectomized rats [WS95, Wat05] (shown in the Appendix Fig. 2.11). The parameters $\bar{c}_\infty$ and b represent the minimum dimensionless level of stored CRH and the decay rate of the function, respectively. The function $h(c_\mathrm{s})$ describes how the rate of CRH release increases with c_s. Since the amount of CRH packaged in releasable vesicles is likely regulated, we assume $h(c_\mathrm{s})$ saturates at high c_s. The choice of a decreasing form for $c_\infty(o)$ implies that increasing cortisol levels will decrease the target level (or production rate) of c_s in Eq. 2.14. The reduced production of c_s will then lead to a smaller $h(c_\mathrm{s})$ and ultimately to a reduced release source for c (Eq. 2.15). As expected, the overall effect of increasing cortisol is a decrease in the release rate of CRH. Finally, since the upregulation of CRH release by circulating CRH is mediated by binding to CRH receptor, $g_c(c)$ will be chosen to be a Hill-type function, with Hill-exponent n, similar in form to the function $g_R(OR)$ used in Eqs. 2.13 and 2.18. The parameter $1-\mu_\mathrm{c}$ represents the basal release rate of CRH relative to the maximum release rate and q_1^{-1} represents the normalized CRH level at which the positive effect is at half-maximum.

2.3 Multiple Timescale Analysis

2.3.1 Fast-slow variable separation and bistability

Since we assume the negative feedback effect of cortisol on synthesis of CRH operates over the longest characteristic timescale t_c in the problem, the full model must be studied across two separate timescales, a *fast timescale* t, and a *slow timescale* $\tau = t/t_\mathrm{c} \equiv \varepsilon t$. The full model (Eqs. 2.14-2.18) can be succinctly written in the form

$$\frac{\mathrm{d}c_\mathrm{s}}{\mathrm{d}t} = \varepsilon(c_\infty(o) - c_\mathrm{s}), \tag{2.20}$$

$$\frac{\mathrm{d}\mathbf{x}}{\mathrm{d}t} = \mathbf{F}(c_\mathrm{s}, \mathbf{x}), \tag{2.21}$$

where $\mathbf{x} = (c, a, o, r)$ is the vector of fast dynamical variables, and $\mathbf{F}(c_\mathrm{s}, \mathbf{x})$ denotes the right-hand-sides of Eqs. 2.15-2.18. We refer to the fast dynamics described by $\mathrm{d}\mathbf{x}/\mathrm{d}t = \mathbf{F}(c_\mathrm{s}, \mathbf{x})$

as a *fast flow*. In the $\varepsilon \to 0$ limit, it is also easy to see that to lowest order c_s is a constant across the fast timescale and is a function of only the slow variable τ.

Under this timescale separation, the first component of Eq. 2.21 (Eq. 2.15) can be written as

$$\frac{\mathrm{d}c}{\mathrm{d}t} = q(c_\mathrm{s}(\tau), I)g_c(c) - q_2 c, \tag{2.22}$$

where $q(c_\mathrm{s}(\tau), I) \equiv q_0 I h(c_\mathrm{s}(\tau)) = q_0 I(1 - e^{-kc_\mathrm{s}(\tau)})$ is a function of $c_\mathrm{s}(\tau)$ and I. Since c_s is a function only of the slow timescale τ, q can be viewed as a bifurcation parameter controlling, over short timescales, the fast flow described by Eq. 2.22. Once $c(t)$ quickly reaches its non-oscillating quasi-equilibrium value defined by $\mathrm{d}c/\mathrm{d}t = qg_c(c) - q_2 c = 0$, it can be viewed as a parametric term in Eq. 2.16 of the pituitary-adrenal (PA) subsystem (Eqs. 2.14-2.18).

Due to the nonlinearity of $g_c(c)$, the equilibrium value $c(q)$ satisfying $qg_c(c) = q_2 c$ may be multi-valued depending on q, as shown in Figs. 2.2A and 2.2B. For certain values of the free parameters, such as $n, 1 - \mu_\mathrm{c}$, and q_1, bistability can emerge through a saddle-node bifurcation with respect to the bifurcation parameter q. Fig. 2.2B shows the bifurcation diagram, *i.e.*, the nullcline of c defined by $qg_c(c) = q_2 c$.

For equilibrium values of c lying within a certain range, the PA-subsystem can exhibit a limit cycle in (a, o, r) [WTL10] that we express as $(a^*(\theta; c), o^*(\theta; c), r^*(\theta; c))$, where $\theta = 2\pi t/t_\mathrm{p}(c)$ is the phase along the limit cycle with period $t_p(c)$.

The dynamics of the PA-subsystem depicted in Fig. 2.3 indicate the range of c values that admit limit cycle behavior for (a, o, r), while the fast c-nullcline depicted in Fig. 2.2B restricts the range of bistable c values. Thus, bistable states that also support oscillating (a, o, r) are possible only for values of c that satisfy both criteria.

Since circulating CRH only feeds forward into a, o, and r in the $\varepsilon \to 0$ limit, a complete description of all the fast variables can be constructed from just c which obeys Eq. 2.22. Therefore, to visualize and approximate the dynamics of the full five-dimensional model, we only need to consider the 2D projection onto the fast c and slow c_s variable. A summary of the time-separated dynamics of the variables in our model is given in Fig. 2.4.

To analyze the evolution of the slow variable $c_\mathrm{s}(\tau)$, we write our equations in terms of

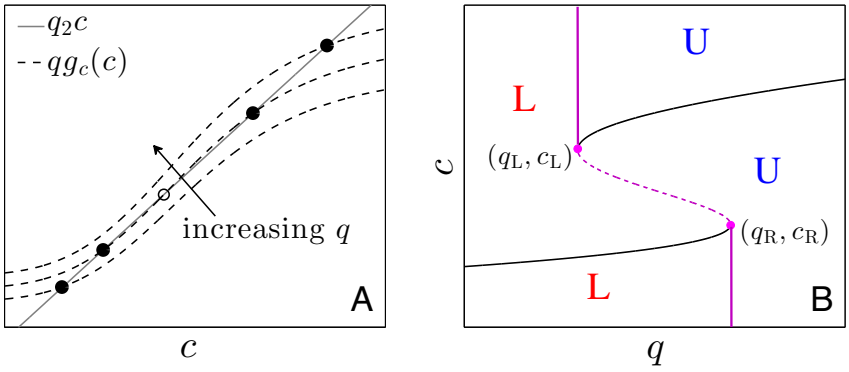

Figure 2.2: **Nonlinear $g_c(c)$ and bistability of fast variables.** (A) The stable states of the decoupled system in Eq. 2.22 can be visualized as the intersection of the two functions $qg_c(c)$ (dashed curve) and $q_2 c$ (gray line). For a given Hill-type function $g_c(c)$, Eq. 2.22 can admit one or two stable states (solid circles), depending on function parameters. The unstable steady state is indicated by the open circle. (B) Bifurcation diagram of the decoupled system (Eq. 2.22) with q as the bifurcation parameter. Solid and dashed segments represent stable and unstable steady states of the fast variables, respectively. L and U label basins of attraction associated with the lower and upper stable branches of the c-nullcline. Left and right bifurcation points (q_L, c_L) and (q_R, c_R) are indicated. Fixed points of c appear and disappear through saddle node bifurcations as q is varied between q_L and q_R.

the scaled time variable $\tau = \varepsilon t$:

$$\frac{\mathrm{d}c_s}{\mathrm{d}\tau} = (c_\infty(o) - c_s), \tag{2.23}$$

$$\varepsilon \frac{\mathrm{d}\mathbf{x}}{\mathrm{d}\tau} = \mathbf{F}(c_s, \mathbf{x}). \tag{2.24}$$

In the $\varepsilon \to 0$ limit, the "outer solution" $\mathbf{F}(c_s, \mathbf{x}) \approx 0$ simply constrains the system to be on the fast c-nullcline defined by $qg_c(c) = q_2 c$. The slow evolution of $c_s(\tau)$ along the fast c-nullcline depends on the value of the fast variable $o(t)$ through $c_\infty(o)$. To close the slow flow subsystem for $c_s(\tau)$, we fix c to its equilibrium value as defined by the fast subsystem and approximate $c_\infty(o(c))$ in Eq. 2.23 by its period-averaged value

$$\langle c_\infty(c) \rangle \equiv \int_0^{2\pi} c_\infty(o^*(\theta; c)) \frac{\mathrm{d}\theta}{2\pi} = \bar{c}_\infty + \int_0^{2\pi} e^{-bo^*(\theta;c)} \frac{\mathrm{d}\theta}{2\pi}. \tag{2.25}$$

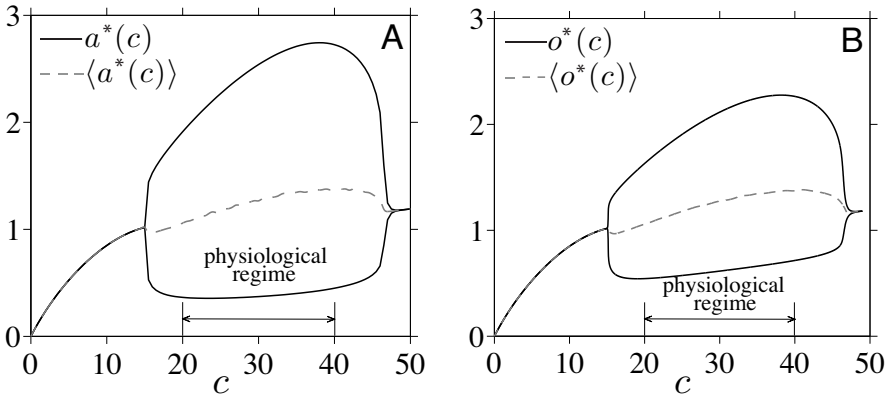

Figure 2.3: **Dynamics of the oscillating PA-subsystem as a function of fixed c.** (A) Maximum/minimum and period-averaged values of ACTH, $a(t)$, as a function of circulating CRH. (B) Maximum/minimum and period-averaged values of cortisol $o(t)$. Within physiological CRH levels, ACTH, GR (not shown), and cortisol oscillate. The minima, maxima, and period-averaged cortisol levels typically increase with increasing c. The plot was generated using dimensionless variables c, a, and o with parameter values specified in [LWA08] and $t_{\rm d} = 1.44$, corresponding to a delay of $T_{\rm d} = 15$min.

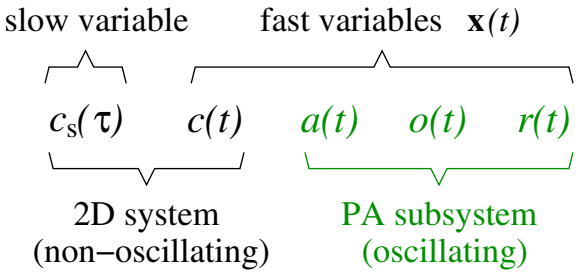

Figure 2.4: **Classification of variables.** Variables of the full five-dimensional model are grouped according to their dynamical behavior. $c_{\rm s}(\tau)$ is a slow variable, while $\mathbf{x}(t) = (c, a, o, r)$ are fast variables. Of these, (a, o, r) form the typically oscillatory PA-subsystem that is recapitulated by c. In the $\varepsilon = 1/t_{\rm c} \ll 1$ limit, the variable $c_{\rm s}(\tau)$ slowly relaxes towards a period-averaged value $\langle c_\infty(o(c))\rangle$. Therefore, the full model can be accurately described by its projection onto the 2D $(c_{\rm s}, c)$ phase space.

Since o^* increases with c (see Fig.2.3B), $\langle c_\infty(c)\rangle$ is a decreasing function of c under physiological parameter regimes. This period-averaging approximation allows us to relate the evolution of $c_{\rm s}(\tau)$ in the slow subsystem directly to c. The evolution of the slow subsystem is approximated by the closed $(c_{\rm s}, c)$ system of equations

$$\frac{\mathrm{d}c_\mathrm{s}}{\mathrm{d}\tau} = \langle c_\infty(c)\rangle - c_\mathrm{s}, \tag{2.26}$$

$$0 = q_0 h(c_\mathrm{s}) I(t) g_c(c) - q_2 c. \tag{2.27}$$

with $\langle c_\infty(c)\rangle$ evaluated in Eq. 2.25. By self-consistently solving Eqs. 2.26 and 2.27, we can estimate trajectories of the full model when they are near the c-nullcline in the 2D (c_s, c)-subsystem. We will verify this in the following section.

2.3.2 Projected dynamics on the reduced system

The separation of timescales results in a natural description of the fast c-nullcline in terms of the parameter q (Fig. 2.2) and the slow c_s-nullcline (defined by the relation $c_\mathrm{s} = \langle c_\infty(c)\rangle$ relating c_s to c) in terms of c. However, the c-nullcline is plotted in the (q, c)-plane while the c_s-nullcline is defined in the (c, c_s)-plane. To plot the nullclines together, we relate the equilibrium value of c_s, $\langle c_\infty(c)\rangle$, to the q coordinate through the monotonic relationship $q(c_\mathrm{s}) = q_0 I h(\langle c_\infty(c)\rangle) = q_0 I(1-e^{-k\langle c_\infty(c)\rangle})$ and transform the c_s variable into the q parameter so that both nullclines can be plotted together in the (q, c)-plane. These transformed c_s-nullclines will be denoted "q-nullclines."

We first consider a fixed basal stress input $I = I_\mathrm{base} = 1$ and plot the q-nullclines in Fig. 2.5A for increasing values of k, the parameter governing the sensitivity of CRH release to stored CRH. From the form $h(\langle c_\infty(c)\rangle) = (1-e^{-k\langle c_\infty(c)\rangle})$, both the position and the steepness of the q-nullcline in (q, c)-space depend strongly on k. Fig. 2.5B shows a fast c-nullcline and a slow q-nullcline (transformed c_s-nullcline) intersecting at both stable branches of the fast c-nullcline. Here, the flow field indicates that the 2D projected trajectory is governed by fast flow over most of the (q, c)-space.

How the fast and slow nullclines intersect each other controls the long-term behavior of our model in the small ε limit. In general, the number of allowable nullcline intersections will depend on input level I and on parameters $(q_0, ..., p_6, b, k, n, \mu_\mathrm{c}, t_\mathrm{d})$. Other parameters such

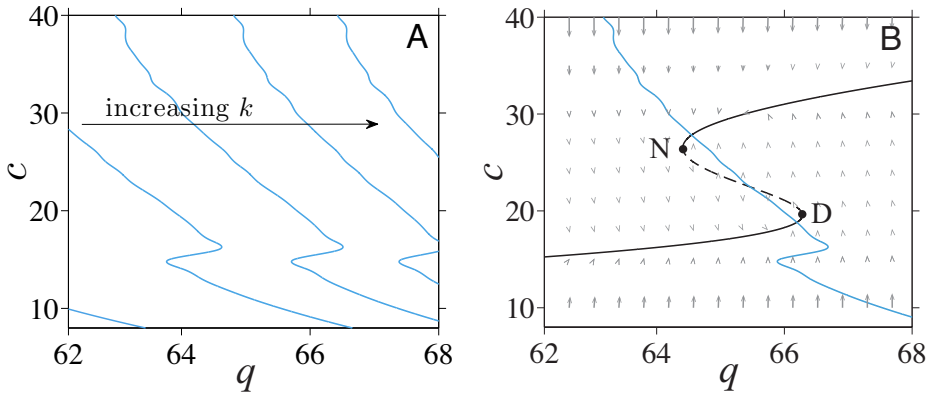

Figure 2.5: **Slow and fast nullclines and overall flow field.** (A) The nullcline of c_s in the $\varepsilon \to 0$ limit is defined by $c_\mathrm{s} = \langle c_\infty(c) \rangle$. To plot these slow nullclines together with the fast c-nullclines, we transform the variable c_s and represent it by q through the relation $q = q_0 h(c_\mathrm{s})$. These transformed nullclines then become a function of c and can be plotted together with the fast c-nullclines. For each fixed value of c, $o(t; c)$ is computed by employing a built-in DDE solver dde23 in MATLAB. The numerical solution is then used to approximate $\langle c_\infty(c) \rangle$ in Eq. 2.25 by Euler's method. The q-nullcline shifts to the right and gets steeper as k increases. (B) The fast c-nullcline defined by $q g_c(c) = q_2 c$ (black curve) is plotted together with the slow c_s-nullcline plotted in the (q, c) plane ("q-nullcline," blue curve). Here, two intersections arise corresponding to a high-cortisol normal (N) stable state and a low-cortisol diseased (D) stable state. The flow vector field is predominantly aligned with the fast directions toward the c-nullcline.

as q_0, q_1, and μ_c appear directly in the fast equation for c and thus most strongly control the fast c-nullcline. Fig. 2.6A shows that for a basal stress input of $I = I_\mathrm{base} = 1$ and an intermediate value of k, the nullclines cross at both stable branches of the fast subsystem. As expected, numerical simulations of our full model show the fast variables (a, o, r) quickly reaching their oscillating states defined by the c-nullcline while the slow variable $q = q_0 I h(c_\mathrm{s})$ remains fairly constant. Independent of initial configurations that are not near the c-nullcline in (q, c)-space, trajectories quickly jump to one of the stable branches of the c-nullcline with little motion towards the q-nullcline, as indicated by ξ_f in Fig. 2.6A.

Once near the c-nullcline, say when $|\mathbf{F}(c_\mathrm{s}, \mathbf{x})| \ll \varepsilon$, the trajectories vary slowly according to Eqs. 2.23. Here, the slow variable c_s relaxes to its steady state value while satisfying the constraint $\mathbf{F}(c_\mathrm{s}, \mathbf{x}) \approx 0$. In $(q, c)-$space, the system slowly slides along the c-nullcline towards

the q-nullcline (the ξ_s paths in Fig. 2.6A). This latter phase of the evolution continues until the system reaches an intersection of the two nullclines, indicated by the filled dot, at which the reduced subsystem in c_s and c reaches equilibrium.

For certain values of k and if the fast variable c is bistable, the two nullclines may intersect within each of the two stable branches of the c-nullcline and yield the two distinct stable solutions shown in Fig. 2.6A. For large k, the two nullclines may only intersect on one stable branch of the c-nullcline as shown in Fig. 2.6B. Trajectories that start within the basin of attraction of the lower stable branch of the c-nullcline ("initial state 2" in Fig. 2.6B) will stay on this branch for a long time before eventually sliding off near the bifurcation point and jumping to the upper stable branch. Thus, the long-term behavior of the full model can be described in terms of the locations of the intersections of nullclines of the reduced system.

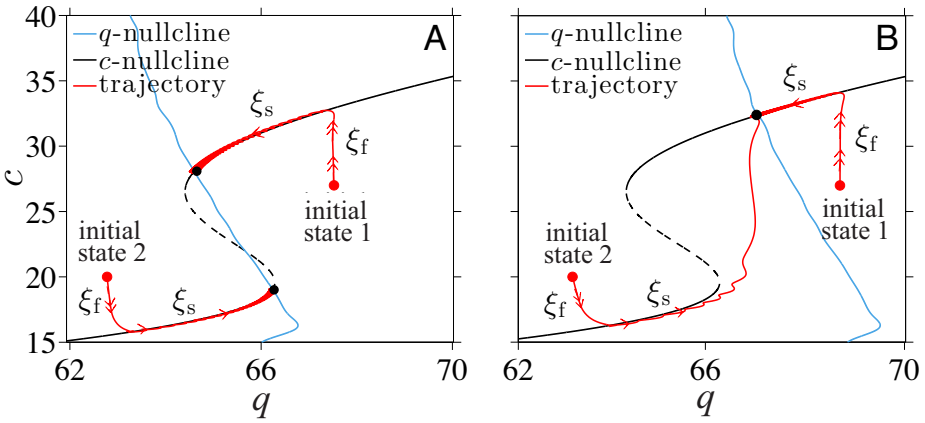

Figure 2.6: **Equilibria at the intersections of nullclines.** (A) For intermediate values of k, there are three intersections, two of them representing stable equilibria. Solid red lines are projections of two trajectories of the full model, with initial states indicated by red dots and final stable states shown by black dots. The full trajectories approach the intersections of the q-nullcline (blue) and c-nullcline (black). (B) For large k there is only one intersection at the upper branch of the c-nullcline. Two trajectories with initial states near different branches of the c-nullcline both approach the unique intersection (black dot) on the upper branch. The scenario shown here corresponds to a Type I nullcline structure as described in the Additional File.

2.4 Discussion

The dual-nullcline structure and existence of multiple states discussed above results from the separation of slow CRH synthesis process and fast CRH secretion process. This natural physiological separation of time scales ultimately gives rise to slow dynamics along the fast c-nullcline during stress. The extent of this slow dynamics will ultimately determine whether a transition between stable states can be induced by stress. How external stress-driven transitions mediated by the fast-slow negative feedback depend on system parameters will be explored in next chapter. The remainder of this chapter will be focused on understanding how our model exhibits bistable attracting limit cycles that characterize the normal and diseased states that preserve the ultradian oscillations. In particular, different types of nullcline structures that may arise depending on system parameters will be identified and analyzed.

Changes in parameters that accompany trauma can lead to shifts in the position of the nullclines. For example, if the stored CRH release process is sufficiently compromised (*e.g.* smaller k), the slow q-nullcline moves to the left, driving a bistable or fully resistant organism into a stable diseased state. Interventions that increase k would need to overcome hysteresis in order to restore normal HPA function. More permanent changes in parameters are likely to be caused by physical rather than by psychological traumas since such changes would imply altered physiology and biochemistry of the person. Traumatic brain injury (TBI) is an example of where parameters can be changed permanently by physical trauma. The injury may decrease the sensitivity of the pituitary to cortisol-GR complex, which can be described by decreasing p_2 in our model. Such change in parameter would lead to a leftward shift of the q-nullcline and an increased likelihood of hypocortisolism. Similarly, various physiological conditions associated with certain parameter changes can be incorporated into our model to predict and analyze their effects on the long-term behavior of the system. In the remainder of this chapter, we will focus on how the new parameters (q_0, q_1, μ_c, k) introduced in our model determine the existence and the type of bistability of the system. A more comprehensive discussion will be included in the following chapter.

To be more concrete in our analysis, we now choose our nullclines by specifying parameter values. We estimate many of the dimensionless parameters by using values from previous studies, as listed in Table 2.1. Of the four remaining parameters, μ_c, q_0, q_1, and k, we will study how our model depends on k while fixing μ_c, q_0, and q_1. Three possible nullcline configurations arise according to the values of μ_c, q_0, and q_1 and are delineated in the following section. We have also implicitly considered only parameter regimes that yield oscillations in the PA subsystem at the stable states defined by the nullcline intersections.

Table 2.1: Dimensionless parameter values of our full model. Analogous parameters from the literature are referenced.

Parameter	Value	Source and Ref.	Description
n	5	assumed	Hill coefficient in upregulation function $g_c(c)$
$\bar{c}_\infty$	0.2	estimated from [Wat05]	baseline stored CRH level
b	0.56	estimated from [Wat05]	relates cortisol to stored CRH level
k	undetermined	·	relates stored CRH to CRH release rate
μ_c	undetermined	·	basal CRH release rate
q_0	undetermined	·	maximum CRH release rate
q_1^{-1}	undetermined	·	circulating CRH for half-maximum self-upregulation
q_2	1.8	estimated from [WWS98]	ratio of CRH and cortisol decay rates
p_2^{-1}	0.067	p_2^{-1} [LWA08]	(or)-complex level for half-maximum feedback
p_3	7.2	p_3 [LWA08]	ratio of ACTH and cortisol decay rates
p_4	0.05	p_4 [LWA08]	(or)-complex level for half-maximum upregulation
p_5	0.11	p_5 [LWA08]	basal GR production rate by pituitary
p_6	2.9	p_6 [LWA08]	ratio of GR and cortisol decay rates
t_c	69.3	assumed	CRH biosynthesis timescale
t_d	1.44	"τ" [LWA08]	delay in ACTH-activated cortisol release

2.4.1 Three types of bistable nullcline structure

To determine how the q-nullcline crosses the c-nullcline, we substitute c_s by its equilibrium period-averaged value $\langle c_\infty(c)\rangle$. If we assume a basal input level $I = 1$, the values of k that will position the basal q-nullcline to just pass through the left and right bifurcation points (q_L, c_L) and (q_R, c_R) can be found by solving $q_{L,R} = q_0(1 - e^{-k\langle c_\infty(c_{L,R})\rangle})$:

$$k_L = \frac{1}{\langle c_\infty(c_L)\rangle} \ln\left(\frac{1}{1 - q_L/q_0}\right), \quad k_R = \frac{1}{\langle c_\infty(c_R)\rangle} \ln\left(\frac{1}{1 - q_R/q_0}\right). \tag{2.28}$$

All possible ways in which the nullclines can cross each other as k is varied are illustrated in Fig. 2.7.

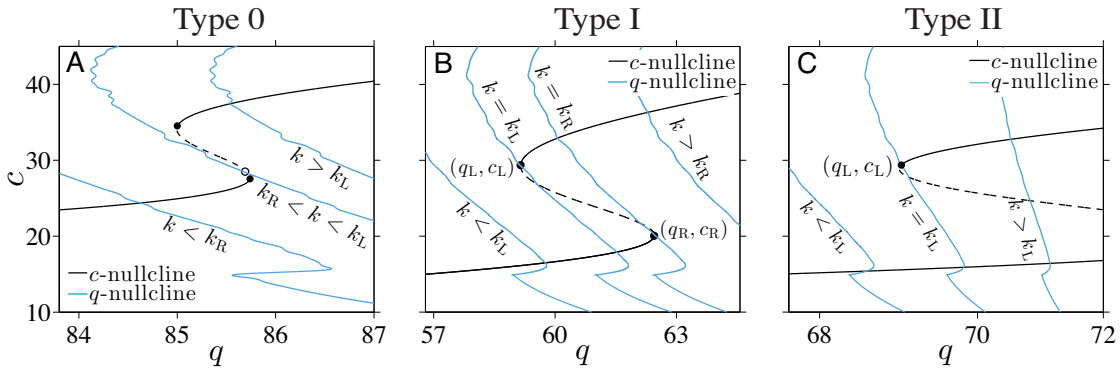

Figure 2.7: **The possible number of equilibria of the reduced (c_s, c) system.** (A) A **Type 0** scenario in which $k_R < k_L$ permits only one nullcline intersection, either one the lower stable branch, the unstable branch, or the upper stable branch. (B) In this **Type I** parameter regime, the c-nullcline is shaped and positioned such that $k_L < k_R$. Therefore, it is possible for the model to exhibit two oscillating stable states provided $k_L < k < k_R$. For $k < k_L$ ($k > k_R$), the q-nullcline shifts to the left(right) and the intersection with the upper(lower) branch of the c-nullcline disappears, leading to only one stable point. (C) A **Type II** c-nullcline. For $k < k_L$, there is only one intersection at the lower branch. For all $k > k_L$ there are two intersections.

The specific locations of the bifurcation points, as well as k_L and k_R, are complicated functions of all parameters. However, Eqs. 2.28 allows us to distinguish three qualitatively different regimes. The first possibility is $k_L > k_R$, where there can be at most only one intersection between the slow and fast nullclines. We denote this as a **Type 0** scenario

(Fig. 2.7A) characterized by having at most a single stable state towards which the system will always return upon cessation of external stress. In Type 0 situations with intermediate values of k, the intersection will arise in the unstable branch of the c-nullcline. In this case, we expect the system to oscillate between the two stable branches of the c-nullcline. Here, the fast variables a, o, and r will cycle periodically between two oscillating levels.

In order for the two nullclines to intersect three times (twice on stable branches of the c-nullcline), the q-nullcline must "fit" within the bistable region of the c-nullcline. As shown in Fig. 2.7, there are two separate subcases of nullclines that intersect twice. If $k_{\mathrm{L}} < k_{\mathrm{R}}$, a value of $k_{\mathrm{L}} < k < k_{\mathrm{R}}$ would imply that the $q-$nullcline can intersect both stable branches of the c-nullcline, leading to two stable solutions. We refer to this case as **Type I** (Fig. 2.7B).

Another possibility is that the right bifurcation point is beyond the maximum value $q = q_0$ dictated by the function $h(\langle c_\infty(c_{\mathrm{R}})\rangle)$. As shown in Fig. 2.7C, the bistable c-nullclines exhibits only one bifurcation point within the domain of q. The lower branch of the c-nullclines in this set extends across the entire range of physiological values of q, ensuring that the q-nullcline will intersect with the lower branch for any value of k. Therefore, to determine if there are two intersections we only need to check that $k_{\mathrm{L}} \leq k$ is satisfied. In this **Type II** case, the system is either perpetually in the diseased low cortisol state, or is bistable between the diseased and normal states; the system will always be at least susceptible to low-cortisol disease. Summarizing,

- **Type 0**: Exactly one solution (one nullcline intersection) exists for the reduced subsystem. Here, $k_{\mathrm{R}} < k_{\mathrm{L}}$ and the intersection may occur on the lower or upper stable branches, or on the unstable branch of the c-nullcline. The system is either permanently diseased, permanently resistant, or oscillates between normal and diseased states.

- **Type I**: At least one solution exists. A stable diseased solution exists if $k < k_{\mathrm{L}}$, two stable solutions (diseased and normal) arise if $k_{\mathrm{L}} \leq k \leq k_{\mathrm{R}}$, and fully resistant state arises if $k > k_{\mathrm{R}}$.

- **Type II**: At least one solution exists. A stable diseased state arises if $k < k_{\mathrm{L}}$ while

both diseased and normal solutions arise if $k > k_{\mathrm{L}}$. A fully disease-resistant state cannot arise.

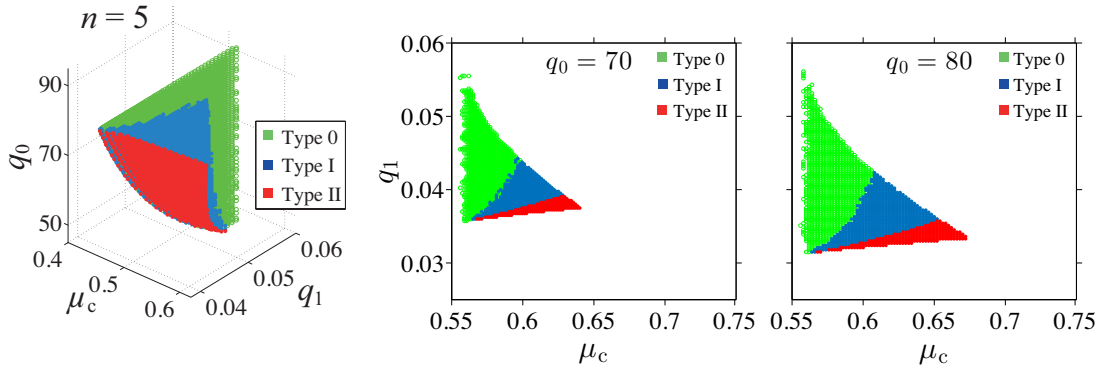

Figure 2.8: **Phase diagram in (μ_c, q_0, q_1)-space.** Regimes for each of the three types of bistable c-nullclines shown in the parameter space (μ_c, q_0, q_1) and (μ_c, q_1) with $n = 5$. The uncolored regions correspond to systems that do not exhibit either bistability or oscillations.

With the parameters fixed according to Table 2.1, we will treat k as a control parameter and exhaustively sweep the three-dimensional parameter space (q_0, q_1, μ_c) to determine the regions which lead to each of the nullcline structural types. In addition, we restrict the parameter domain to regions which admit oscillating solutions of the full problem. In other words, parts of both stable branches of the c-nullclines must fall within values of c which support oscillations in the PA-subsystem (Fig. 2.3). The regions in (μ_c, q_0, q_1) space that satisfy these conditions and that yield each of the types of nullcline crossings are indicated in Fig. 2.8.

Based on measurements of self-upregulation of CRH secretion during stress [OCM85], $\mu_c = 0.6$ is chosen to set the baseline level of the Hill function $g_c(c = 0) \approx 0.4$. q_1 is approximated by setting the inflection point of $g_c(c)$ to arise at $c \approx 25$, the average value used by Walker *et al.* [WTL10]. Assuming $c \approx 25$ is a fixed point of Eq. 2.15 when $I = 1$ and $c_s \approx \langle c_\infty(25) \rangle$, q_0 can be estimated as a root of the right-hand-side of Eq. 2.15. This choice for the remaining parameters puts our nullcline system into the **Type I** category that can exhibit one or two stable states with oscillating (a, o, r) subsystems. We restricted the analysis of our model to **Type I** systems.

Given these considerations, we henceforth chose $\mu_c = 0.6$, $q_1 = 0.04$, and $q_0 = 77.8$ for the rest of our analysis. This choice of parameters is motivated in the Additional File and corresponds to a so-called "Type I" nullcline structure. In this case, three possibilities arise: one intersection on the lower stable branch of the c-nullcline if $k < k_L$, two intersections if $k_L < k < k_R$ (Fig. 2.6A), and one intersection on the upper stable branch of the c-nullcline if $k > k_R$ (Fig. 2.6B). For our chosen set of parameters and a basal stress input $I = 1$, the critical values $k_L = 2.5 < k_R = 2.54$ are given above by Eq. 2.28.

2.4.2 Bistable limit cycle attractors

2.4.3 Normal stress response

Activation of the HPA axis by acute stress culminates in an increased secretion of all three main hormones of the HPA axis. Persistent hypersecretion may lead to numerous metabolic, affective, and psychotic dysfunctions [MS93,McE98]. Therefore, recovery after stress-induced perturbation is essential to normal HPA function. To model the change in the amount of synaptic input experienced by the PVN during stress response, we consider time-dependent synaptic input strength, $I(t)$. Since the majority of neural circuits that project to the PVN are excitatory [HFM03], we assume external stress stimulates CRH neurons to release CRH above its unit basal rate and that $I(t) = 1 + I_{ext}(t)$ ($I_{base} = 1$) with $I_{ext} \geq 0$. We explore the stability of the HPA axis by initiating the system in the upper of the two stable points shown in Fig. 2.9A and by then imposing a 120min external stress input $I_{ext} = 0.1$. The HPA axis responds with an increase in the peak level of cortisol before relaxing back to its original state after stress is terminated (Fig. 2.9B). This transient process is depicted in the projected (q, c)-space in Fig. 2.9A.

Upon turning on stress, the lumped parameter q and the slow nullcline shift to the right by 10% since $q = q_0(1+I_{ext})h(\langle c_\infty(c)\rangle)$ (see Fig. 2.9A). The trajectory will then move rapidly upward towards the new value of c on the c-nullcline; afterwards, it moves very slowly along the c-nullcline towards the shifted q-nullcline. After 120min, the system arrives at the "$\times$" on the c-nullcline in Fig. 2.9A. Once the stress is shut off the q-nullcline returns to its original

position defined by $I = 1$. The trajectory also jumps horizontally back to near the initial q value and subsequently quickly returns to the original upper-branch stable point.

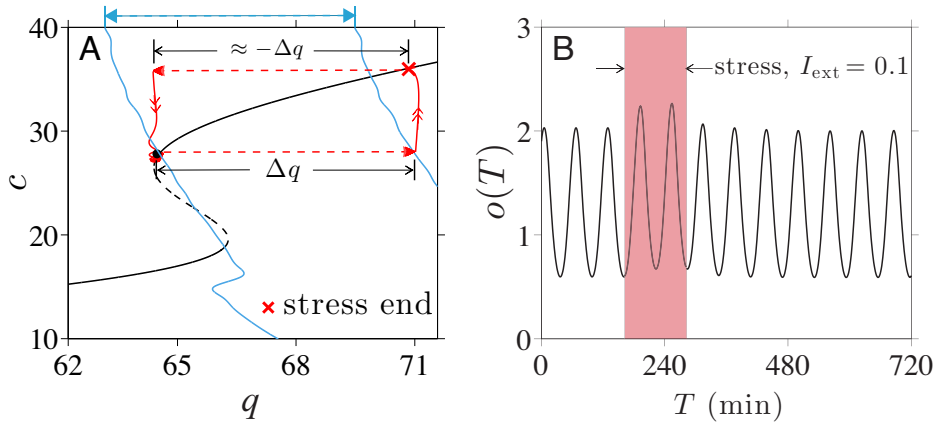

Figure 2.9: **Normal stress response.** Numerical solution for the response to a 120min external stress $I_{\text{ext}} = 0.1$. (A) At the moment the external stress is turned on, the value of (q, c) increases from its initial stable solution at $(64.4, 27)$ to $(71, 27)$ after which the circulating CRH level c, quickly reaches the fast c-nullcline (black) before slowly evolving along it towards the slow q-nullcline (blue). After short durations of stress, the system returns to its starting point within the normal state basin. (B) The peaks of the cortisol level are increased during stress (red) but return to their original oscillating values after the stress is turned off.

2.4.4 Timing of stress onset and transient response

Here, we show how the transient response of the system during stress is dependent on the timing of the stress initiation. In previous studies [WWS98, WWL98], changes in corticosterone levels in rats were measured in response to stress induced by noise applied at different phases of the animals oscillating cortisol cycle. It was observed that the timing of the stress onset relative to the ultradian phase was crucial in determining the magnitude of corticosterone response. Increases in corticosterone levels were markedly higher when noise was initiated during the rising phase than when initiated during the falling phase.

We can frame these experimental observations mechanistically within our theory. Following the experimental protocol [WWS98, WWL98], we simulate the stress response using a brief stressor with a duration of 30min. As shown in Fig. 2.10A, an external stress that is

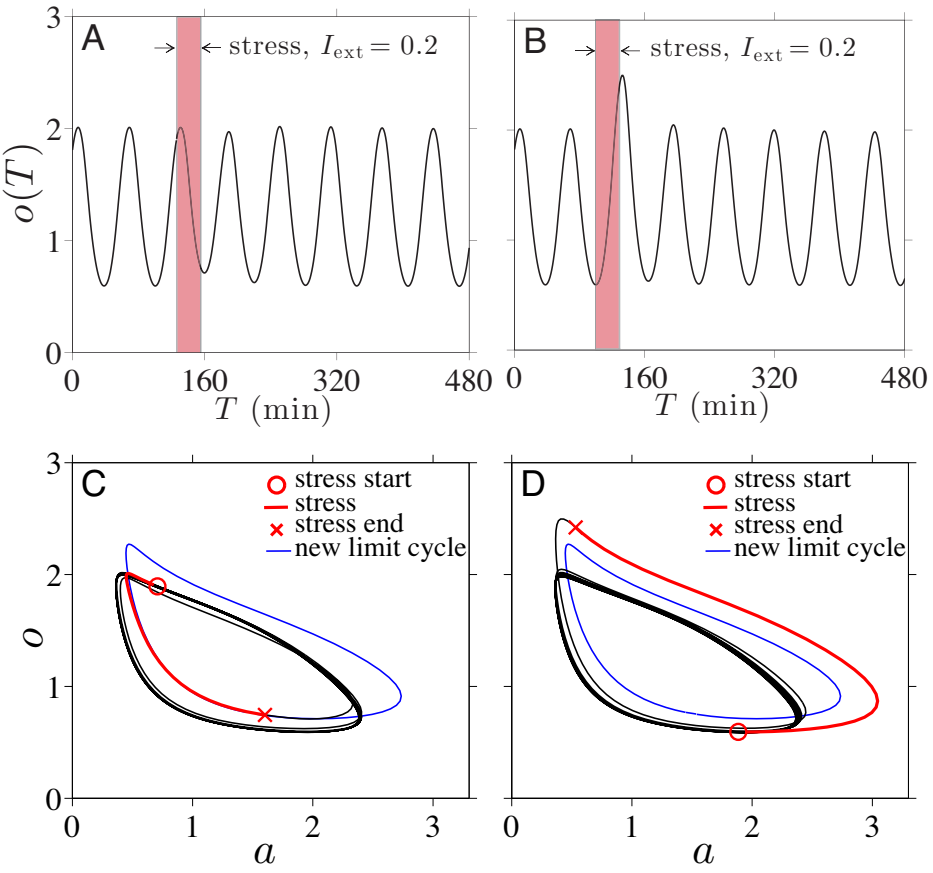

Figure 2.10: **Stress timing and cortisol response.** (A) A stressor of duration of 30min with magnitude $I_{\text{ext}} = 0.2$ was applied mainly over the falling phase of the underlying cortisol oscillation. The first peak after the stress onset was almost unchanged, but the first nadir was elevated. (B) The same stressor used in (A) applied during the rising phase led to a significantly increased subsequent peak while the first nadir was unaffected. (C) The trajectory of the system (red) is projected onto the cortisol-ACTH plane. The new limit cycle of the PA-subsystem corresponding to fixed $I(t) = 1.2$ is indicated by the blue curve. During stress, the trajectory of the system is attracted towards the new limit cycle. The system recovers after making a smaller cycle within the normal limit cycle, reaching a higher nadir. (D) The trajectory of the system deviates then recovers back through a trajectory above the normal limit cycle, reaching a higher peak.

applied mostly over the falling phase of the cortisol oscillation results in a higher subsequent nadir in $o(t)$ than one that is applied predominantly during a rising phase. However, as shown in Fig. 2.10B, stress applied mainly during the rising phase leads to a higher subsequent peak level. This observation is consistent with the results of the experiment on rats

and can be explained by the dynamics inherent in our model.

The immediate increase in $q = q_0 I h(c_s)$ associated with the increase in I leads to a rapid increase in c, as shown in Fig. 2.9. This higher level of circulating CRH shifts the stable limit cycle of the PA subsystem to a new one with higher minimum and maximum values of ACTH and cortisol (as shown in Fig. 2.3). This new limit cycle is shown by the blue curve in Figs. 2.10C,D. Under external stress, a trajectory of the system quickly deviates and approaches the new limit cycle, but quickly returns to the original limit cycle after cessation of stress. Thus, depending on the position of the trajectory relative to that of the new stressed limit cycle, the initial deviation may try to reach the new limit cycle in the falling or rising cortisol phases as shown in Figs. 2.10C,D. Moreover, if the duration of the stress is shorter than the period of the inherent oscillation, the trajectory will return to its original limit cycle before completing a full cycle of the new limit cycle. These properties of the limit cycle dynamics explain the difference in the level of subsequent peak following the stress onset depending on the timing of the stress onset.

2.5 Summary and Conclusions

We developed a theory of HPA dynamics that includes stored CRH, circulating CRH, ACTH, cortisol and glucocorticoid receptor. Our model incorporates a fast self-upregulation of CRH release, a slow negative feedback effect of cortisol on CRH synthesis, and a delay in ACTH-activated cortisol synthesis. These ingredients allow our model to be separated into slow and fast components and projected on a 2D subspace for analysis.

Depending on physiological parameter values, there may exist zero, one, or two stable simultaneous solutions of both fast and slow variables. For small k, CRH release is weak and only the low-CRH equilibrium point arises; an individual with such k is trapped in the low-cortisol "diseased" state. For large k, only the high-CRH normal state arises, rendering the individual resistant to acquiring the long-term, low-cortisol side-effect of certain stress disorders. When only one stable solution arises, HPA dysregulation must depend on changes in parameters resulting from permanent physiological modifications due to *e.g.,*

aging, physical trauma, or stress itself [McE98, DRM14a]. For example, it has been observed that older rats exhibit increased CRH secretion while maintaining normal levels of CRH mRNA in the PVN [HTP94]. Such a change could be interpreted as an age-dependent increase in k, which, in our model, implies that aging makes the organism more resistant to stress-induced hypocortisolism. Indeed, it has been suggested that prevalence of PTSD declines with age [AB00, RBB88].

Other regulatory systems that interact with or regulate the HPA axis can also affect parameter values in our model. Gonadal steroids, which are regulated by another neuroendocrine system called the hypothalamic-pituitary-gonadal (HPG) axis, activate the preoptic area (POA) of the hypothalamus [SSC90, GAT01], which in turn attenuates the excitatory effects of medial amygdala stimulation of the HPA axis [FCS90]. Thus, low testosterone levels associated with hypogonadism would effectively increase $I(t)$ within our model, shift the q-nullcline in the (q, c)-space, and in turn increase cortisol levels. One might consider this as a possible explanation for chronically elevated cortisol levels observed in major depressive disorder patients who suffers from hypogonadism. Although it is beyond the scope of this paper, one may further investigate role of gonadal hormones, or role of any other interacting systems, in mediating stress response by considering which parameters would be affected in our model.

Within certain parameter regimes and for intermediate k, our theory can also exhibit bistability. When two stable solutions arise, we identify the states with low oscillating levels of cortisol as the diseased state associated with hypocortisolism. Thus our model implies that HPA dysregulation may develop without permanent "structural" or physiological changes, but via "transitions" between two modes of behavior that correspond to basins of attraction of the dynamical system. How such transitions, or onset of a disease, can be induced by stressors will be investigated in the next chapter. Besides the magnitude and duration of the stressor, we will also consider the effect of the relative timing of stress initiation to the intrinsic oscillation of the system on stress-driven transitions, as its importance was demonstrated in the normal stress response simulations.

2.6 Appendix

2.6.1 Nondimensionalization

Our equations are nondimensionalized in a manner similar to that used by Walker *et al.* [WTL10]:

$$\begin{aligned} &t = d_O T, && c_{\mathrm{s}} = C_{\mathrm{s}}/\bar{C}_{\mathrm{s}}, && c = (\mu_{\mathrm{R}} p_{\mathrm{R}})^{-1} d_O C, \\ &a = (\mu_{\mathrm{R}} p_{\mathrm{R}} p_{\mathrm{A}})^{-1} d_O^2 A, && r = (\mu_{\mathrm{R}} p_{\mathrm{R}})^{-1} d_O R, && o = (\mu_R p_{\mathrm{R}} p_{\mathrm{A}} p_{\mathrm{O}})^{-1} d_O^3 O, \end{aligned} \tag{A1}$$

Here, $c_{\mathrm{s}}, c, a, r, o$ are the dimensionless versions of the original concentrations $C_{\mathrm{s}}, C, A, R, O$, respectively. C_{s} is normalized by $\bar{C}_{\mathrm{s}}$, which denotes the typical maximum amount of releasable CRH in the physiological range. Upon using these variables, the dimensionless forms of Eqs. 2.9-2.13 are expressed in Eqs. 2.14-2.18. The parameters q_i, p_i are dimensionless combinations conveniently defined to be analogous to those used by Walker *et al.* [WTL10]:

$$\begin{aligned} &t_c = d_O T_C, && t_{\mathrm{d}} = d_O T_{\mathrm{d}}, && q_0 = p_C/(\mu_R p_R), \\ &q_2 = d_C/d_O, && p_2 = \mu_R^2 p_R^2 p_A p_O/(d_O^4 K_A), && p_3 = d_A/d_O, \\ &p_4 = d_{\mathrm{O}}^8 K_{\mathrm{R}}^8 (p_{\mathrm{A}} p_{\mathrm{O}})^{-2} (\mu_{\mathrm{R}} p_{\mathrm{R}})^{-4}, && p_5 = (1-\mu_{\mathrm{R}})/\mu_{\mathrm{R}}, && p_6 = d_R/d_O. \end{aligned} \tag{A2}$$

Using these scalings, we arrive at the dimensionless Eqs. 2.14-2.19.

2.6.2 Parameter estimates

Many of the numerous physiological parameters in our model can be estimated or constructed from previous studies on the HPA axis. For example, as shown in Fig. 2.11, the parameters forming the function $c_\infty(o)$ are derived from fitting to data on adrenalectomized male rats [Wat05]. From the fitting, we estimate the baseline level $\bar{c}_\infty \simeq 0.2$, and the decay rate $b \simeq 0.6$ [Wat05]. Furthermore, the dimensionless parameters $p_2, \ldots, p_5$ and t_{d} will be fixed to those used in Walker *et al.* [WTL10]: $p_2 = 15$, $p_3 = 7.2$, $p_4 = 0.05$, $p_5 = 0.11$, $p_6 = 2.9$

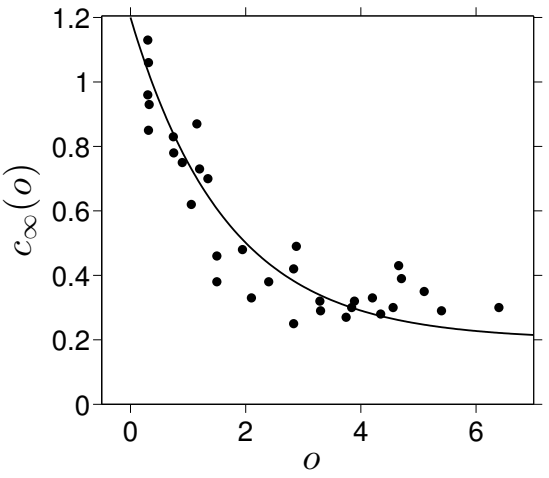

Figure 2.11: **Fitting $c_\infty(o)$ to rat data.** Nondimensionalized data taken from Watts [Wat05] and fitted using the form for $c_\infty(o)$ given in Eq. 2.19. Cortisol levels were arbitrarily rescaled according to 125ng/ml = 3.

and $t_\mathrm{d} = 1.44$ ($T_\mathrm{d} = 15$ min). Although it is not possible to determine all of the remaining parameters from data, we will use reasonable estimates. The half-life of cortisol was estimated to be about 7.2min [WWS98] while the half-life of CRH has been estimated to be about 4min [SAG84]. Therefore, $q_2 = d_C d_O^{-1} \approx 1.8$. Of the remaining parameters $(n, \mu_\mathrm{c}, q_0, q_1, k)$, the dependence on n will turn out to be quantitative so we henceforth set $n = 5$. These estimated parameters are listed in Table 2.1.

Even though one expects the values of these effective parameters to be highly variable, we fix them in order to concretely investigate the mathematical structure and qualitative predictions of our model. The parameters μ_c, q_0, q_1, and k remain undetermined; however, it is instructive to treat k as a control parameter and explore the nullcline structure in μ_c, q_0, q_1 parameter space.

CHAPTER 3

The HPA axis and PTSD

3.1 Introduction

As introduced in the previous chapter, the hypothalamic-pituitary-adrenal (HPA) axis is a neuroendocrine system that regulates the secretion of cortisol by the adrenal cortex in response to stressors. In order to understand how the HPA axis functions, especially in the context of post-traumatic stress disorder (PTSD), a number of challenge tests have been developed. These tests typically involve measuring changes in key endogenous hormone levels after the administration of their synthetic analogues in both PTSD and normal subjects. In this paper, we will interpret the outcomes and dynamics of the challenge tests through mechanistic models of HPA axis dynamics.

Cortisol (a type of glucocorticoid steroid hormone) is a "stress hormone" that regulates or supports a variety of important cardiovascular, metabolic, immunologic, and homeostatic functions [WBB16]. As typical for hormones, maintaining cortisol concentrations within appropriate ranges during both stress response and in the basal state is essential for normal physiological function. A stress response is typically initiated when neurons in the paraventricular nucleus (PVN) of the hypothalamus receive increased synaptic inputs from various regions of the brain, each containing information about certain types of stressors. These synaptic inputs induce the PVN neurons to release corticotropin-releasing peptide hormone (CRH) into the portal blood vessel connecting the hypothalamus to the anterior pituitary. Released CRH travels to the anterior pituitary and activates the secretion of adrenocorticotropin hormone (ACTH). ACTH travels via the bloodstream to the adrenal cortex, located above the kidneys, where it stimulates cortisol secretion. Finally, cortisol

travels back to both the pituitary and the hypothalamus to suppress their activities, completing the negative feedback loop and returning cortisol to a basal level. Both ACTH and cortisol exhibit ultradian (hourly) and circadian (daily) oscillations. The basic interactions regulating the HPA axis dynamics are summarized in Fig. 3.1. When the HPA axis is dysregulated, cortisol may fail to return to basal levels, disrupting other functions and causing comorbidities. For example, excessive cortisol is associated with major depressive disorder (MDD) [GG02] while low cortisol is reported among PTSD patients. Clinical observations that confirm lower than normal cortisol levels in the urine of PTSD patients collected over a 24-hour period [Mas68, YSN90, YKB95] and in blood samples drawn at 15 minutes intervals over a 24 hours [BVK07]. In one measurement, cortisol levels collected in urine of PTSD subjects was 40.9 ± 12.3 μg/day and appreciably lower than the 62.8 ± 22.2 μg/day collected in urine of normal subjects [YSN90]. Blood samples also showed that plasma cortisol levels were consistently lower among PTSD patients over the 24-hour period and significantly lower in the afternoon [BVK07].

Despite the general trend of lower cortisol under PTSD, a few contradicting reports may be found in the literature. Most of them are surveyed in a recent meta-analysis [MRV07]. For example, urine measurements in [RLW01] showed a marginally significant increase of cortisol in premenopausal women with PTSD; the basal cortisol level in [YGY04a] showed no difference between PTSD and control groups. The overall pooled estimate of the mean cortisol level from the meta-analysis [MRV07] indicated cortisol was lower within the PTSD group (standardized mean difference= -0.12 with p-value of 0.24), but concluded that the difference was not significant. On the other hand, the difference between PTSD and control subjects was shown to be significant in some subgroups, such as females and those exposed to certain types of trauma [MRV07]. Most importantly, the meta-analysis found that cortisol levels were significantly lower among PTSD patients when compared to subjects who had not been previously exposed to trauma (standardized mean difference = -0.35 with p-value of 0.007). One of the goals of our study is to propose a theory to explain how trauma exposure can lead to altered cortisol dynamics and understand why certain subgroups are likely to express lower post-traumatic cortisol levels.

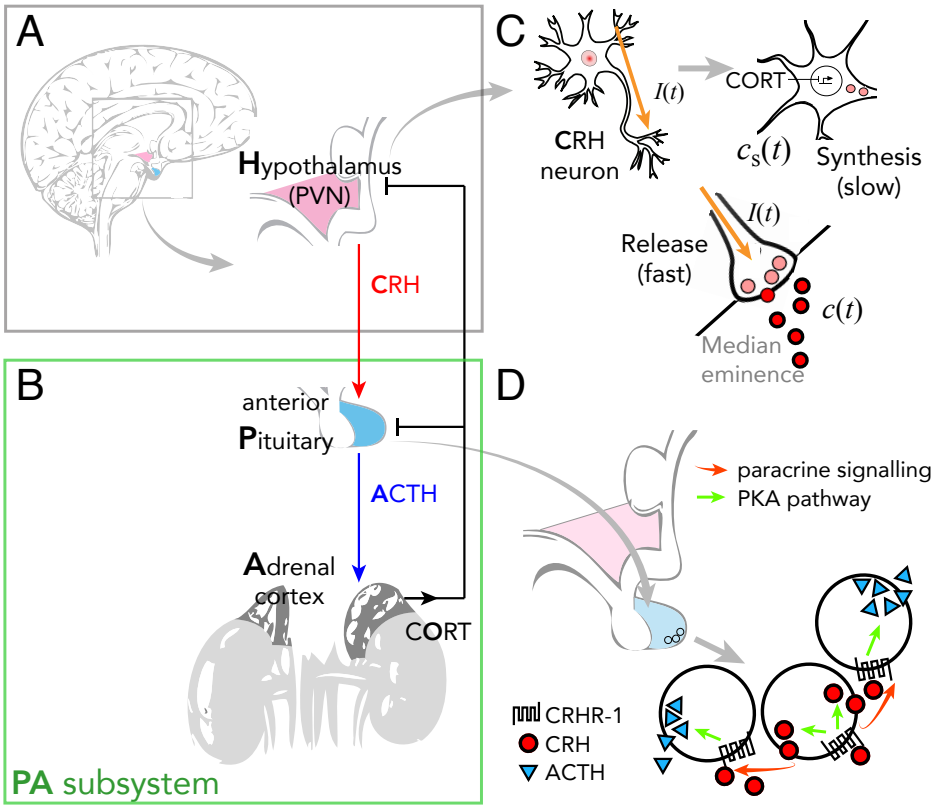

Figure 3.1: **Schematic of the HPA axis.** (A) Stress is processed in the central nervous system (CNS) and a signal is relayed to the paraventricular (PVN) in the hypothalamus to activate CRH secretion into the hypophyseal portal system. (B) CRH diffuses to the pituitary gland and activates ACTH secretion. ACTH travels down to the adrenal cortex to activate cortisol (CORT) release. Cortisol inhibits both CRH and ACTH secretion to down-regulate its own production, forming a closed loop. (C) Negative feedback of cortisol suppresses CRH synthesis in the PVN, ultimately reducing the amount of stored CRH and its subsequent release. External inputs such as stressors and circadian inputs directly affect the release rate of CRH at the axonal terminal. (D) CRH released by the PVN stimulates the protein kinase A (PKA) pathway to activate release of CRH by the anterior pituitary, contributing to ACTH secretion in a auto/paracrine fashion.

In previous chapter, we developed a dynamical model of the HPA axis to describe the interactions among the key hormones mentioned above and the glucocorticoid receptor (GR) that mediates feedback activity of cortisol. Here, we consider a self-upregulation process of CRH through the auto/paracrine function in the anterior pituitary for a more accurate description of the physiology. This modification of the original model does not change its overall qualitative features. A detailed comparison between the original mode and the current model is included in the Appendix. For appropriate sets of parameters, our model exhibits bistability with two attracting limit cycles over which cortisol and ACTH oscillate with an ultradian (hourly) rhythm. Of the two distinct oscillating states, the one with lower averaged cortisol level was characterized as a diseased state and the one with higher cortisol level was associated with the normal state. In previous chapter, all parameters were fixed except for the one representing the net synaptic input experienced by the PVN neurons.

In reality, many of parameters may vary due to aging [GM14], life experience [DRM14b], gender differences [SSW01,UCO06], the use of medication [SSH08], and especially in response to injuries. For example, selective serotonin reuptake inhibitor (SSRI) treatment was shown to increase hippocampus volume [TDD14]. This may in turn modulate the tonic inhibition exerted by the hippocampus on the PVN and subsequently change the baseline synaptic input to CRH neurons in the PVN. On the other hand, traumatic brain injury (TBI) can produce diffuse axonal injuries (DAI) [SSL14] that can affect the synaptic strength or activation pattern of the hypothalamus [MSS02]. Recent studies on the influence of maternal HPA function in neonatal rats have suggested that early life experience can have long-lasting impacts on responsivity of HPA axis activation [DRM14b]. Finally, the strength of the negative feedback of cortisol in the pituitary is hypothesized to be enhanced under PTSD [Yeh02]. These examples are only a few of many conditions that may be associated with anatomical/physiological changes that can be interpreted, and thus incorporated, as alterations in the parameters of our model [KDC16].

Here, we briefly analyze the nullcline structure of the new model as a function of parameters and analyze the conditions under which normal-diseased bistability arises, whether or not stress-induced transitions are possible between the bistable states, and whether or

not the experimentally observed ultradian oscillations can be reproduced. We also systematically investigate how the dynamics depend on relevant parameters. Understanding how changes in parameters affect transient and long-term behavior of the HPA axis could guide the diagnosis and therapeutic strategies. We specifically include perturbations that represent existing pharmacological challenge tests used to assess HPA axis function.

For example, dexamethasone (DEX) has been used as an exogenous steroid that suppresses ACTH release in the pituitary. DEX suppression tests have shown that the relative decrease in cortisol is greater in PTSD patients than those in a control group. The current viewpoint is that the greater decrease in cortisol seen in PTSD subjects is due to an enhanced negative feedback of cortisol. Within a mathematical framework, this effect would typically be modeled by changing the physiological parameters describing the negative feedback. Our model allows for a novel mechanism: cortisol suppression may be due to transitions between bistable steady states without necessarily invoking parameter changes.

Moreover, we demonstrate how our mathematical analysis can help address previously unresolved observations of challenge experiments. ACTH stimulation tests performed to assess adrenal sensitivity in PTSD subjects showed slightly increased cortisol response to ACTH administration among PTSD subjects [RDP09]. This observation contradicts the authors' speculation of decreased adrenal sensitivity in PTSD subjects. We show that this experimental result is in fact consistent with the decreased adrenal sensitivity hypothesis and emphasize that the interplay between all components of the HPA axis must be taken into account to fully understand its overall dynamics.

Finally, we investigate how transitions between the normal and diseased states may be induced within our model. The synaptic input of the PVN is varied over time with different duration and magnitude to understand how *stress-driven transitions* between normal and diseased states can arise when a two-stage negative feedback (of cortisol on CRH) mechanism is incorporated. The possibility of such transitions lead to a number of novel features in the overall system. Within our model, prolonged stress-induced secretion of CRH can trigger transitions between normal and diseased states, suggesting a possible mechanism leading to the emergence of a low cortisol state after a traumatic experience. In this picture, disruptions

to the HPA axis could be alleviated by externally controllable inputs that lead to transitions between the bistable states, rather than by permanently altering specific physiological parameters.

Our model provides an alternative hypothesis on the origin of the lowered cortisol levels of PTSD patients, in which the onset of the disease is described as a transition from one basin of attraction to another. However, the hypothesis does not necessarily exclude the current view in which the dysregulated hormone dynamics is attributed to change of parameters of the system. To further validate our model and its implications, we propose a novel challenge test that could further assess and discriminate the two views.

3.2 Parameters and long-term dynamics

Our nondimensionalized model of the HPA axis based on the interactions shown in Fig. 3.1 consists of a system of delay differential equations as follows

$$\frac{\mathrm{d}c_\mathrm{s}}{\mathrm{d}t} = \frac{1}{t_c}(\underbrace{(\bar{c}_\infty + e^{-bo})}_{c_\infty(o)} - c_\mathrm{s}), \tag{3.1}$$

$$\frac{\mathrm{d}c}{\mathrm{d}t} = q_0 I(t) \underbrace{(1 - e^{-kc_\mathrm{s}})}_{h(c_\mathrm{s})} + \underbrace{g_{\mathrm{c,max}} \frac{(q_1 c)^n}{1 + (q_1 c)^n}}_{g_c(c)} - q_2 c, \tag{3.2}$$

$$\frac{\mathrm{d}a}{\mathrm{d}t} = c \underbrace{\frac{1}{1 + p_2(or)}}_{f_a(or)} - p_3 a, \tag{3.3}$$

$$\frac{\mathrm{d}r}{\mathrm{d}t} = \underbrace{\frac{(or)^2}{p_4 + (or)^2} + p_5}_{g_r(or)} - p_6 r, \tag{3.4}$$

$$\frac{\mathrm{d}o}{\mathrm{d}t} = a(t - t_\mathrm{d}) - o, \tag{3.5}$$

where c_s represents the amount of *stored* CRH at the axonal terminal of CRH secreting neurons in the PVN, c is the level of circulating CRH, a defines the level of circulating

ACTH, r describes the level of available glucocorticoid receptor in the anterior pituitary, and o is the level of circulating cortisol. In Eqs. 3.3 and 3.4, the cortisol-receptor complex is assumed to form and dissociate under fast dynamics and this level will be approximated as that of steady-state by the product $o \times r$. All parameters are listed in Table 3.1.

The introduction of c_s is the most distinctive feature of our model in comparison to others [GAG07, WTL10, AVO13b, SRD12] and allows us to more realistically model aspects of CRH dynamics that occur on different timescales. The two variables, c_s and c, distinguish the two stages of the CRH secretion process: (i) the "slow" synthesis and packaging process of CRH peptides as regulated by cortisol and (ii) the "fast" release process of CRH into the median eminence governed by synaptic activities and nongenomic effects of cortisol. The constant t_c reflects the slow timescale (minutes to hours) over which the amount of stored CRH, c_s, relaxes towards a target value $c_\infty(o)$ relative to the timescale of CRH release (milliseconds). The target value $c_\infty(o)$ is set by circulating cortisol levels $o(t)$ and embodies its negative feedback on CRH synthesis.

The two state variables, c_s and c, are coupled by Eq. 3.2 through a saturating and monotonically increasing function $h(c_\mathrm{s}) = 1 - e^{-kc_\mathrm{s}}$ so that the average release rate of CRH increases with more stored CRH available. Self-upregulation of CRH release by the hypothalamic PVN neurons was included in our previous model [KDC16] and was based on an experiment [OCM85] that showed that when CRH is injected into the third ventricle, PVN neurons increase their rate of CRH release into the median eminence. Thus, this experiment indicates self-upregulation only if the CRH released in the median eminence directly and immediately increases the CRH level in the cerebrospinal fluid (CSF) filling the third ventricle. This is certainly a plausible mechanism. Yet, since a direct connection between the two pools of CRH is not yet well established, we improve our model by considering another relevant source of CRH activity.

Other measurements [GC98] have demonstrated that CRH is also produced and secreted by the pituitary itself and that ACTH secretion in the anterior pituitary is upregulated in an auto/paracrine fashion by CRH secretion. We correspondingly revise the model presented in [KDC16] and in Eq. 3.2 of the current work include both CRH secretion due to the

stimulation of the PVN neurons, as modulated by the synaptic input $I(t)$ and the amount of stored CRH c_s, and CRH secretion due to the auto/paracrine activity of the anterior pituitary, as described by the increasing Hill-type function $g_c(c)$. Its amplitude $g_{\mathrm{c,max}}$ can be estimated by isolating the self-upregulated CRH activity of the pituitary [GC98]. Together with the decaying term, our new Eq. 3.2 describes the time rate of change of the total CRH concentration that can influence the anterior pituitary.

To include changes in synaptic input under stress, $I(t)$ is modeled as a time-dependent parameter $I(t) = I_0 + I_{\mathrm{ext}}(t)$, where I_0 is the minimum basal input level and $I_{\mathrm{ext}}(t)$ is the increase in the synaptic input induced by external stress.

The concentrations of ACTH a, cortisol in circulation o and the availability of glucocorticoid receptor GR in the pituitary r obey Eqs. 3.3,3.4 and 3.5, respectively, and comprise the pituitary-adrenal (PA) subsystem, in which c can be viewed as a control parameter. The nonlinear multistate dynamics are defined by the decreasing and saturating regulation terms $f_a(or)$ and $g_r(or)$, respectively. The characteristic timescale constant t_d is normalized by the decay rate of cortisol and is proportional to the time required for cortisol synthesis and release by the adrenal cortex after stimulation by ACTH. More details of the model, its dimensional form, and the choice of the functional forms used in Eqs. 3.1-3.5 can be found in Appendix 3.7.1 and in [KDC16]. A comprehensive list of all parameters and their descriptions is included in Table 3.1.

[WTL10] showed that the PA subsystem (Eqs. 3.3-3.5) exhibits a limit cycle for a range of fixed time delay, t_{d}. For concreteness, we consider a time delay of 15 minutes ($t_{\mathrm{d}} = 1.44$) for the rest of this paper. Moreover, the amplitude and the frequency of the limit cycle was shown to depend continuously on c, so that the limiting behavior of the PA subsystem could be unequivocally determined by the value of c. The separation of the two timescales – the faster timescale of the (a, r, o) limit cycle in the PA subsystem and the slower timescale governing the CRH synthesis process – allows us to study the dynamics of the entire system (Eqs. 3.1-3.5) by confining our analysis to the reduced system on the (c_{s}, c)-phase plane. This means that the long-term behavior of the entire system can be characterized by the structures of the nullclines of c_{s} and c projected onto the (c_{s}, c)-plane.

In particular, for certain sets of parameters, the nullcline structure exhibits bistable fixed points on the (c_s, c)-plane that can be characterized as the diseased and normal modes of the PA subsystem, each marked by ultradian oscillations and distinct mean cortisol levels. None of the earlier models [SKO00, SJB06, GAG07, WTL10, AVO13b, SRD12, GTO14, BO17] has captured both multistability and endogenous ultradian oscillations. More details on bifurcation and fast/slow analysis of the previous models can be found in [KDC16] and [Ber15].

There is no consensus on which mathematical model is mechanistically the most accurate. [HRW15] selected five pulications [VAO11,SRD12,AVO13b,JSC05,CHF09] to compared model predictions with cortisol and ACTH levels obtained from 17 healthy individuals. Measured ACTH levels were substituted into the equation for cortisol for each of the models, and cortisol data was generated. Later, the role of cortisol and ACTH was reversed: measured cortisol levels were used to numerically determine ACTH. Simulated data and actual measurements were then compared.

None of the five models analyzed provided good fit with data: the best overall model by [AVO13b] still yielded a difference of an order of magnitude between simulations and data. It also did not exhibit ultradian oscillations. Attempts at better calibrating the model for a more accurate description of the circadian rhythm yielded some improvement, with the mean percentage error decreasing from 94% to 66%. It is important to note that when computing the goodness of fit on the data of 17 subjects, parameters were fixed at the original values provided by the authors. Individual differences and/or variations in environments were not taken into account. These attempts at matching models with actual data show how challenging the task actually is. Many variables must be taken into account, including personalized parameter sets, circadian and ultradian rhythms, external inputs, and other factors, some of which may still be unidentified.

The focus of our work is not to exactly match data to our model, but rather to provide a mechanistic framework to better understand the interplay between various components of the HPA axis and its overall qualitative behaviors. Our goal is to gain insight on how variations in parameters may affect the HPA equilibrium for each individual, and how transitions may

be induced between multiple equilibria if they exist. Moreover, truly validating our model would require extensive data measured both before and after exposure to trauma. Such data do not exist to best of our knowledge, and we hope that our work could motivate new, specific measurements that may yield a complete picture of the HPA axis and its dynamics.

In the following sections we outline the analysis of the present model described by Eqs. 3.1-3.5.

3.2.1 Parameter dependencies

In this section, we investigate how the model (Eqs. 3.1-3.5) behaves as its parameters are varied. This is important since some of the ones used in previous studies [WTL10, KDC16] were estimated from insufficient data or arbitrarily selected. We will first examine the robustness of the long-term behavior of our model to changes in individual parameters. Since the long-term behavior of the model can be characterized by the nullcline structures of Eqs. 3.1-3.5 projected onto the (c_s, c)-plane, in the following subsections we will study how parameter changes affect the c_s- and c-nullclines. Descriptions of each parameter and their effects on the nullclines are listed in Table 3.1.

3.2.2 Nullcline analysis: c-nullcline

The c-nullcline is defined as the set of (c_s, c) that satisfies the following relation (obtained by setting Eq. 3.2 equal to zero):

$$0 = q_0 I h(c_s) + g_c(c) - q_2 c, \tag{3.6}$$

where

$$h(c_s) = 1 - e^{-k c_s} \qquad \text{and} \qquad g_c(c) = \frac{g_{c,\max}(q_1 c)^n}{1 + (q_1 c)^n}. \tag{3.7}$$

There are a total of seven parameters in the constraint defining the c-nullcline in Eq. 3.6: $q_0, q_1, q_2, I, g_{c,\max}, n$, and k. Our first approach is to study how time-dependent changes in

Table 3.1: Parameters and their effects on nullcline structure

Parameter	Description	Effects on nullclines (when increased)
q_0	maximum release rate of CRH in basal state	an upward shift of the upper branch and a leftward shift of both knees of the c-nullcline.
q_1	circulating CRH for half-maximum self-upregulation	an upward shift of the upper branch and a leftward shift of both knees of the c-nullcline.
q_2	ratio of CRH and cortisol decay rates	a downward shift of the upper branch and a rightward shift of both knees of the c-nullcline.
$g_{\mathrm{c,max}}$	maximum auto/paracrine effect of CRH in the pituitary	a rightward shift of the lower and upper knee of the c-nullcline and a upward shift of the upper branch.
n	Hill coefficient of $g_c(c)$ describing the self-upregulation of CRH	a leftward shift of the left knee and a rightward shift of the right knee of the c-nullcline
k	relates stored CRH to CRH release rate	a leftward shift of the middle branch of the c-nullcline and an upward shift of the lower branch of the c-nullcline
b	relates cortisol to stored CRH level	a leftward shift of the middle branch of the c_{s}-nullcline
p_2	(or)-complex level for half-maximum negative feedback	a rightward shift and elongation of the oscillatory regime of the c_{s}-nullcline.
p_3	ratio of ACTH and cortisol decay rates	a rightward shift and elongation of the oscillatory regime of the c_{s}-nullcline.
p_4	(or)-complex level for half-maximum positive feedback on r production	elongation of the oscillatory branch of the c_{s}-nullcline.
p_5	basal GR production rate by pituitary	shortening of the oscillatory branch of the c_{s}-nullcline.
p_6	ratio of GR and cortisol decay rates	a rightward shift and shortening of the oscillatory branch of the c_{s}-nullcline.
t_{d}	delay in the adrenal cortex in response to ACTH	elongation of the oscillatory branch of the c_{s}-nullcline [WTL10].

the synaptic input I affect the dynamics of the system. Since I and q_0 form a product, changes in I and q_0 are equivalent; therefore we only consider changes q_0, q_1, q_2, μ_c, n, and k. In Fig. 3.2 we vary one parameter at a time while all others are kept fixed at nondimensional reference values $q_0 = 28.0, q_1 = 0.04, q_2 = 1.8, I = 1, g_{\mathrm{c,max}} = 42, n = 5$ and $k = 2.83$, as detailed in [KDC16] and in Appendix 3.7.1.

Increasing q_0 narrows and shifts the bistable region in the (c_s, c)-plane towards lower values of c_s, while extending the nullclines to larger values of c (Fig. 3.2A). When q_1 is increased, the bistable region also narrows and shifts toward lower c_s values, but the range of the corresponding c values on the nullclines do not change significantly (Fig. 3.2B). Increasing q_2 (Fig. 3.2C) appears to have the opposite effect: the bistable region is widened and the range of corresponding c values decreases. This behavior is expected since it can be shown that the roots of Eq. 3.6 depend on the ratio q_0/q_2. When $g_{c,max}$ is increased, the upper branch of c-nullcline shifts towards higher values of c and the bistable regime moves towards the lower c_s values (Fig. 3.2D). The Hill coefficient n of $g_c(c)$ (in Eq. 3.2) also exhibits a saddle-node bifurcation at a critical point $4 < n^* < 5$ (Fig. 3.2E). Once bistability emerges, the upper and lower knees of the c-nullcline shift towards lower and higher values of c_s as n increases. The bistable regime in c_s is elongated as the two knees shift in the opposite direction from each other. Lastly, increasing k (Fig. 3.2E) shifts the bistable region towards lower c_s values without appreciably changing the values of c over which bistability exists.

By understanding how each parameter affects the c-nullcline, we can identify and predict which parameter changes disrupt HPA axis function. For example, we predict that increasing k will make the lower cortisol state less accessible since the range of c_s covered by the lower branch of the c-nullcline narrows as k increases. Furthermore, we can use our results to interpret experimental reports of perturbations to the HPA axis. Any physiological disruption observed or associated with changes in long-term HPA function can be mapped to relevant parameter changes in our model.

3.2.3 Nullcline analysis: c_s-nullcline

The c_s-nullcline is defined as the set of (c_s, c) that satisfies the relation (obtained by setting Eq. 3.1 equal to zero):

$$0 = c_\infty(o) - c_s. \tag{3.8}$$

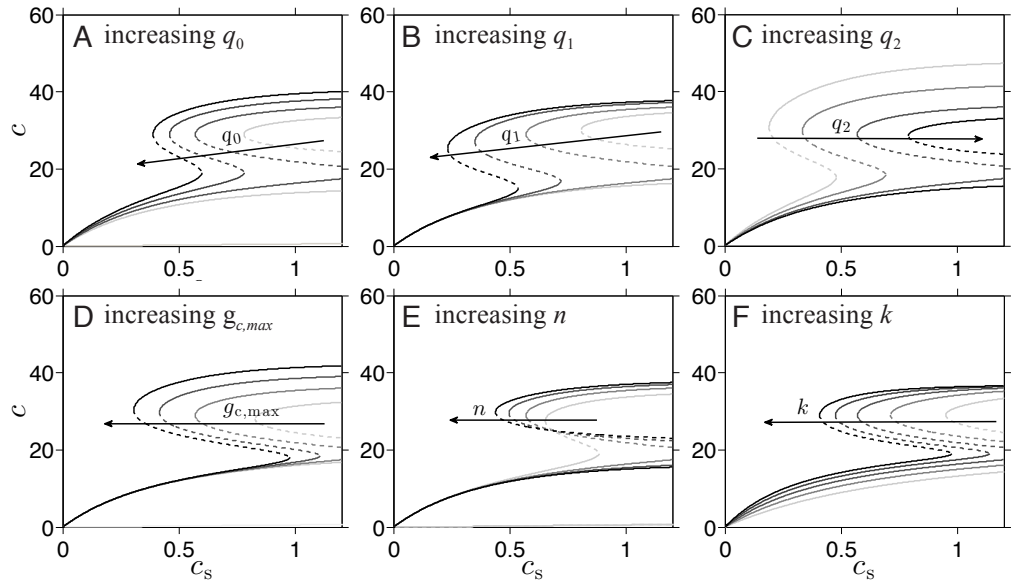

Figure 3.2: **Effects of changing parameters on the c-nullcline.** One of the nondimensionalized six parameters that affect the c-nullcline is varied over a range of values (from 80% to 120% of their reference values) and the corresponding c-nullclines are plotted. The dashed segment of the nullcline indicates the unstable steady states. Darker color indicates a greater value of the corresponding parameter. When not varied, parameters are set to the reference values $q_0 = 28.0 (I = 1), q_1 = 0.04, q_2 = 1.8, g_{\mathrm{c,max}} = 42, n = 6$ and $k = 2.83$. (A) q_0 is varied from 22.4 to 33.6. (B) q_1 is varied from 0.032 to 0.48, (C) q_2 is varied from 1.44 to 2.16.(D) $g_{\mathrm{c,max}}$ is varied from 33.6 to 50.4. (E) n is varied from 1 to 8. A saddle-node bifurcation occurs between $n = 4$ and $n = 5$. (F) k is varied from 2.26 to 3.40.

Eq. 3.8 does not directly relate c_{s} to c but couples the two through o, which exhibits oscillatory behavior for physiological values of c. To directly relate c to c_{s}, we average o over one full cycle of its oscillation, the values of which are fully determined by c through the PA subsystem as illustrated in the previous section. The nullcline relation (Eq. 3.8) can thus be approximated and rewritten as

$$0 = \langle c_\infty(c) \rangle - c_{\mathrm{s}}, \tag{3.9}$$

where

$$\langle c_\infty(c)\rangle \equiv \int_0^{2\pi} c_\infty(o^*(\theta;c))\frac{\mathrm{d}\theta}{2\pi} = \bar{c}_\infty + \int_0^{2\pi} e^{-bo^*(\theta;c)}\frac{\mathrm{d}\theta}{2\pi}. \tag{3.10}$$

The term $o^*(\theta;c)$ represents the trajectory of $o(t)$ with phase θ along the limit cycle of the PA subsystem defined by a given c. Therefore the c_s-nullcline depends on the dynamics of the PA subsystem (Eqs. 3.3-3.4) and its parameters b, p_2, p_3, p_4, p_5, and p_6. We can now vary one of these parameters while fixing the others to [KDC16, WTL10]: $b = 0.6, p_2 = 15, p_3 = 7.2, p_4 = 0.05, p_5 = 0.11$, and $p_6 = 2.9$ as illustrated in Fig. 3.3. The part of the c_s-nullcline that is approximated by averaging $c_\infty(o)$ over a full period of the limit cycle is indicated by dashed segments.

Fig. 3.3A shows that increasing b shifts the c_s-nullcline to the left in the (c_s, c)-plane. This shift towards lower values of stored CRH, c_s, is expected since higher b corresponds to stronger cortisol-induced suppression of the CRH synthesis. On the other hand, as shown in Figs. 3.3B and C, increasing p_2 or p_3 lengthens the oscillatory regime of the c_s-nullcline and shifts it towards the right. Increasing p_4 elongates the oscillatory regime while increasing p_5 shrinks it. In both cases, a relatively small horizontal shift of the c_s-nullcline is observed (Figs. 3.3D and E). Finally, increasing p_6 increases the upper limit of c of the oscillatory branch and shifts it to smaller values of c_s, as shown in Fig. 3.3F.

The long-term behavior of the HPA axis to corresponding parameter changes are now mapped out. We can use these results to predict what long-term changes would emerge under various pathological conditions, as illustrated in the next section. Note that many physiological disruptions may alter more than one parameter and that changing multiple parameters simultaneously can lead to a qualitatively different deformation of the c_s- and c-nullcline. The effect of multiple parameter changes is beyond the scope of this paper. However, we can easily extend our analysis to address the issue by altering all the parameters of interest when generating the nullclines.

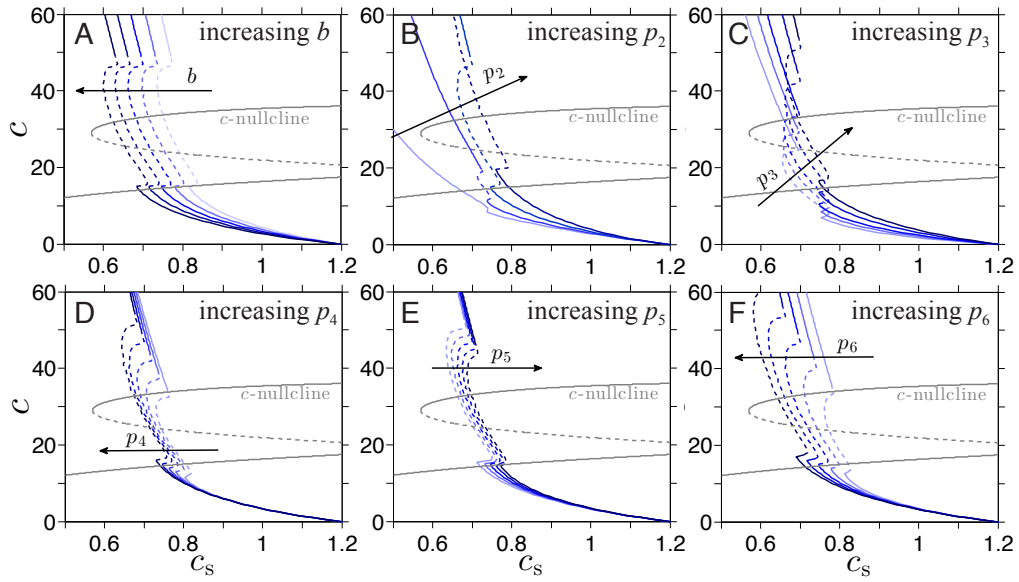

Figure 3.3: **Effect of changing parameters on c_s-nullcline** One of the six parameters that affect the c_s-nullcline is varied over a range of values (from 80% to 120% of their reference values) and corresponding c_s-nullclines are plotted. The dashed segment of the nullcline indicates the time-averaged value of c_s over the limit cycle corresponding to the value of c (Eqs. 3.9 and 3.10). Darker color indicates a greater value of the corresponding parameter. When not varied, these parameters are set at the reference values: $t_d = 1.44, b = 0.6, p_2 = 15, p_3 = 7.2, p_4 = 0.05, p_5 = 0.11$, and $p_6 = 2.9$. (A) b is varied from 0.48 to 0.71 (B) p_2 is varied from 1.5 to 27, (C) p_3 is varied from 3.6 to 7.92.(D) p_4 is varied from 0.04 to 0.06. (E) p_5 is varied from 0.09 to 0.14. (F) p_6 is varied from 2.3 to 3.8.

3.3 Pharmacological Challenge Tests

In the previous section, we have shown that the long-term dynamics of the system are determined by the crossing of the c- and c_s-nullclines defined by Eqs. 3.6 and 3.9. Thus, we only need to understand how the intersections change upon varying model parameters to study how alterations in parameters will affect the system. Having studied how the HPA axis responds to parameter changes, we use our model to better understand a series of pharmacological challenge tests used to assess HPA function in PTSD. We re-examine some current interpretations by comparing them to our predictions and uncover unforeseen intricacies underlying the response of the HPA axis. Our analysis allows us to present novel, alternative interpretations of the observed experimental data. Indeed, this is one the main

virtues of mathematical models as they allow to probe complex, non-linear dependencies and to craft non-trivial predictions. Although the model presented in Eqs. 3.1-3.5 can be used to study any condition or experimental protocol that involves parameter alterations in the HPA axis, we will focus, in this paper, on experiments related to PTSD.

3.3.1 Dexamethasone suppression test (DST)

The dexamethasone suppression test (DST) is a pharmacological challenge test typically used to identify the cause of abnormal cortisol levels observed in diseases such as Cushing syndrome. In DST, a cortisol analogue (dexamethasone, DEX) is used to probe the negative feedback of cortisol on ACTH secretion in the pituitary. In particular, some studies have used DST to test whether lower basal cortisol levels in PTSD result from an enhanced negative feedback of cortisol on pituitary activity. DEX is a synthetic glucocorticoid compound that suppresses ACTH secretion, and subsequently cortisol secretion, when it binds to glucocorticoid receptors (GR) in the pituitary [CKK00]. In DEX suppression studies, cortisol levels are measured pre-DEX and post-DEX and used to calculate the percent suppression of cortisol, defined as

$$s = \frac{\text{pre-DEX cortisol - post-DEX cortisol}}{\text{pre-DEX cortisol}} \times 100. \tag{3.11}$$

The mean percent suppression of cortisol s was shown to be greater in PTSD subjects ($s = 83\%$) than in the control group without PTSD ($s = 74\%$) [YGG04]. The difference in s was interpreted as due to heightened sensitivity of the negative feedback of cortisol in the pituitary [SYK97, YGY04b]. This interpretation implicitly assumes that the suppression effect of cortisol (and dexamethasone) is directly proportional to its concentration. The linear relationship is convenient but neglects the contribution of other components of the system that can interact with the suppression activity to yield a more complex, possibly non-linear relationship. We use our mathematical model to examine how exogenous DST affects the dynamics of the HPA axis. We model DEX administration by replacing $o(t)$ with

$o(t) + o_{\text{exo}}(t)$ in Eqs. 3.3 and 3.4 to yield

$$\frac{\mathrm{d}c_{\text{s}}}{\mathrm{d}t} = \frac{c_{\infty}(o) - c_{\text{s}}}{t_c}, \tag{3.12}$$

$$\frac{\mathrm{d}c}{\mathrm{d}t} = q_0 I(t) h(c_{\text{s}}) + g_c(c) - q_2 c, , \tag{3.13}$$

$$\frac{\mathrm{d}a}{\mathrm{d}t} = \frac{c}{1 + p_2((o + o_{\text{exo}}(t))r)} - p_3 a, \tag{3.14}$$

$$\frac{\mathrm{d}r}{\mathrm{d}t} = \frac{((o + o_{\text{exo}}(t))r)^2}{p_4 + ((o + o_{\text{exo}}(t))r)^2} + p_5 - p_6 r, \tag{3.15}$$

$$\frac{\mathrm{d}o}{\mathrm{d}t} = a(t - t_{\text{d}}) - o, . \tag{3.16}$$

Here $o_{\text{exo}}(t)$ denotes the concentration of circulating DEX converted to equivalents in cortisol concentrations based on the relative potency of DEX from [Ste97]. Note that we do not include DEX in Eq. 3.12 since it was shown that DEX retention is much lower in the brain [SKR05] and that DEX does not affect GR in brain tissue [CKK00]. In a typical DEX challenge test, cortisol levels are measured in the morning (8 am) to obtain basal pre-DEX cortisol levels. DEX is then orally administered, typically at night (11 pm), and post-DEX cortisol levels are measured again the following morning (8 am). We assume circulating DEX levels follow a simple pharmacokinetic law

$$\frac{\mathrm{d}o_{\text{exo}}}{\mathrm{d}t} = \Pi_{\text{o}}(t) - p_7 o_{\text{exo}}, \tag{3.17}$$

where p_7 represents the decay rate of DEX relative to the decay rate of cortisol. For simplicity, we use a rectangle function for $\Pi_{\text{o}}(t)$. The width (30min) of $\Pi_{\text{o}}(t)$ is estimated based on the at peak concentration of DEX [PRS98] and the height (2 in nondimensionalized unit of o) is set to match the dosage used in the experiment [YGG04]. Based on the half-life of DEX ($\sim$ 240min [PRS98]) and cortisol ($\sim$ 7.2min [LWA08]), we set $p_7 = 0.03$.

The numerical solutions of cortisol levels during DEX suppression test within our model

(Eqs. 3.12-3.16) are shown in Figs. 3.4A and B for normal and PTSD subjects, respectively. The parameters used in both figures are identical: normal and PTSD subjects are characterized solely by which one of the two stable states they initially reside in (c_s, c) space. Initial (c_s, c) values are plotted in Fig. 3.4C and labeled N_{pre} and D_{pre} for normal and PTSD subjects. We take the average of o over a full cycle of oscillation to estimate pre-DEX cortisol values $\langle s \rangle_N = 63\%$ and $\langle s \rangle_D = 73\%$ for normal and PTSD subjects. These predicted values are in qualitative agreement with the experimentally reported percent suppression $s_N = 74\%$ and $s_D = 83\%$ for normal and PTSD subjects [YGG04]. Due to the oscillatory behavior of cortisol in the basal sate, the percent suppression depends on the phase of the oscillation at the time of pre-DEX measurement. For example, if the pre-DEX measurement time is set near the peak of the oscillations, our model predicts $s_N = 76\%$ for normal subjects and $s_D = 81\%$ for PTSD subjects. For a more accurate comparison between our predictions and data, the *timing* of DEX administration with respect to the phase of the oscillating cortisol levels should be carefully controlled in experiments.

To understand the behavior of our HPA axis model under DEX administration, we observe how $o_{\text{exo}}(t)$ affects the (c_s, c)-nullcline structure. Since $o_{\text{exo}}(t)$ contributes only to the PA subsystem (Eqs. 3.3-3.5), it only affects the c_s-nullcline. The latter is shown in Fig. 3.4C (dark blue) near the time of measurement, 9 hrs from DEX administration. Normal and diseased states initially resting at the intersection of the c_s- and c-nullclines slowly evolve towards the shifted intersections (labeled N_{post} and D_{post} for normal and PTSD subjects, respectively) defined by the new c_s-nullcline under DEX administration.

We use the decrease in $f_a(or) = 1/(1 + p_2(or))$ in Eq. 3.3 due to DEX administration as a measure of suppression of pituitary activity under the challenge test. Recall that $f_a(or)$ is a modulating factor of the ACTH production rate and represents the negative feedback of the cortisol on the pituitary. For the pre-DEX value of $f_a(or)$, we take the period-averaged value of or, denoted $\langle or \rangle_N$ and $\langle or \rangle_D$ for normal and diseased initial states, respectively. Note that the new shifted c_s-nullcline under DEX administration is not associated with oscillatory behavior and the new intersections represent non-oscillating equilibria. The cortisol levels depicted in Figs. 3.4A and B confirm that cortisol oscillations cease under DEX suppression,

which has not yet been experimentally tested. The non-oscillating equilibrium value for o and r are denoted o^*_α and r^*_α, where $\alpha = N, D$ indicate normal and PTSD states. In Fig. 3.4C, pre-DEX values of $f_a(\langle or \rangle_\alpha)$ and post-DEX values of $f_a((o^*_\alpha + o_{\text{exo}})r^*_\alpha)$ are plotted for normal ($\alpha = N$) and PTSD ($\alpha = D$) subjects. The decreases in $f_a(or)$ denoted as $\Delta f_{a,\alpha}$ in Fig. 3.4D indicate that suppression is greater for PTSD subjects than for normal subjects, despite the comparable change in or values. This is because of the form of $f_a(or)$: decreases in $f_a(or)$ due to increases in o are greater for lower initial values of or. In other words, the state with low initial or value will experience greater suppression as o increases to $o + o_{\text{exo}}$ since $f_a(or)$ is convex ($f_a(or)'' > 0$) and decreasing ($f_a(or)' < 0$) for $o \geq 0$ and $r \geq 0$.

Our model provides an additional interpretation of DEX administration results in PTSD patients. The enhanced suppression effect on cortisol may be due to the *intrinsic* dynamics rather than parametric changes; within our model, the negative feedback effect is dependent on the state of the system at the time of DEX administration, which in turn depends on dynamics and history of the system. Thus, increased suppression of cortisol levels in PTSD subjects during DEX administration may simply indicate that PTSD subjects were in the low cortisol state *before* the test, rather than implying that permanent changes had occurred in their system in the course of developing PTSD.

This alternate explanation has a direct implication on how one should design therapeutic protocols for PTSD or other stress-related disorders associated with cortisol disruption. Under the enhanced negative feedback hypothesis, therapies or medications would attempt to lower the pituitary sensitivity to cortisol to bring it back to normal levels. Our model shows that this "straightforward" approach would fail and suggests that therapies should instead focus on devising appropriate perturbations to the system. For example applying externally controlled inputs $I(t)$, could induce transitions back to the normal stable state as shown in [KDC16]. This framework is consistent with current recommendations for treatment of stress disorders via exposure therapy and cognitive-behavioral techniques in which an individual is re-exposed to trauma or stress in a controlled way.

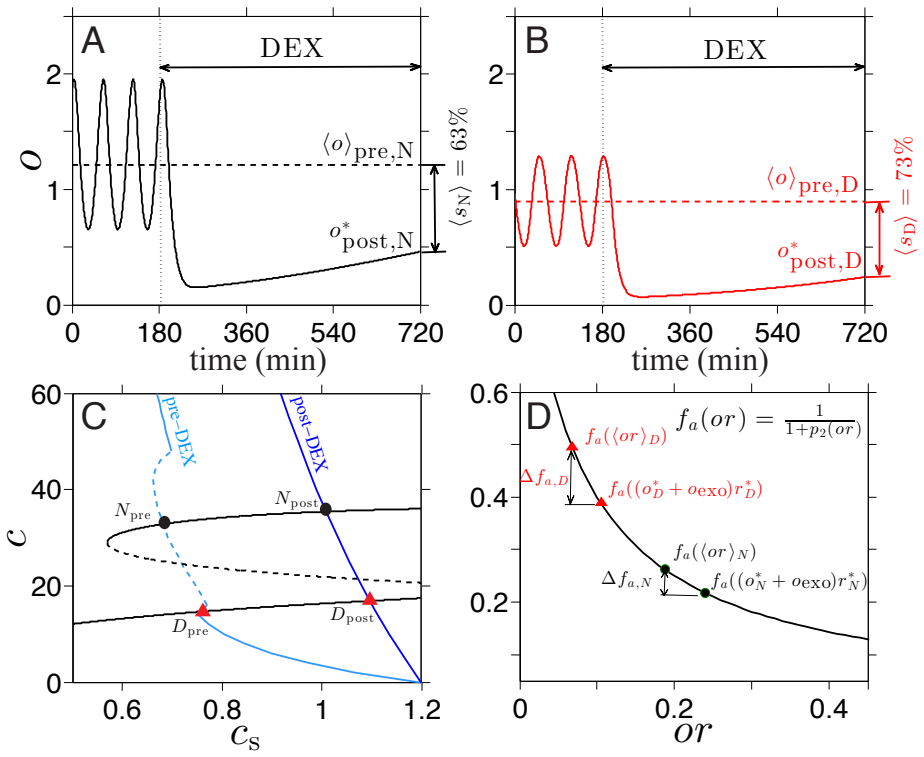

Figure 3.4: **Numerical simulation of DEX challenge test on normal and PTSD subjects.** (A) Numerical simulation of cortisol response in a "normal" subject during DEX suppression test. The average percent suppression of cortisol in this scenario is $\langle s_N\rangle = 63\%$ (B) Numerical simulation of cortisol response in a PTSD subject during DEX suppression test. Here, the average percent suppression of cortisol is $\langle s_D\rangle = 73\%$, significantly greater than that of a normal subject. (C) Intersections of the c-nullcline with pre-DEX (light blue) and post-DEX (blue) c_{s}-nullclines. Normal and PTSD subjects are represented as black circles and red triangles, respectively. (D) The values of $f_a(or)$ pre- and post-DEX treatment are plotted for normal (black circles) and PTSD states (red triangles)

3.3.2 ACTH stimulation test

In this section, we consider the ACTH stimulation test typically used to diagnose conditions associated with insufficient adrenal activity. Cortisol levels are measured after the administration of cosyntropin, a synthetic derivative of ACTH. Exogenous ACTH stimulates cortisol secretion to the same extent of endogenous ACTH and thus effectively increases $a(t)$ in our model. As in the analysis of the DEX suppression test, we can model cosyntropin administration by replacing $a(t)$ with $a(t) + a_{\mathrm{exo}}(t)$, where $a_{\mathrm{exo}}(t)$ denotes the concentration of the

cosyntropin in circulation.

In a previous study [RDP09], an ACTH stimulation test was administered to PTSD and normal subjects to measure potential differences adrenal gland response between the two groups. It was hypothesized that a bolus of cosyntropin would lead to a *smaller* pulse of cortisol secretion in PTSD patients due to hypo-reactivity of their adrenal glands. Adrenal hypo-reactivity would also suggest lower baseline cortisol levels, consistent with a number of observations [YGG04, YGY04b]. Surprisingly, the main experimental finding was that cortisol response to cosyntropin *was not* significantly altered in PTSD subjects. Moreover, the baseline cortisol levels observed under PTSD were actually slightly higher than normal [RDP09]. It was thus concluded [RDP09] that either adrenal reactivity is not altered in PTSD patients or that potential alterations do not affect HPA dynamics.

This interpretation relies on the intuition that a proportional relationship exists between adrenal reactivity and cortisol response so that upon stimulation, in this case by cosyntropin, any adrenal hypo-reactivity in PTSD subjects would lead to smaller cortisol increases. This picture would be valid if the stimulating activity of ACTH in the adrenal gland were isolated from other ACTH interactions within the HPA axis. However, cortisol suppresses endogenous ACTH secretion in the pituitary, which in turn, indirectly reduces cortisol secretion. In addition, glucocorticoid receptor (GR) concentration is coupled to cortisol through the dependence on or in Eq. 3.4 and thus influences the negative feedback in the pituitary. As a result of these various nonlinear interactions, particularly those embodied by $g_r(or)$ and $f_a(or)$, cortisol response to ACTH stimulation is more complex than a simple proportionality relationship. We now use our model to explore these nonlinear interactions and develop a more nuanced interpretation of the experimental observations.

In particular, we will contrast and compare our results to the above described experimental data and show that indeed, upon taking into consideration the full dynamics of the HPA axis, laboratory observations [RDP09] *may be consistent* with the hypothesis of reduced adrenal reactivity in PTSD subjects, in contrast to the original interpretation. Within our model adrenal gland reactivity to ACTH determines the parameters p_2 and p_4 in Eqs. 3.1-3.5 (refer to Appendix 3.7.1 for details). To model hypo-reactivity we adjust both parameters

to reflect 10% decrease in the adrenal gland reactivity in PTSD subjects. The resulting numerical solutions are plotted in Fig. 3.5A and show that basal cortisol levels are indeed *increased* in the basal state of PTSD subjects, consistent with the baseline cortisol measurements in [RDP09]. This result emphasizes that the simple intuition of a direct relationship between adrenal reactivity and cortisol response is *not accurate.*

To now describe the response of cortisol under an ACTH stimulation test, we modify our model by rewriting Eq. 3.5 as

$$\frac{\mathrm{d}o}{\mathrm{d}t} = a(t - t_{\mathrm{d}}) + a_{\mathrm{exo}}(t - t_{\mathrm{d}}) - o, \tag{3.18}$$

where $a_{\mathrm{exo}}(t)$ denotes the concentration of exogenous cosyntropin in circulation. We model the dynamics of $a_{\mathrm{exo}}(t)$ using a pharmacokinetic description similar to that used for DEX:

$$\frac{\mathrm{d}a_{\mathrm{exo}}}{\mathrm{d}t} = \Pi_a(t) - p_8 a_{\mathrm{exo}}. \tag{3.19}$$

Here p_8 represents the clearance rate of cosyntropin scaled by the clearance rate of cortisol and $\Pi_a(t)$ is a rectangle function. We set $p_8 = 1.7$, based on the half-life of exogenous ACTH (4.1min [MRJ72]). We compare cortisol's response to cosyntropin administered near the nadir of its ultradian oscillation for hypo-reactive and near the peak for normal adrenal glands in Fig. 3.5B. In this case, the response of a hypo-reactive subject is higher than that of a normal subject. To study the dependence of cortisol response on the timing of cosyntropin administration, in Fig. 3.5C we plot the peak levels of cortisol under cosyntropin administration against the phase of the oscillation at which the administration took place. Overall, cortisol response is predicted to be slightly *greater* in normal subjects with the maximum peak response of a hypo-sensitive subject (dashed red in Fig. 3.5C) comparable to the minimum peak response of a normal subject (solid red in Fig. 3.5C). This prediction implies that depending on the phase of the intrinsic oscillation at the time of cosyntropin

administration, the response of a hypo-reactive adrenal gland could be greater than normal. However, the corresponding *mean* cortisol response should be lower if a sufficiently large sample size is used without controlling for the phase of cortisol at the time of cosyntropin administration.

Our model predicts that reduced adrenal reactivity to ACTH will *increase* baseline cortisol levels. This implies that the experimental result reported in [RDP09] may indeed reflect a reduced adrenal reactivity in PTSD subjects, amending previous interpretations. The increase in cortisol response seen among PTSD patients can also vary depending on the timing of cosyntropin administration. For example, the relative increase in cortisol is greatest upon administering cosyntropin during the increasing phase near the nadir of cortisol's intrinsic oscillation as seen in Fig. 3.5C. Note that if experiments on normal and PTSD individuals are not phase-matched, the response of a normal subject may be less than the response of a PTSD subject, as observed from the experiment. Since the sample size used in the experiment was small ($N = 8$ subjects for PTSD and $N = 9$ subjects for control), the increased cortisol response among PTSD subjects may be explained as a confounding effect arising from the timing of ACTH/cosyntropin administration. Phase-matching would be required for a proper interpretation of the measurement.

3.4 Stress-driven Transitions

We now discuss how transitions from a normal to a diseased state can be induced by *positive* (excitatory) external stress of sufficient duration. In Fig. 3.6, we start the system in the normal high-c state.

3.4.1 External stress induces transition from normal to diseased state

Upon stimulation of the CRH neurons through $I_{\text{ext}} > 0$, both CRH and average glucocorticoid levels are increased while the average value of $c_\infty(o(t))$ is decreased since $c_\infty(o)$ is a decreasing function of o. As $c_{\text{s}}(\tau)$ slowly decays towards the decreased target value of $\langle c_\infty(o(c))\rangle$, $h(c_{\text{s}}(\tau))$, and hence $q(c_{\text{s}})$, also decrease. As shown in Fig. 3.6A, much of this

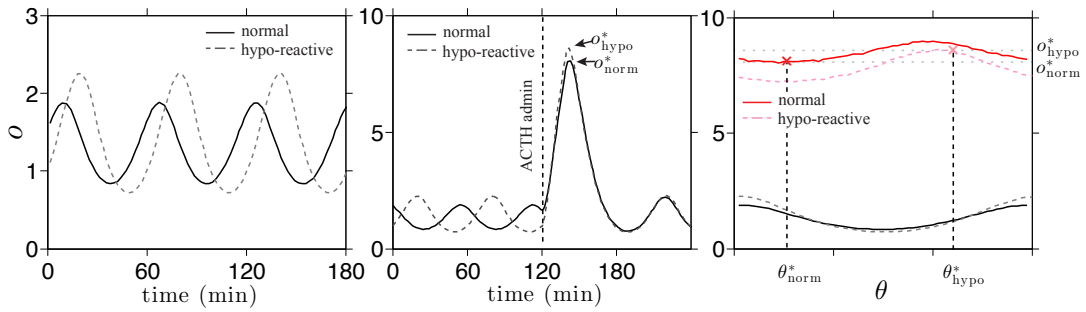

Figure 3.5: **Numerical solutions of ACTH stimulation test.** (A) The oscillating stable state of the system with normal (solid) and hypo-reactive (dashed) adrenal gland sensitivity are plotted. For direct comparison, the nondimensionalized o is scaled by the same factor (the normal adrenal sensitivity) in both cases for a direct comparison. Details of the scaling of the state variables are provided in Appendix 3.7.1. The hypo-reactive subject with p_2 and p_4 adjusted to represent lower adrenal sensitivity exhibited slightly higher basal cortisol levels. (B) Cortisol response to exogenous ACTH administration is plotted for normal (solid) and for hypo-reactive (dashed) adrenal sensitivity. The phase of the oscillation at the time of administration was different in each simulation. (C) The peak cortisol levels reached during exogenous ACTH administration are plotted as a function of the phase of of the intrinsic oscillations at the time of ACTH administration for normal (solid red) and hypo-reactive (dashed red) subject. The phase and the peaks shown in (B) are marked in the plot as an example. The maximum peak cortisol level of the hyposensitive subject and the minimum peak cortisol level of the hypo-reactive subject are both around $o = 8$.

decrease occurs along the high-c stable branch of the c-nullcline. Once the external stress is switched off, q will jump back down by a factor of $1/(1 + I_{\text{ext}})$. If the net decrease in q is sufficient to bring it below the bifurcation value $q_L \approx 64$ at the leftmost point of the upper knee, the system crosses the separatrix and approaches the alternate, diseased state. Thus, the normal-to-diseased transition is more likely to occur if the external stress is maintained long enough to cause a large net decrease in q, which includes the decrease in q incurred during the slow relaxation phase, plus the drop in q associated with cessation of stress. The minimum duration required for normal-to-diseased transition should also depend on the magnitude of I_{ext}. The relation between the stressor magnitude and duration will be illustrated in the Additional Files.

A numerical solution of our model with a 30hr $I_{\text{ext}} = 0.2$ was performed, and the tra-

jectory in (q, c)-space is shown in Fig. 3.6A. The corresponding cortisol level along this trajectory is plotted in Fig. 3.6B, showing that indeed a stable transition to the lower cortisol state occurred shortly after the cessation of stress. In addition to a long-term external

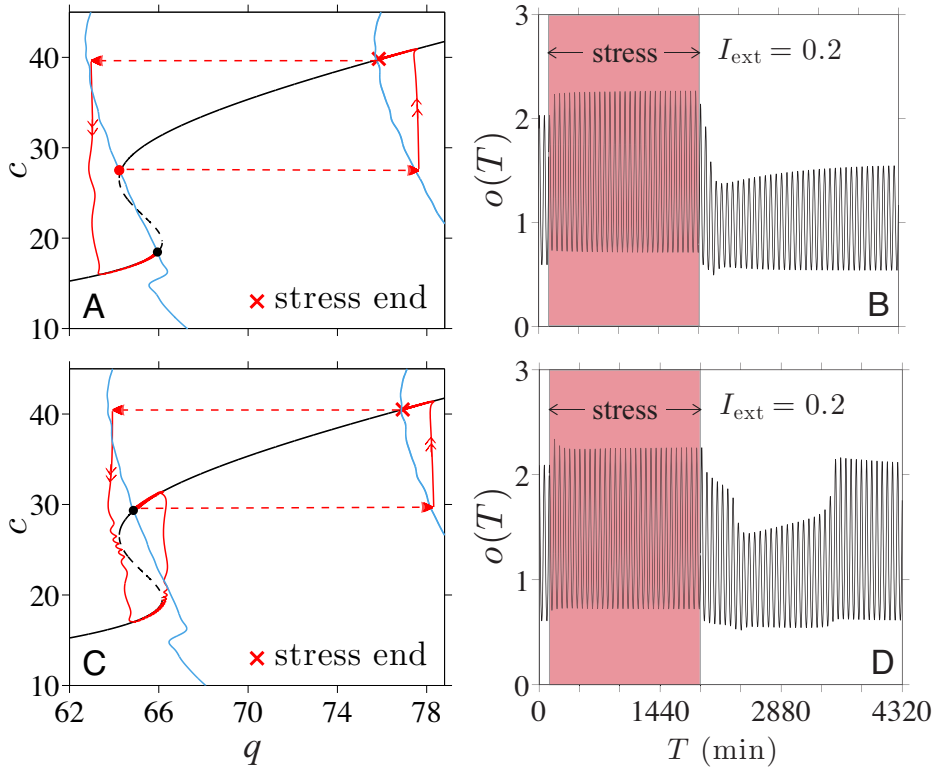

Figure 3.6: **Stress-induced transitions into an oscillating low-cortisol diseased state.** An excitatory external stress $I_{\text{ext}} = 0.2$ is applied for 30hrs. Here, the system reaches the new stable point set by $I = 1.2$ before stress is terminated and the q-nullcline reverts to its original position set by $I = 1$. (A) At intermediate values of $2.5 < k < 2.54$, when two stable state arise, a transition from the normal high-cortisol state into the diseased low-cortisol state can be induced by chronic external stress. (B) Numerical solutions of cortisol level $o(T)$ plotted against the original time variable T shows the transition to the low-cortisol diseased state shortly after cessation of stress. (C) and (D) If $k > k_{\text{R}} = 2.54$, only the normal stable state exists. The system will recover and return to its original normal state after a transient period of low cortisol.

stress, the stable transition to a diseased state requires $2.5 < k < 2.54$ and the existence of two stable points. On the other hand, when $k > k_{\text{R}} = 2.54$, the enhanced CRH release stimulates enough cortisol production to drive the sole long term solution to the stable upper normal branch of the c-nullcline, rendering the HPA system *resistant* to stress-induced

transitions.

The response to chronic stress initially follows the same pattern as described above for the two-stable-state case, as shown in Fig. 3.6C. However, the system will continue to evolve along the lower branch towards the q-nullcline, eventually sliding off the lower branch near the right bifurcation point (indicated in Fig. 2.7 by $(q_{\mathrm{R}}, c_{\mathrm{R}})$) and returning to the single normal equilibrium state. Thus, when k is sufficiently high, the system may experience a transient period of lowered cortisol levels after chronic stress but will eventually recover and return to the normal cortisol state. The corresponding cortisol level shown in Fig. 3.6D shows this recovery at $T \approx 3400$min, which occurs approximately 1500min after the cessation of stress.

3.4.2 Transition to diseased state depends on stress timing

We have shown how transitions between the oscillating normal and diseased states depend on the duration of the external stress I_{ext}. However, whether a transition occurs also depends on the *time* – relative to the phase of the intrinsic ultradian oscillations – at which a fixed-duration external stress is initiated. To illustrate this dependence on phase, we plot in Figs. 3.7A and B two solutions for $o(T)$ obtained with a 250min $I_{\mathrm{ext}} = 0.1$ initiated at different phases of the underlying cortisol oscillation. If stress is initiated during the rising phase of the oscillations, a transition to the low-cortisol diseased state occurs and is completed at approximately $T = 1000$min (Fig. 3.7A,C). If, however, stress is initiated during the falling phase, the transition does not occur and the system returns to the normal stable state (Fig. 3.7B,D). In this case, a longer stress duration would be required to push the trajectory past the low-q separatrix into the diseased state.

As discussed earlier, an increase in period-averaged cortisol level during stress drives a normal-to-diseased state transition. We see that the period-averaged level of cortisol under increased stress is different for stress started at 120min from stress started at 150min. As detailed in the Additional File, the amplitude of the first cortisol peak after the start of stress is significantly lower when the applied stress is started during the falling phase

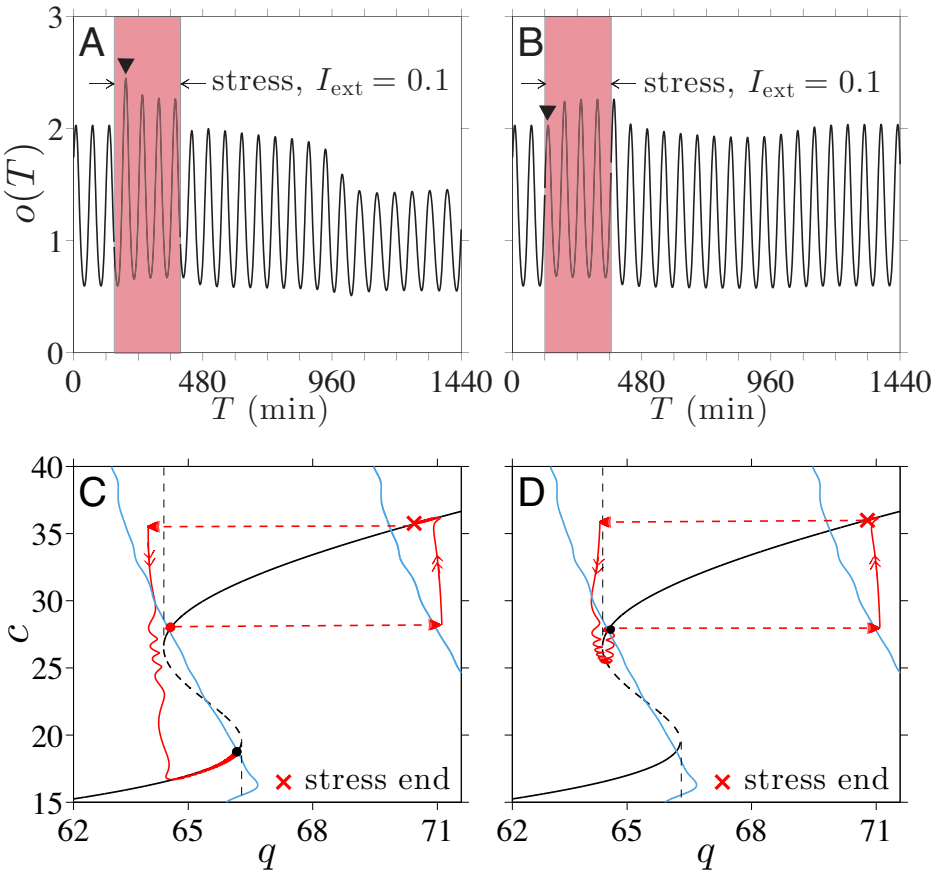

Figure 3.7: **Stress timing and transition to low-cortisol oscillating state.** Cortisol levels in response to $I_{\text{ext}} = 0.1$ applied over 250min. (A) If stress is initiated at $T = 150$min, a transition to the low-cortisol diseased state is triggered. (B) If stress is initiated at $T = 120$min, the system returns to its normal high-cortisol state. Note that the first peak (marked by "▼") during the stress in (A) is higher than the first peak in (B). (C) If stress is initiated at $T = 150$min, stress cessation and the slow relaxation along the c-nullcline during stress are sufficient to bring q just left of the separatrix, inducing the transition. (D) For initiation time $T = 120$min, q remains to the right of the separatrix, precluding the transition.

of the intrinsic cortisol oscillations. The difference between initial responses in $o(t)$ affects the period-averaging in $\langle c_\infty(o)\rangle$ during external stress, ultimately influencing c_{s} and consequently determining whether or not a transition occurs. Note that this phase dependence is appreciable only when stress duration is near the threshold value that brings the system close to the separatrix between normal and diseased basins of attraction. Trajectories that pass near separatrices are sensitive to small changes in the overall negative feedback of cortisol

on CRH synthesis, which depend on the start time of the stress signal.

3.4.3 Stress of intermediate duration can induce "reverse" transitions

We can now use our theory to study how *positive* stressors I_{ext} may be used to induce "reverse" transitions from the diseased to the normal state. Understanding these reverse transitions may be very useful in the context of exposure therapy (ET), where PTSD patients are subjected to stressors in a controlled and safe manner, using for example, computer-simulated "virtual reality exposure." Within our model we can describe ET as external stress ($I_{\text{ext}} > 0$) applied to a system in the stable low-c diseased state. The resulting horizontal shift in q causes the system to move rightward across the separatrix and suggests a transition to the high-c normal state can occur upon termination of stress. As shown in Fig. 3.8A, if stressor of sufficient duration is applied, the trajectory reaches a point above the unstable branch of the c-nullcline upon termination leading to the normal, high-cortisol state (Fig. 3.8B). Since the initial motion is governed by fast flow, the minimum stress duration needed to incite the diseased-to-normal transition is short, on the timescale of minutes. However, if the stressor is applied for too long, a large reduction in q is experienced along the upper stable branch. Cessation of stress might then lower q back into the basin of attraction of the low-cortisol diseased state (Fig. 3.8C). Fig. 3.8D shows the cortisol level transiently increasing to a normal level before reverting back to low levels after approximately 1400min.

Within our dynamical model, stresses need to be of *intermediate* duration in order to induce a stable transition from the diseased to the normal state. The occurrence of a reverse transition may also depend on the phase (relative to the intrinsic oscillations of the fast PA subsystem) over which stress was applied, especially when the stress duration is near its transition thresholds. For a reverse diseased-to-normal transition to occur, the decrease in c_{s} cannot be so large that it brings the trajectory past the left separatrix, as shown in Fig. 3.8C. Therefore, near the maximum duration, stress initiated over the falling phase of cortisol oscillation will be more effective at triggering the transition to a normal high-

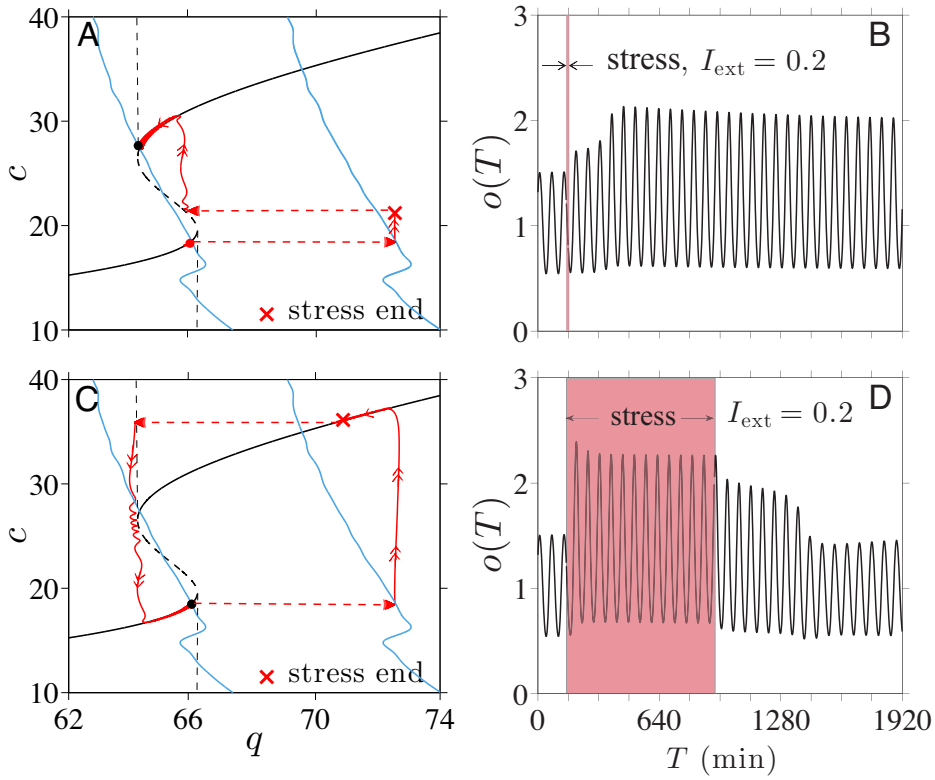

Figure 3.8: **Stress-induced transitions to high-cortisol oscillating state.** (A) Projected 2D system dynamics when a stressor of amplitude $I_{\text{ext=0.1}}$ is applied for 9min starting at $T = 120$min. c is increased just above the unstable branch ($c \approx 20$) to allow the unstressed system to cross the separatrix and transition to the normal high-c stable state. (B) The plot of $o(T)$ shows the transition to the high-cortisol, high-oscillation amplitude state shortly after the 9min stress. (C) A stressor turned off after 780min (13hrs) leaves the system in the basin of attraction of the diseased state. (D) Cortisol levels are pushed up but after about 1400min relax back to levels of the original diseased state.

cortisol state. Overall, these results imply that exposure therapy may be tuned to drive the dynamics of the HPA axis to a normal state in patients with hypocortisolism-associated stress disorders.

3.5 Proposal and Predictions for a new two-stage challenge tests

In the previous section, we re-examined the hypothesis that changes in physiological parameters (specifically p_2) can result in a greater suppression of pituitary activity by dexamethasone

or cortisol. This enhanced negative feedback has been proposed as the cause for lower basal cortisol levels in PTSD subjects. Using our model and analyses, we presented an alternative hypothesis based on the nonlinear interactions in our dynamical system. Here, we outline new experiments that could be used to further evaluate and distinguish these two hypotheses. If the negative feedback of cortisol on the pituitary is enhanced in PTSD subjects, their response to stressors should *be reduced*, especially when the pharmacological suppression is in effect. One way to further probe the system is to combine a non-pharmacological, psychological stressor with the DST. The ensuing cortisol response can be used to probe the purported enhanced negative feedback on the pituitary.

As in the previous section, we assume $I_{\text{ext}}(t)$ to be a positive constant when the external stressor is on, and zero while off. We turn on I_{ext} for sixty minutes starting nine hours after DEX administration, when post-DEX cortisol levels are usually measured. In contrast to the enhanced negative feedback hypothesis, our model shows that cortisol response is generally greater in the low cortisol PTSD state (Fig. 3.9A,B) than in the normal state. Moreover, the peak of cortisol under PTSD can surpass that of cortisol under normal conditions if I_{ext} is sufficiently large.

To understand this unexpected "reversed" phenomenon, consider the nullcline structure during DEX administration and after the stressor is applied (Fig. 3.9C and D). Upon turning on the stressor, the perturbation in I increases the secretion rate of CRH of the PVN neurons, effectively changing q_0 in Eq. 3.2. We have previously shown that increasing q_0 shifts the upper branch of the c-nullcline and moves the bistable regime towards the left in the (c_{s}, c)-plane, as shown in Fig. 3.2A. For a stressor with $I_{\text{ext}} = 0.5$, the c-nullcline is shifted so that the PTSD state on the lower branch is no longer in the bistable regime in the (c_{s}, c)-plane and consequently the PTSD state *jumps* to the upper branch and relaxes towards the only available steady state, approximated by the intersection of the two nullclines in Fig. 3.9D. Meanwhile, the normal state residing on the upper branch of the c-nullcline also jumps to the shifted nullcline, but the size of the jump is significantly *smaller* compared to the jump from the lower branch (as seen in Fig. 3.9D).

The proposed two-step challenge protocol directly contrasts our model prediction and

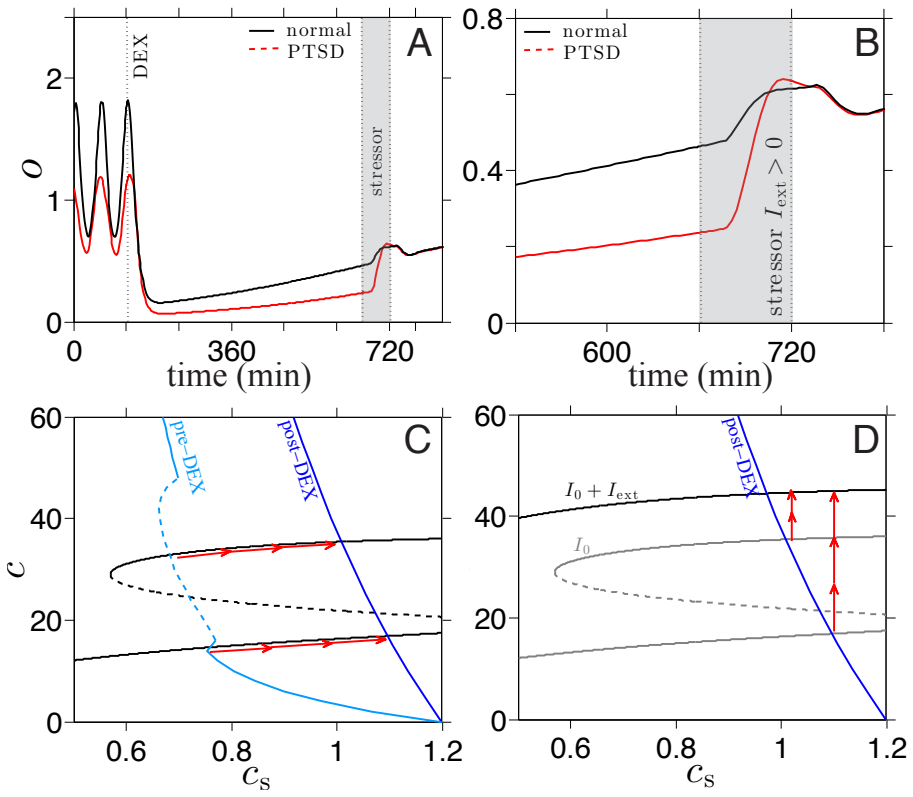

Figure 3.9: **Numerical solutions of a combined two-step challenge test.** We propose a new challenge test in which a non-pharmacological stress challenge is given after DEX administration. (A) The cortisol responses of normal and diseased state systems to a non-pharmacological stressor $I_{\text{ext}}(t)$ at the typical time (9 hours) of post-DEX measurement in DST (shaded region). The response is greater in the system with lower cortisol level (dashed red, PTSD group) than the control (solid black) despite the larger suppression induced by DEX prior to the stressor. (B) A close-up of (A) shows that the peak cortisol level in PTSD subjects surpasses that in normal subjects during the external stress. (C) Nullcline structure during DEX suppression is similar to the one in Fig. 4C (in the main manuscript) before the external stressor I_{ext} is applied. The c_s-nullcline jumps immediately after DEX administration (light blue to dark blue) and relaxes very slowly back to its original position. The stable points slide along the upper and the lower branches of the c-nullcline towards the new intersection with the temporarily shifted c_s-nullcline (dark blue). (D) The c-nullcline is shifted leftward and upward during application of the stressor I_{ext}. The states on the upper and lower branch of the original c-nullcline quickly move toward the new c-nullcline (red arrows). The increase during the shift in c (and subsequently in o) is greater for the PTSD state.

the previous hypothesis. The increase in cortisol response in a subject with lower basal cortisol level cannot be explained by an altered negative feedback strength, while it can be understood as a natural consequence of the changing dynamical structure of the system due to perturbations in the parameter. The experiment also eliminates a confounding effect of the timing of the measurement due to the ultradian oscillation in cortisol level.

3.6 Summary and Conclusions

The HPA axis is a dynamical system continuously evolving to meet changing physiological needs and environmental stimuli. Even at equilibrium, key hormones such as cortisol and ACTH exhibit ultradian oscillations. To accurately interpret the response of the HPA axis to internal, anatomical changes or external inputs, such as the injection of exogenous hormones, we need to understand how the response depends on the state of the system itself and the interplay between its different components. To this end, we developed a mathematical model of HPA dynamics where changes in parameter values and exogenous sources of key hormones could be explicitly included. Of particular importance is the understanding of how pharmacological intervention might affect the long-term dynamics of the HPA axis. Our model is useful in this respect since the effect of medication, trauma, or disease can be mapped onto changes in given parameters. We thus performed a parameter sweep and were able to predict possible modifications to long-term behaviors induced by corresponding pharmacological challenge tests.

Measurements taken during an ACTH stimulation test have shown higher baseline cortisol levels in PTSD subjects and unchanged cortisol responses to exogenous ACTH administration [RDP09]. This result was interpreted as evidence against altered adrenal reactivity in PTSD subjects. Upon incorporating the altered adrenal gland reactivity into our model as a parameter change, we found that data from [RDP09] *can* be explained by adrenal hypo-reactivity in PTSD. Our simulations show that a hypo-reactive adrenal gland can lead to raised baseline cortisol with similar cortisol response to exogenous ACTH administration compared to that of normal subjects. We believe that the phase of the intrinsic oscillations

in cortisol at the time of exogenous ACTH administration should be controlled for more accurate interpretation of experiments.

The most well-known feature of HPA dysfunction in PTSD patients is the low secretion of cortisol. The current viewpoint is that lowered cortisol levels are a consequence of an enhanced negative feedback in the HPA axis [YTL96, BVK07]. This conclusion is based on DEX suppression tests that show a greater percent suppression of cortisol among PTSD subjects. Extending our model to include DEX administration, we have provided an additional mechanism to explain low cortisol levels in PTSD, namely that it arises as a feature of an alternate stable state of the dynamical system. The diseased low-cortisol stable state exhibits greater percent suppression of cortisol *without* enhancing the sensitivity of the negative feedback of cortisol in the pituitary. Thus, enhanced cortisol suppression is an inherent feature of a stable state in our bistable model.

Our model can help understand the many ways trauma might dysregulate cortisol dynamics and identify subgroups of PTSD patients that may require different treatment approaches. For instance, one could measure specific parameters for subjects within one of the subgroups that showed a significant difference in cortisol level [MRV07] and verify whether the associated nullcline structure would allow for bistability. If so, our model supports possible treatments in the form of appropriate external inputs to the system to induce the transition between the stable states. To the contrary, if bistability does not arise, treatment protocols should focus on adjusting the parameter values to correct the dynamics.

Although our model has provided a mechanistic description of the HPA axis behavior under two distinct pharmacological challenge tests, it does not provide a direct explanation for the variability observed in baseline cortisol levels in PTSD patients. One possibility is that the discrepancy merely reflects different stages or effects of disruptions in the HPA axis induced by exposure to trauma.

The literature on PTSD has been driven by diagnostic criteria that rely heavily on non-quantitative and subjective self-reports. This is also true with research on neuroendocrine alterations in PTSD, where the definition of PTSD often failed to take into account important

factors such as gender and type of trauma. Such issues have likely contributed to conflicting reports on how basal cortisol levels are affected by PTSD. Our mathematical model provides a framework to help interpret how external perturbations, such as pharmacological challenge tests, lead to abnormal dynamics and long-term behavior. Analysis of our model allows us to characterize, more mechanistically, PTSD by identifying specific components of the HPA axis that can be affected by trauma or medication.

Our model offers a mechanistic explanation to the seemingly counter-intuitive phenomenon of lower cortisol levels after stress-induced *activation* of cortisol production. Solutions to our model demonstrate that the negative-feedback effect of a temporary increase in cortisol on the synthesis process of CRH can slowly accumulate during the stress response and eventually shift the system into a different basin of attraction. Such a mechanism provides an alternative to the hypothesis that hypocortisolism in PTSD patients results from permanent changes in physiological parameters associated with negative-feedback of cortisol [YTL96, YL07].

We also find that external stress can induce the "reverse" transition from a diseased low-cortisol state to the normal high-cortisol state. Our results imply that re-exposure to stresses of *intermediate* duration can drive the system back to normal HPA function, possibly "decoupling" stress disorders from hypocortisolism.

Interestingly, we show that the minimum durations required for either transition depends on the time at which the stress is initiated relative to the phase of the intrinsic oscillations in (a, o, r). Due to subtle differences in cortisol levels immediately following stress initiation at different phases of the intrinsic cortisol oscillation, the different cumulative negative-feedback effect on CRH can determine whether or not a trajectory crosses a separatrix (Fig. 3.7). When the duration of external stress is near its threshold, normal-to-diseased state transitions are easier to induce when stress is initiated during the rising phase of cortisol oscillations. Reverse diseased-to-normal transitions are more easily induced when stress is initiated during the falling phase.

In summary, our theory provides a mechanistic picture that connects cortisol dysregulation with stress disorders and a mathematical framework one can use to study the down-

stream effects of therapies such as brief eclectic psychotherapy (BEP) and exposure therapy (ET). Both therapies involve re-experiencing stressful situations directly or through imagination, and have been consistently proven effective as first-line treatments for PTSD symptoms [OVG07,FKF08,RER12]. Our results suggest that ET can directly alter and "decouple" the expression of cortisol from an underlying upstream disorder. Changes in neuronal wiring that typically occur over slower times scales is also expected after ET [TST13]. In our model, such changes would lead to slow variations in the basal input $I(t)$. Thus, cortisol level may not be tightly correlated with PTSD, particularly in the context of ET.

It is important to emphasize that we modeled neuroendocrine dynamics downstream of the stress input I_{ext}. How the form of the stress function I_{ext} depends on the type of stress experienced requires a more detailed study of more upstream processes, including how hormones might feed back on these higher-brain processes. Since *higher* cortisol levels are found among female PTSD patients with a history of childhood abuse [LC95] and among PTSD patients who have experienced a nuclear accident [Bau93], future studies of such divergent, experience-dependent dysregulation will rely on more complex input functions $I_{\text{ext}}(t)$. For example, under periodic driving, complex resonant behavior should arise depending on the amplitude and frequency of the external stress $I_{\text{ext}}(t)$ and the nullcline structure of the specific system. Moreover, effects of other regulatory networks that interacts with the HPA axis can be included in our model through appropriate forms of $I_{\text{ext}}(t)$. This leads us to the topics of the next chapter. We first investigate the circadian rhythm input, which is one of the most well known and studied driving forces of the HPA axis. Then we will elaborate $I_{\text{ext}}(t)$ by including the description of synaptic signaling that regulates the initiation and termination of activation of the PVN.

3.7 Appendix

3.7.1 Nondimensionalization

For completeness, we reproduce the dynamical system model first introduced in Chapter 2. The original model was described by the delay-differential equations

$$\frac{\mathrm{d}C_\mathrm{s}}{\mathrm{d}T} = \frac{C_\infty(O) - C_\mathrm{s}}{T_C}, \tag{3.20}$$

$$\frac{\mathrm{d}C}{\mathrm{d}T} = p_C I(T) h(C_\mathrm{s}) g_C(C) - d_C C, \tag{3.21}$$

$$\frac{\mathrm{d}A}{\mathrm{d}T} = p_A C \left(\frac{K_A}{K_A + OR} \right) - d_A A, \tag{3.22}$$

$$\frac{\mathrm{d}R}{\mathrm{d}T} = p_R \left(1 - \frac{\mu_R K_R^2}{K_R^2 + (OR)^2} \right) - d_R R, \tag{3.23}$$

$$\frac{\mathrm{d}O}{\mathrm{d}T} = p_O A(T - T_d) - d_O O, \tag{3.24}$$

where C_s, C, A, R, and O represent concentrations of stored CRH in the PVN, circulating CRH, circulating ACTH, glucocorticoid receptors on the pituitary, and circulating cortisol, respectively. In our new model, Eq. 3.21 is modified as:

$$\frac{\mathrm{d}C}{\mathrm{d}T} = p_C I(T) h(C_\mathrm{s}) + g_C(C) - d_C C. \tag{3.25}$$

The parameters p_α relate the production rate of species α's to their corresponding modulating factors. Greater values of p_α's indicate increased reactivity. For instance, an increase in p_O will yield a greater production rate for a given ACTH level $A(t)$. Modulating functions in the production terms of Eqs. 3.20-3.23 are equivalent to those used in the nondimensionalized Eqs. 3.1-3.4, expressed in terms of dimensional parameters and variables. Lastly, parameters d_α denote the linear decay rate of species α.

The dimensionless form of our model (Eqs. 3.1-3.5) is derived from the dimensional model in the previous subsection with similar scalings used by [WTL10]:

$$
\begin{aligned}
t &= d_O T, & c_\mathrm{s} &= C_\mathrm{s}/\bar{C}_\mathrm{s}, \\
c &= (\mu_R p_R)^{-1} d_O C, & a &= (\mu_R p_R p_A)^{-1} d_O^2 A, \\
r &= (\mu_R p_R)^{-1} d_O R, & o &= (\mu_R p_R p_A p_O)^{-1} d_O^3 O.
\end{aligned} \tag{3.26}
$$

Here, the original time variable T is scaled by the decay rate of cortisol. The original concentrations C_s, C, A, R, O are nondimensionalized to c_s, c, a, r, o, respectively. C_s is normalized by $\bar{C}_\mathrm{s}$, which denotes the maximum stored CRH in the physiological range. For the term describing the additional sources of CRH (from auto/paracrine activity of the pituitary) in the new model, we denote the rate parameter that sets the maximum secretion rate of CRH by the pituitary cells as $g_{\mathrm{c,max}}$. The parameters q_0 and $g_{\mathrm{c,max}}$ should add up to the total secretion rate of CRH in the previous model. From the measurements in [GC98], we estimate the relative contribution of the auto/paracrine activity of the pituitary in CRH production to be in the range of $40\% - 80\%$. For concreteness, we set it to be 60% in our simulations. Note that the adrenal reactivity p_O is one of the scaling factors of the nondimensionalized cortisol level o. When comparing the cortisol responses with altered adrenal reactivity, one needs to take into account for the altered scaling factor for o. The numerical solutions shown in Fig. 3.5 are scaled appropriately to compensate for the altered scaling factor caused by the increased adrenal reactivity p_O.

Finally, the nondimensionalized parameters q_i, p_i are defined analogously to those used by [WTL10]:

$$
\begin{aligned}
t_c &= d_O T_C, & t_\mathrm{d} &= d_O T_\mathrm{d}, \\
q_0 &= p_C/(\mu_R p_R), & q_2 &= d_C/d_O, \\
p_2 &= \mu_R^2 p_R^2 p_A p_O/(d_O^4 K_A), & p_3 &= d_A/d_O, \\
p_4 &= d_\mathrm{O}^8 K_\mathrm{R}^8 (p_\mathrm{A} p_\mathrm{O})^{-2} (\mu_\mathrm{R} p_\mathrm{R})^{-4}, & p_5 &= (1-\mu_\mathrm{R})/\mu_\mathrm{R}, \\
p_6 &= d_R/d_O.
\end{aligned} \tag{A2}
$$

Here, $p_2 \propto p_O$ and $p_4 \propto p_O^{-2}$ and both parameters should be adjusted accordingly when considering changes in adrenal gland sensitivity, p_O, in our model.

3.7.2 Comparison of new and previous model

We briefly describe the effect of including the auto/paracrine activity of the pituitary on the nullcline structure and the behavior of the model. In our previous model Chapter 2, the upregulation of CRH release was assumed to act on the release process of the PVN neuron itself and the auto/paracrine activity of the pituitary was not considered. The equation for c in the previous model analogous to Eq. 3.2 of current model is:

$$\frac{\mathrm{d}c}{\mathrm{d}t} = q_0 I(t) \underbrace{(1 - e^{-kc_\mathrm{s}})}_{h(c_\mathrm{s})} \underbrace{\left(1 - \frac{\mu_\mathrm{c}}{1 + (q_1 c)^n}\right)}_{g_c(c)} - q_2. \tag{3.27}$$

Since both previous and the new model include an increasing Hill-type function $g_c(c)$, we expect both of them to have bistability. Indeed, we have shown that the new model also exhibits bistability in appropriate parameter regimes. Changing each parameter also had a similar effect on the c-nullcline, but the new model retained the bistable regime more robustly. Here we provide analogous plots of Fig. 3.2 generated with the previous model for a direct comparison in Fig. 3.10.

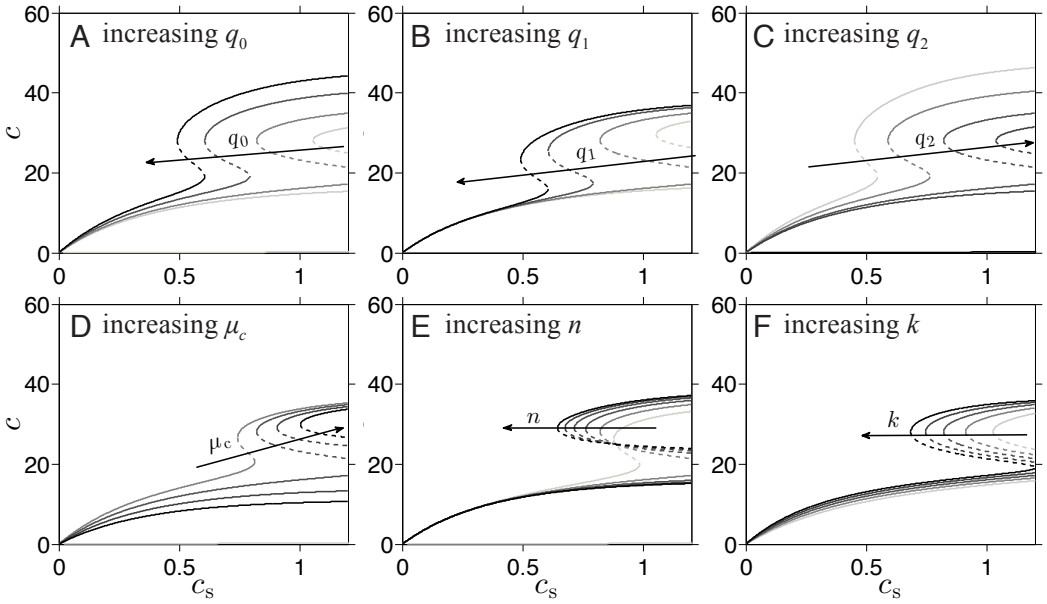

Figure 3.10: **Effects of changing parameters on the c-nullcline.** One of the nondimensionalized six parameters that affect the c-nullcline is varied over a range of values (from 80% to 120% of their reference values) and the corresponding c-nullclines are plotted for the previous model in Chpater 2. Darker color indicates a greater value of the corresponding parameter. When not varied, parameters are set to the reference values $q_0 = 70(I = 1), q_1 = 0.04, q_2 = 1.8, \mu_c = 0.66, n = 6$ and $k = 2.83$. (A) q_0 is varied from 66 to 84. (B) q_1 is varied from 0.032 to 0.48, (C) q_2 is varied from 1.44 to 2.16.(D) μ_c is varied from 0.48 to 0.72. A saddle-node bifurcation occurs near $\mu^* \approx 0.56$ (thicker nullcline). (E) n is varied from 1 to 8. A saddle-node bifurcation occurs between $n = 4$ and $n = 5$. (F) k is varied from 2.26 to 3.40.

CHAPTER 4

Circadian rhythms in the HPA axis

4.1 Introduction

We have developed a dynamical model of the HPA axis that describes the known interactions among the three key hormones responsible for regulating the stress response in the HPA axis. The model exhibited bistable oscillating (ultradian) states that characterized the normal and diseased states. A generalized and simplified form of the external input via a direct projection of the higher brain areas to the PVN was considered. It is important to note that the HPA axis is extensively co-regulated by immune, endocrine, and nervous system. For example, the activity of the hypothalamus-pituitary-gonadal (HPG) axis affects the excitatory inputs to the PVN through the regulation of the sex steroids [FCS90], in addition to various pathways that project to the PVN during the stress response. Notable among these are catecholamine-producing pathways from the brainstem that directly relay information of physiological stress via visceral pathways [HC97]. Other pathways from the limbic area such as the amygdala and the bed nucleus of the stria terminalis (NST) are activated by stressors involving higher-order sensory processing. Each of these pathways will have a particular form of $I_{\text{ext}}(t)$ with its own magnitude and waveform. These stressor-specific forms of $I_{\text{ext}}(t)$ have not yet been studied and fall beyond the scope of this work. Nonetheless, our work provides a general framework on ways to analyze their effect on the HPA dynamics if such information were available.

In this chapter, we will consider another type of external input of the HPA axis to capture the circadian rhythm observed in cortisol levels, in addition to the ultradian rhythm. The circadian rhythm refers to biological oscillations of a period that is approximately of 24-hour

that is highly conserved from cyanobacteria to humans. The suprachiasmatic nucleus (SCN) of the hypothalamus is known as the main pacemaker responsible for the circadian rhythm in mammals [SS06]. The circadian rhythm drives the rest-activity cycle and diurnal variations in many physiological processes such as metabolism and hormone secretion. The current consensus is that the circadian rhythm in cortisol is also regulated by the SCN, supported by the experiments that showed the loss of the rhythm when the SCN was disrupted [AKG79].

We will incorporate the circadian input from the SCN into our model based on clinical observations and then compare i to the approach employed by previous models. Thereafter, we will apply the methods presented in the previous chapter to analyze the behavior of the HPA stress system under the circadian input. Finally, the effects of the external input generated by the stressor combined with the circadian input will be studied. Stress-induced transitions from normal to diseased states under the circadian rhythm within our model predict a new property in which the onset of the lower cortisol level state is dependent on the timing of the stressor termination relative to the circadian phase.

4.2 Suprachiasmatic nucleus and the HPA axis

The suprachiasmatic nucleus (SCN) of the hypothalamus is a group of neurons that is considered to be the central circadian oscillator. The SCN receives the information about the day-night cycle from the photosensitive retinal ganglion cells and uses it to synchronize the internal circadian timing system with respect to the environment [SS06, SS02]. This hypothesis is supported by findings that showed that the ablation of the SCN leads to a complete loss of circadian rhythmicity [SZ72]. Another study demonstrated that the transplantation of an intact SCN restores circadian rhythmicity in arrhythmic mutant animals [RFD90]. The circadian rhythm generated in the SCN is transformed into neuronal or hormonal signals that affect various processes in the body including the HPA axis.

Previous models that included circadian oscillations [JSC05, VAO11, WTL10] have assumed that the PVN receives a direct neuronal input from the SCN that drives the HPA axis through the modulation of the PVN activity. This assumption was realized through

the variation of the secretion rate of CRH over time. Within our model, this corresponds to a periodic $I_{\text{ext}}(t)$ with a period of 24 hours. One can easily extend the work on pulse-like $I_{\text{ext}}(t)$ from the previous chapter to predict the model's behavior under a circadian $I_{\text{ext}}(t)$. However, a recent study [MEI76] showed that the circadian rhythm in cortisol persisted in rodents when their pituitaries were removed, indicating that the circadian rhythm in cortisol may not depend on the rhythmic release of ACTH and CRH. On the other hand, there is evidence suggesting that the circadian input from the SCN acts on the adrenal gland. Autonomic control of the cortisol rhythm is shown to be influenced by adrenal sensitivity to ACTH [JE97, UAE06, KKS81] that is modulated by splanchnic nerve innervation from the SCN to the adrenal gland [JE97, UAE06]. The splanchnic nerves are visceral nerves that relays synaptic signals from the central nervous system to the peripheral sympathetic neurons and ganglia. Based on these observations we consider the effect of circadian modulation of the adrenal sensitivity to be driven directly by the SCN via the sympathetic nervous system. The dynamics of the HPA axis including the circadian input from the SCN is summarized in Fig. 4.1.

The sensitivity of the adrenal cortex represented by the parameter p_O appears in Eq. 2.12 of the original model with dimensional variables. In the nondimensionalized system (Eqs. 3.1-3.5), parameters p_2 and p_4 and the state variable o are dependent on p_O. To describe the varying sensitivity of the adrenal cortex, we consider a time-dependent $p_O(T)$, and subsequently time-dependent $p_2(t)$ and $p_4(t)$ (refer to the nondimensionalization in the Appendix of Chapter 2). The periodic input from the SCN and its modulating effect can be described by some periodic function with a period of 24 hours. For concreteness and simplicity, we first consider a sinusoidal function, $I_{\text{circ}}(t) = 1 + 0.2(1 + \sin(2\pi\omega t))$, where ω^{-1} is equivalent to 24 hours in the dimensional time variable T. Specifically, time-dependent parameter $p_O(t) = \bar{p_O} I_{\text{circ}}(t)$ (Fig. 4.2A), and subsequently $p_2(t) = \bar{p_2} I_{\text{circ}}(t)$ and $p_4(t) = \bar{p_4}(I_{\text{circ}}(t))^{-2}$ are used in the model. Here $\bar{p_i}$'s are the reference parameter values used as the fixed values in the previous chapter. As the scale of $o(t)$ is also dependent on $I_{\text{circ}}(t)$ ($o(t) \propto (p_O(T))^{-1} O(T)$), we will refer to $I_{\text{circ}}(t)o(t)$ as $o(t)$ in the plots of this chapter to reflect the change in the actual cortisol level.

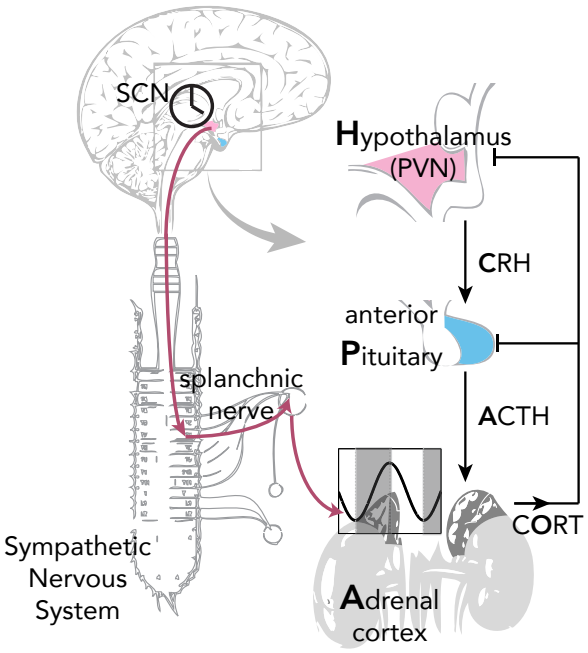

Figure 4.1: **Modulation of adrenal sensitivity by the SCN.** The circadian rhythm in cortisol secretion is mediated by splanchnic nerve innervation of the adrenal gland. The adrenal sensitivity to ACTH stimulation is modulated over a circadian rhythm.

As discussed in the previous chapter, changes to the parameter p_2 and p_4 affect the c_s-nullcline of the system. We have numerically generated a few c_s-nullclines in Fig. 4.2B with selected p_O values across its circadian range, $p_O \in [\bar{p_O}, 1.4\bar{p_O}]$. The plot shows that increasing p_O, and p_2 and p_4 adjusted accordingly, shift the c_s-nullcline horizontally to the right, while shifting the oscillatory regime of the c_s-nullcline downward in the (c_s, c) plane. The c_s-nullclines shifts continuously between the two c_s-nullclines that corresponds to the minimum and the maximum of p_O over 24 hours. Numerical solutions with the time-dependent adrenal sensitivity (Fig. 4.2C) show that the peak and nadir of the hourly oscillation increase with adrenal sensitivity. The cortisol level exhibits a circadian rhythm superimposed on top of the underlying ultradian oscillations, consistent with the observations of plasma cortisol levels. Note that when the c-nullcline has a bistable regime as the one shown in Fig. 4.2B, the bistability of the system can be preserved. The stable oscillating state with lower cortisol levels (characterizing PTSD and other diseased states) also exhibits the circadian rhythm, as shown in Fig. 4.2D.

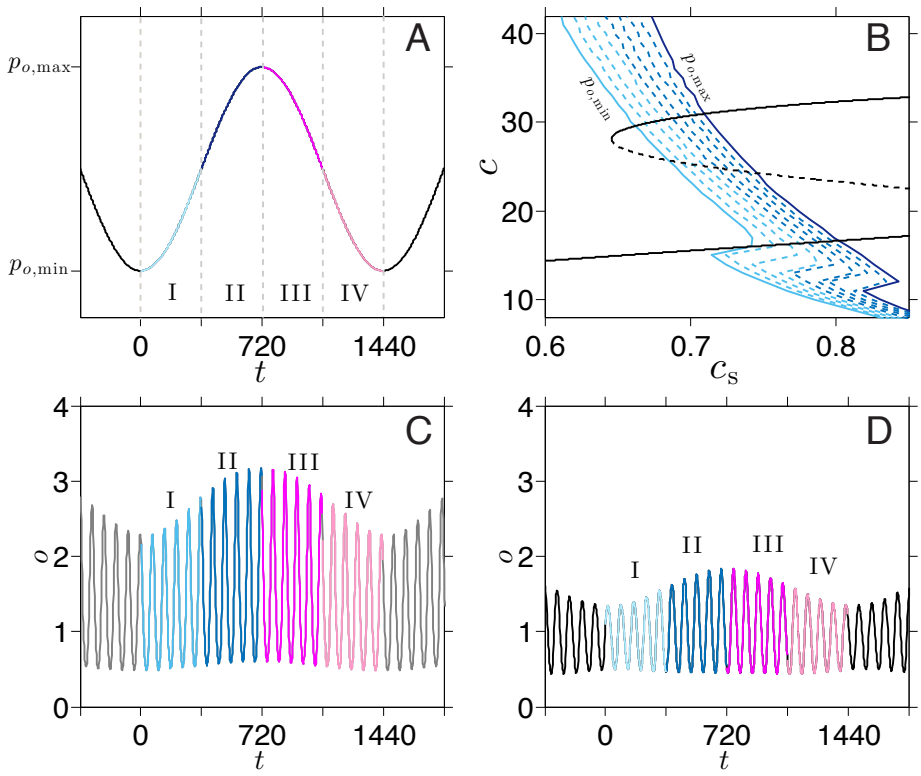

Figure 4.2: **Response of the HPA axis to circadian adrenal sensitivity.**(A) A sinusoidal function is selected to represent the modulation of the adrenal sensitivity. The circadian rhythm is decomposed into four phases (labeled as I, II, III, and IV) of the sinusoidal function. (B) Effects of circadian adrenal sensitivity on the c_s-nullcline. (C) Model prediction for circadian adrenal sensitivity demonstrates increased pulse amplitude in the cortisol level during the peak of the adrenal sensitivity. (D) The bistability of the model is preserved under the circadian rhythm. The parameters used in the simulations are the same as those from the previous chapter except for p_2 and p_4 varying from 13.2 to 18.4 and from 0.44 to 0.62, respectively.

4.3 Projected dynamics on the reduced system

We have previously seen that if the external inputs are assumed to be fixed over time, the long-term behavior of the system can be summarized by the equilibrium points of the reduced system (located at the intersections of nullclines on the (c_s, c) plane). The equilibrium "point" on the reduced system represented a limit cycle in the (a, o, r) space, of which the amplitude and frequency of the oscillation were determined by the value of c. Here, the intersection of the nullclines moves back and forth along the c-nullcline as the c_s-nullcline oscillates over time

due to the time-varying adrenal sensitivity. The question here is determining the system's behavior in the long-term with the time-dependent intersection.

First, we look at the trajectory of the system projected on the (c_s, c) plane after the system has reached its steady state. In Fig. 4.3, the trajectory is decomposed into four segments according to the four phases of the circadian rhythm shown in Fig. 4.2A. Recall that in the slow time variable τ, the dynamics of the system can be approximated by the following set of equations:

$$\frac{\mathrm{d}c_s}{\mathrm{d}\tau} = \langle c_\infty(c;\tau)\rangle - c_s, \tag{4.1}$$

$$0 = q_0 h(c_s) I(t) g_c(c) - q_2 c. \tag{4.2}$$

Note that $\langle c_\infty(c;\tau)\rangle$ is now a periodic function of time (with a period of 2 units of τ), and that c_s is subject to the periodic driving force, which gives rise to a time-dependent c_s-nullcline. At any given time, τ, c_s evolves towards the direction of the moving c_s-nullcline, sliding along the c-nullcline (since c is constrained by the relation in Eq. 4.2, which defines the c-nullcline). As the movement of c_s-nullcline is faster than that of the state variable in this case, the c_s-nullcline moves further away from the state variable until it changes its direction of movement at the peak (nadir) of $I_{\mathrm{circ}}(\tau)$. Once the change in the direction of the c_s-nullcine occurs, the state of the system keeps on moving towards the c_s-nullcline, until the c_s-nullcline and the state eventually intersect and pass each other on the (c_s, c) plane. Once the passing occurs, the direction of the state reverses as its relative position to the c_s-nullcline changes to the opposite side. Similar dynamics occur during the rest of the circadian period until the state of the system reverses its direction of movement again, and the cycle is repeated. Thus the reduced system in steady state is also oscillatory with the same period of the circadian drive. To demonstrate this, the state of the whole system projected on the (c_s, c) plane and the c_s-nullcline at specified times are plotted in Fig. 4.3B. As c is oscillatory, the amplitude and frequency of the limit cycle in the (a, o, r) space also change accordingly in a periodic manner. In total, the system exhibits an hourly oscillation with its amplitude modulated in a circadian rhythm. We have plotted the trajectories of

the system for each of the four phases of the circadian rhythm in Fig. 4.3 to illustrate the evolution of the system in respect to the movement of the c_s-nullcline.

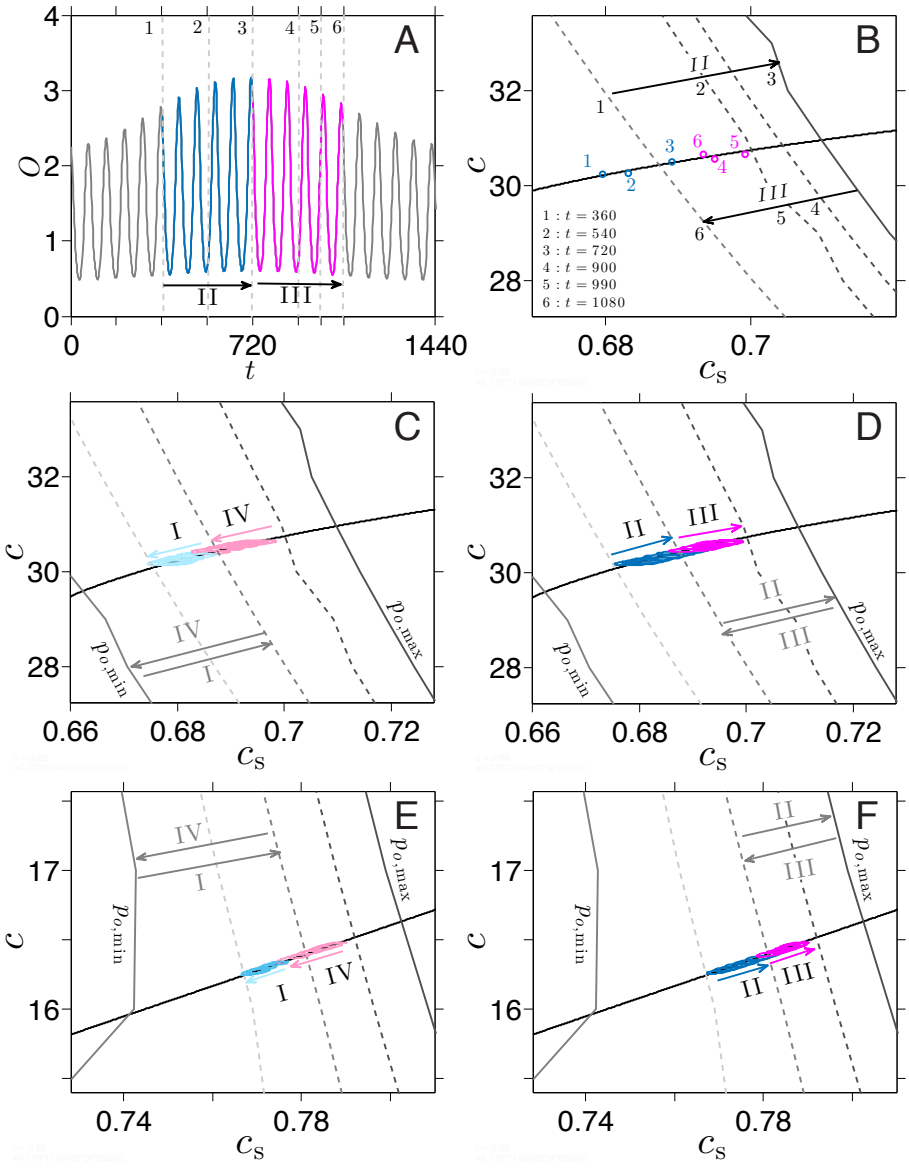

Figure 4.3: **Long-term behavior under periodic c_s-nullcline.** (A) Labels 1-6 indicates the time of the corresponding c_s-nullclines plotted in (B). (B) Each open circle is the projection of the state at the time of the corresponding label. The relative positions of the state from the c_s-nullcline at each time point demonstrate that the system is always relaxing towards the c_s-nullcline but lags behind and never catches up. (C)-(F) The trajectory of the system at each phase on the upper branch ((C)-(D)) and the lower branch ((E)-(F)) of the c-nullcline is plotted. The grey arrows indicate the region swept by the c_s-nullcline during the labeled phase.

4.4 Circadian rhythm and Stress-driven transitions

In this section, we investigate the ways in which transitions between the two stable states are influenced by the inclusion of the circadian rhythm. The activation of the HPA axis by a stressor is described as increasing the synaptic input strength $I_{\text{ext}}(t) > 0$, transiently increasing the secretion rate of CRH by the modulating factor $I(t) = I_0 + I_{\text{ext}}(t)$. We consider a simple rectangular pulse function for $I_{\text{ext}}(t)$ as before. We have seen in the previous chapter that the transition from normal to diseased state was dependent on the duration and the magnitude of the stressor. The change in $I(t)$ affects the c-nullcline and changes the nullcline structure. If the stressor is kept on for a sufficient duration, the system relaxes towards the new steady state. The steady state during the influence of the stressor is also oscillatory and can be analyzed in a similar manner as in the previous section. Fig. 4.4A and B are analogous to Fig. 4.3B and C that illustrate the long-term behavior of the system under stress.

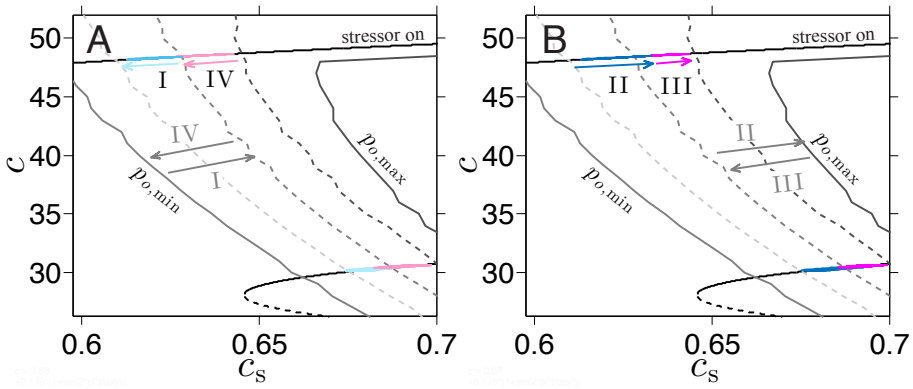

Figure 4.4: **Long-term dynamics under stress.** The trajectory of the state under stress ($I_{\text{ext}}(t) = 2$) during (A) phase IV and I (B) phase II and III.

Increased $I(t)$, or equivalently q_0, during the stress response shifts the c-nullcline upward and contracts the bistable regime in the (c_s, c) plane. The intersections of the c_s- and c-nullclines, and consequently the steady state of the reduced system, generally moves towards the left in the plane due to the decreasing direction of the c_s-nullcline, while still oscillating between the region determined by the range of the c_s-nullcline. This implies that with a

stressor with sufficient magnitude, the system will generally move towards the left, beyond the basins of attraction of the non-stressed system. In Fig. 4.4, we can confirm that the steady state under stress is shifted over to the other side of the separatrix of the fast variables (solid green line). When the stressor is turned off and the c-nullcline returns to its original position, the system will lie in the basins of attraction of the diseased state. This is how transitions from the normal to the diseased state were induced in the previous chapter without considering the circadian input. However, the c_s-nullcline now moves under the influence of circadian rhythm. Consequently, the fast timescale dynamic depends on the position of the c_s-nullcline at the time of stressor initiation and termination. In other words, the transition will now depend on the phase of the circadian rhythm at the time of stress termination. The dependency on the circadian phase at the stress termination is confirmed in Figs. 4.5 and 4.6, in which the stressor is terminated at the end of the four phases.

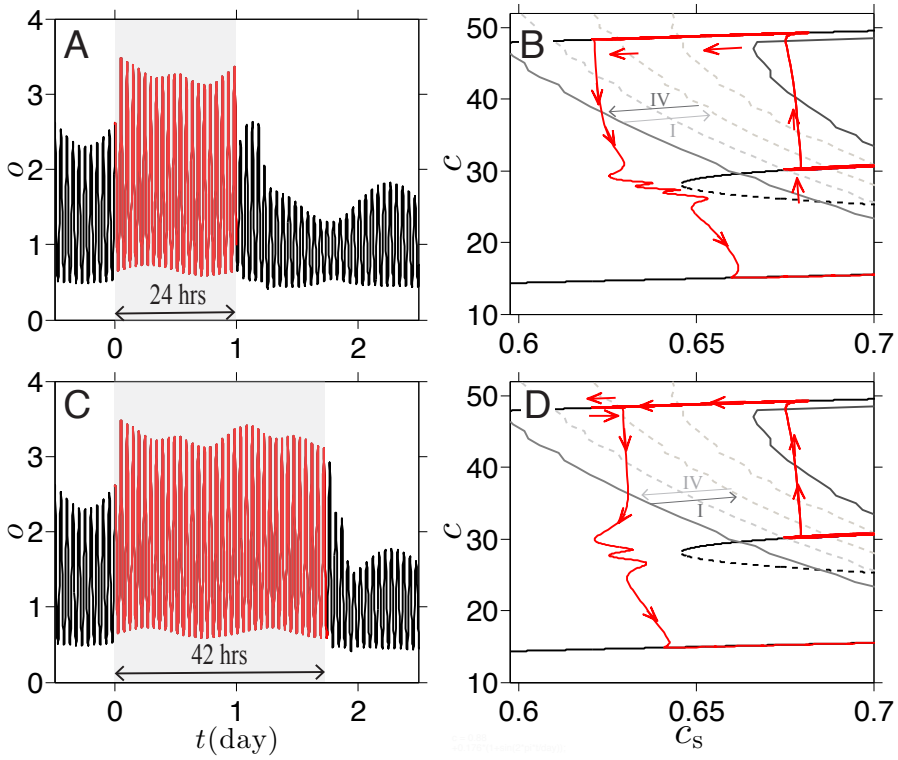

Figure 4.5: **Stress-induced transitions under circadian rhythm.** The system transitions to the diseased branch when the stress is terminated at the end of (A) phase IV and (C) phase I. (B,D) The projected trajectories of the system show that the state is sufficiently repositioned to the other side of the separatrix at the end of (B) phase IV and (D) phase I.

When the stressor is terminated between the end of phase IV and the end of phase I, transitions to the lower branch were induced when the duration was sufficiently large ($\gtrapprox$ 23hrs). The trajectory during the stressor plotted in Figs. 4.5B and C show that the position of the state at the time of stressor termination is on the left half of the steady state oscillation as expected. Note the position of the c_s-nullcline at the time of termination (highlighted in Figs. 4.5B and C).

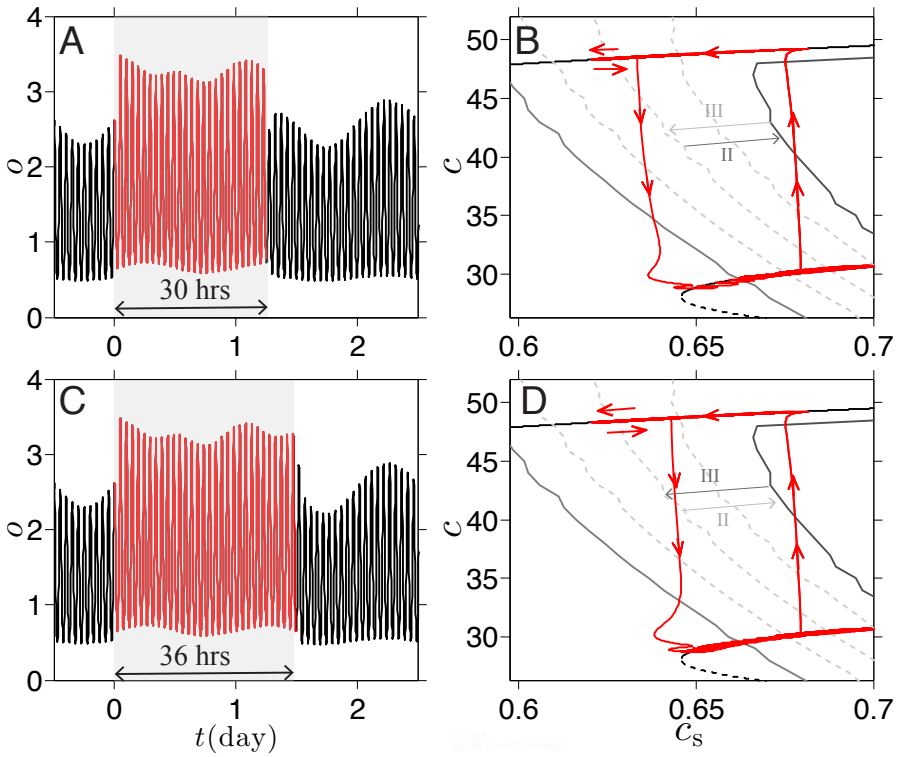

Figure 4.6: **Stress-induced transition under circadian rhythm during phase I and III** The system fails to make the transition to the diseased branch when the stress is terminated at the end of (A) phase II and (C) phase III. (B,D) The projected trajectories of the system show that the state has sufficiently shifted to the other side of the separatrix at the end of (B) phase II and (D) phase III. Note that the stress durations are longer than the one in Fig. 4.5A.

On the other hand, when the stressor is terminated between the end of phase II and III, transitions do not occur regardless of the stress duration. Since the system is in the right half of the steady state oscillation at the time of stress termination (Figs. 4.6), the state of the system is closer from the separatrix while it descends towards the c-nullcline after the

stress. Moreover, the c_s-nullcline are also further to the right, "pulling back" the trajectory towards the basin of attraction of the normal state.

4.5 Conclusion

We have included circadian input from the SCN into our model in a more physiologically relevant way. The circadian input from the SCN modulates the adrenal sensitivity, which is described as the time-varying parameter that oscillates over a period of 24 hours. The bistable structure of the HPA axis dynamics is preserved under the circadian drive. The two distinct stable states exhibit both ultradian and circadian oscillations superimposed upon each other. We can use the model to investigate the ways of the circadian and ultradian rhythm interact and influence the overall dynamics of the cortisol dynamics and stress response. Transitions between the two distinct stable states are considered again with the circadian rhythm in a similar manner as the previous chapter. The model implies that the transitions from normal to lower cortisol state, or the onset of PTSD, are dependent on the phase of the circadian rhythm at the time of stressor termination as well as the duration and magnitude of the stressor. Stress-induced transitions occur when the activation of the PVN elicited by the stressor terminates in the first half of the increasing phase of the sinusoidal circadian rhythm. Such prediction motivates us to investigate the mechanisms underlying the initiation and termination process of the stress response. In other words, a more physiologically relevant form of $I_{\text{ext}}(t)$ may be important in understanding and controlling the onset of PTSD or other causes of dysregulations in cortisol dynamics.

Recent findings suggest that endocannabinoid (eCB) system is an integral regulator of the stress response. In particular, the retrograde neurotransmitter controls the initiation and the termination of the HPA axis activation through modulation of the synaptic input in the PVN. In the following chapter, we will give a brief introduction to the eCB system and present some preliminary models and simulations.

CHAPTER 5

Prospective works

5.1 Endocannabinoid system and the HPA axis

The eCB system is a group of retrograde neurotransmitters and their receptors, which are widely distributed throughout the cortico-limbic and hypothalamic circutiry that regulates the activation of the HPA axis [HT12]. There are two types of eCB molecules that are relevant to the HPA axis: anadamide (AEA) and 2-arachidonoyl glycerol (2-AG). Both AEA and 2-AG are synthesized within the PVN cells and released into the synaptic cleft in a retrograde manner. Their receptors, cannabinoid type 1 (CB1) are primarily localized to axon terminals and are coupled through G-protein that inhibits adenylyl cyclase pathway that ultimately suppress the synaptic activity [MPB16]. Stressor elicits bidirectional changes in AEA and 2-AG during acute stress response.

Under steady state conditions, there is a tonic signal of AEA from the PVN cells that inhibits the synaptic input of the pre-synaptic neurons of the PVN. Exposure to stressor rapidly increases the CRH signaling of basolateral amygdala (BLA) projecting onto the PVN. The CRH receptor of the PVN neurons subsequently increases the enzymatic activity that hydrolyzes and deactivates AEA. This decrease in AEA signaling disinhibits the pre-synaptic neurons and results in the activation of the PVN neurons. Note that CRH acts as a neurotransmitter and does not directly affect the CRH level in the portal vein, *c*. After the initial decrease following the stressor exposure, AEA level slowly recovers over time, typically on the timescale of hours [HT12] The pathway responsible for AEA synthesis is not currently known.

On the other hand, studies suggest that stressors act to increase 2-AG synthesis. Mea-

surements of 2-AG after restraint and footshock stress showed an increase in hypothalamus [ETH10]. The increase induced by stressors was blocked by glucocorticoid receptor antagonist, indicating that the glucocorticoid mediates the regulation of 2-AG synthesis during stress. The exact mechanisms by which cortisol upregulates 2-AG synthesis is not yet fully understood. However, the typical timescale of the process ranging from 20 min to 60 min suggests that the effect is nongenomic and is mediated by membrane-associated receptors.

5.1.1 A preliminary model of the eCB + HPA axis

We modify the model of the overall synaptic input strength received by the PVN as a function of AEA and 2-AG levels as following:

$$\begin{aligned} I(E_1, E_2, t) &= I_{\text{base+}} I_{\text{ext}}(E_1, E_2, t) \\ &= I_{\text{base}} + f_{\text{ext}}(E_1, E_2) I_{syn}(t), \end{aligned} \tag{5.1}$$

where E_1 and E_2 denote the AEA and 2-AG level, respectively, in the PVN neurons. The overall magnitude of the external input, $I_{\text{ext}}(t)$ is modulated by a decreasing function $f_{\text{ext}}(E_1, E_2)$ that represents the retrograde inhibitory action of AEA and 2-AG on the pre-synaptic neurons of the PVN neurons. $I_{\text{syn}}(t)$ is a rectangular pulse function that is nonzero during the course of stressed state and zero during the non-stressed state. The function $I_{\text{syn}}(t)$ indicates whether the pre-synaptic neurons of the PVN active or not. Note that if we set $f_{\text{ext}}(E_1, E_2)$ be constant and independent of E_1 and E_2 we recover the previous $I_{\text{ext}}(t)$ of a rectangular pulse function. The functional form of $f_{\text{ext}}(E_1, E_2)$ has not yet been studied to best of our knowledge. We assume it also takes the form of a Hill function as

$$f_{\text{ext}}(E_1, E_2) = V_{\text{ext}} \frac{K_{\text{e}}^{n_{\text{e}}}}{K_{\text{e}}^{n_{\text{e}}} + (E_1 + E_2)^{n_{\text{e}}}}, \tag{5.2}$$

where V_{ext} and K_{ext} denote the maximum synaptic strength and half-maximal effective eCB concentration, respectively.

5.1.2 Decay of AEA at stress response initiation

For simplicity, let us assume that degradation of AEA induced by a stressor occurs instantaneously.

$$E_1(t) = \begin{cases} E_{1,\mathrm{ON}} & \text{stressor is on } (I_{\mathrm{syn}}(t) > 0) \\ E_{1,\mathrm{OFF}} & \text{otherwise} \end{cases}$$

where $E_{1,\mathrm{OFF}}$ and $E_{1,\mathrm{ON}}$ denote the non-stressed (stressor "OFF") steady state AEA level and the stressed (stressor "ON") steady state AEA level, respectively. Recent measurements show that AEA quickly decreases in response to the stressor (reaches the nadir about 5min after the stressor initiation [HT12]) and it slowly recovers back to its non-stressed steady state. Our current model does not capture the recovery phase but assumes that it stays at the low AEA state until the stressor is over. Alternatively, one may consider a function of the following form:

$$E_1(t) = E_{1,\mathrm{OFF}} - H(t - t_i)E_{1,\mathrm{ON}}(t - t_i)e^{-r(t-t_i)}, \tag{5.3}$$

where $H(t)$ is the Heaviside step function and t_i is the time of the most recent stressor initiation. The AEA level, $E_1(t)$ decreases from the beginning of the stressor and reaches its nadir around time $t = r^{-1}$ before increasing back to the non-stressed basal state level $E_{1,\mathrm{OFF}}$. The characteristic time constant r can be estimated as $5\mathrm{min}^{-1}$ based on the time course of AEA given in [HT12].

5.1.3 Synthesis of 2-AG during stress response

Glucocorticoids (cortisol) upregulates 2-AG synthesis, mediated by membrane-associated receptor action that acts over a fast timescale. We assume that the change in synthesis rate of 2-AG brought by changes in cortisol level is immediate. The increased level of cortisol, $o(t)$ during acute stress response will increase 2-AG level and eventually terminate the activation of the PVN.

Based these observations, we model the dynamic of 2-AG level as following:

$$\frac{\mathrm{d}E_2}{\mathrm{d}t} = \gamma(g_{E_2}(o(t)) - E_2), \tag{5.4}$$

where $g_{E_2}(o)$ is an increasing positive function of cortisol o, which reflects the increased synthesis rate of 2-AG induced by the increase in cortisol level. We assume a simple linear decay rate of d_{E_2} for 2-AG degradation. The timescale constant γ reflects how fast the synthesis and degradation process of 2-AG take place relative to other interactions in the HPA axis. It should be adjusted to match the observed peak time around 50min after the stressor initiation.

5.1.4 Preliminary results: Habituation in stress response

The eCB system and its effect on the synaptic strength of the afferent input to the PVN has been described in the previous section. Since $E_2(o(t))$ is dependent on cortisol level $o(t)$, we can couple the eCB system described above with the mathematical model of the HPA axis developed in the previous chapters. The activation and termination of the HPA axis response to acute stress is dependent on the dynamics of the two eCB molecule levels in the modified model. With estimated parameters in Eqs. 5.2-5.4, we can simulate the response of HPA axis under repeated stressors. We arbitrarily select $V_{\text{ext}} = 2$, $K_e = 1.75$, $n_e = 4$, $E_{1,\text{OFF}} = 1$, $E_{1,\text{ON}} = 1$, and $\gamma = 0.01$ for concreteness. The synthesis rate of 2-AG in Eq. 5.4, $g_{E_2}(o)$ is assumed to be an increasing function that saturates:

$$g_{E_2}(o) = 1 - e^{-ro},$$

where r is the parameter that relates the cortisol level and the synthesis rate of 2-AG and set at $r = 0.5$. More physiologically accurate parameters and functional forms for the eCB model will be estimated in future work. Using the preliminary model, we illustrate and suggest a possible role of eCB signaling in the habituation of the HPA axis response to repeated stress. Circadian rhythm is not included in this preliminary study for simplicity.

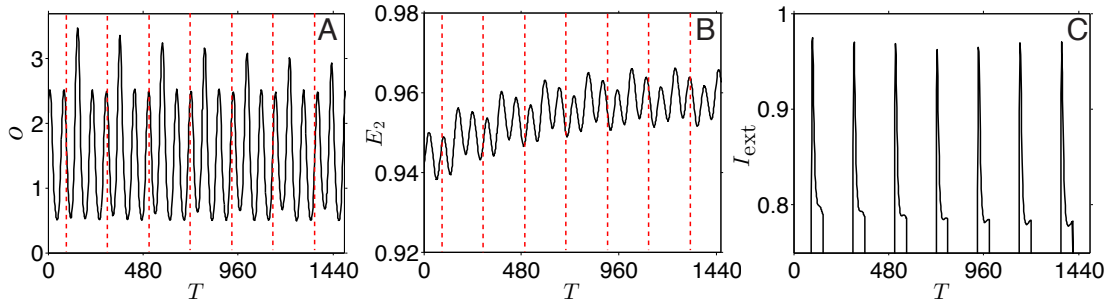

Figure 5.1: **Habituation of HPA response to a repeated stress.**(A) A same type of stressor is repeated for seven times with intervals of 210min. Each stressor lasted for 60min. The peak of cortisol response decreased over the repeated stressors. The time at the initiation of each stressor is marked by a red dashed line. (B) The average level of 2-AG increases over the repeated stressors. (C) Due to increased level of 2-AG, the overall synaptic input received by the PVN during each stressor decreases more rapidly over repetition.

Fig. 5.1A shows that the peak level of cortisol during a stressor decreases over the repetition of the same type of stressors. 2-AG level increases in response to the increased cortisol level during a stress response but decreases back to its basal level as cortisol returns to its basal state. When another stressor arrives before 2-AG level is dropped back to its steady state value, 2-AG level begins to increase from a higher level than the level before the first stressor and increases to a higher level relative to the level reached after the previous stressor. Overall, the average level of 2-AG gradually increases over the repeated stressors(Fig. 5.1B) and consequently the magnitude of pulses of synaptic input received by the PVN decreases more rapidly over the repetition (Fig. 5.1C). The time intervals between stressors was set approximately equal to the period of the intrinsic oscillation to eliminate the effect of timing on the cortisol response (refer to Discussion 2.4). More complex patterns in the cortisol response appear for some other intervals due to the timing effect (not shown), but the cortisol response eventually decreases over repetition and exhibits habituation. Note we assume that the timescale of the changes in 2-AG is set to be comparable to that of the c_{s}. The habituation process was preserved with timescales that are comparable the fast timescale of the HPA axis model (PA subsystem). Once better estimations of parameters and functional forms used in Eqs. 5.2-5.4 become available, the effect of timing, different timescales of 2-AG

(γ), and bistability on the habituation process can be further analyzed. Furthermore, the role of eCB signaling in PTSD and other stress disorders may be further investigated with those estimations available.

5.2 Novelty detection in retina-tectum neural network

5.2.1 Background

The detection of novelty, or detection of violations in the expected patterns in environmental stimulus, is essential for adapting to a constantly changing environment. These processes occur at various levels of our cognitive system in response to different types of sensory or cognitive stimulus. For instance, preliminary *in vitro* experiments on the turtle and mouse tectum cells show various activity patterns in response to different types of novel stimuli (Jian-Young Wu, personal communication, March 11, 2015). On the other hand, recognizing and establishing a regular pattern in stimulus and storing the information is another aspect of detecting novelty. The local field potential measurements (Jian-Young Wu, personal communication, March 11, 2015) demonstrate that neurons in the tectum show a vigorous response to the first flash and gradually subdue over repeated flashes, establishing an expectation of regularity. When the regular pattern is broken by an omitted flash or extra flash, there is a response in the local field potential. At the network level, the tectum shows distinct spatiotemporal patterns depending on the type of novelty. For example, pseudo-color activity maps of the voltage-sensitive dye amplitude from the tectum surface show distinct spatiotemporal patterns with the highest amplitude occurring in different locations in response to the beginning, omission, addition, and end of the stimulus (Jian-Young Wu, personal communication, March 11, 2015).

In this section, we introduce a framework on ways to model and analyze novelty detection in the retina-tectum network. We develop a phenomenological model of the building blocks of a neural field model that can describe the various spatiotemporal activity patterns of the retina-tectum network. From the model, we aim to understand how dynamic networks can

establish and store an expectation of regularity and how particular spatiotemporal patterns may emerge in response to each type of violation in the sensory stream. We will focus on developing the building block models that describe the novelty detection activity in one of the processing stages in the retina-tectum (the ganglion cell layer) and characterize different types of behaviors observed.

There are four basic types of neurons consisting the retina-tectum network: photoreceptor cells, bipolar cells, ganglion cells in the retina and the tectum neurons (a homologous structure to the superior colliculus in mammals). Each type of neurons reside in separate layers in the retina, where synaptic connections are made between one layer and another. When a photon hits a photoreceptor in the retina, it hyperpolarizes the cell through a cascade of reactions that eventually close cGMP gated ion channels [Yau94]. Thereafter, photoreceptors make glutamatergic projections onto ON- and OFF-bipolar cells. The released glutamate has an opposite effect on two types of bipolar cells due to different types of receptors expressed: excitatory effect on OFF-bipolar cells and inhibitory effect on ON-bipolar cells [PBC08]. Both types of bipolar cells (BC) synapse onto ganglion cells (GC) only of the same type (OFF-bipolar to OFF-ganglion and ON-bipolar to ON-ganglion), as their sites of synapses are separated in two discrete layers [FK76]. ON- or OFF-bipolar cells can modulate the activity of the same type of ganglion cells, through inhibitory interneurons called amacrine cells (AC). Only the GC generate action potentials, while all other cells communicate through graded potential [KSJ00]. Finally, the axons of GC form the optic nerve, which projects to the tectum; where we assume the signals from ON- and OFF-paths are integrated.

In summary, the activity in the tectum is driven through four main feed-forward processing stages: photoreception, transmission to bipolar cells, transmission to ganglion cells, and transmission along the optic nerve to neurons in the tectum. Within photoreception and transmission to ganglion cells stage, there are lateral connections. Horizontal cells receive excitatory input from photoreceptors and send inhibitory input to their post-synaptic photoreceptor cells. Amacrine cells receive excitatory input from ON- or OFF-bipolar cells and send inhibitory input to their post-synaptic ON- or OFF-ganglion cells. A schematic

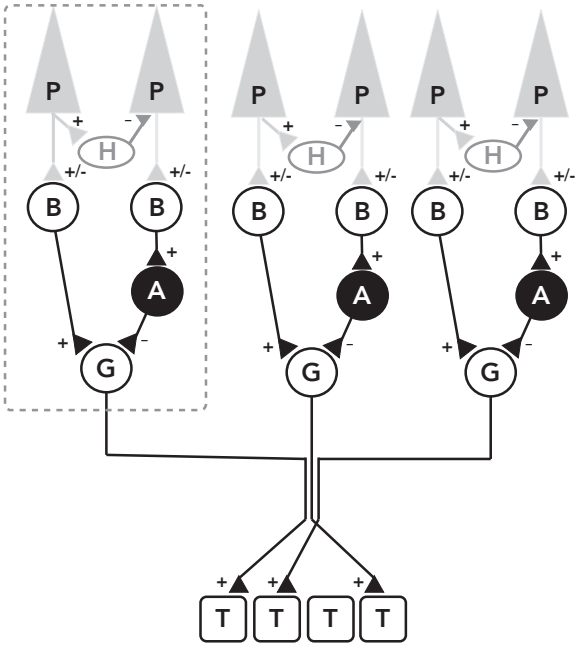

Figure 5.2: **A schematic diagram of the retina-tectum network.** The light stimulus hyperpolarizes the photoreceptors (P) that effectively disinhibits and activates ON-bipolar cells and inhibits OFF-bipolar cells. Horizontal cells are activated by photoreceptors and feed back into neighboring photoreceptors, generating spatial inhomogeneity in the input layer for the bipolar cell layer. ON- or OFF-bipolar cells (B) directly form synapses with and activate the ganglion cells or indirectly form synapses with and inhibit the ganglion cells. The two pathways (direct and indirect) are integrated at the ganglion cell layer. Ganglion cells project onto tectum cells, in which novelty-specific spatiotemporal patterns emerge. The dashed box represents a building block of the network. **P**: photoreceptor, **H**: horizontal cells, **B**: ON- or OFF-bipolar cells, **A**: amacrine cells, **G**: ganglion cell, and **T**: tectum cells. $+$: excitatory synapse, $-$: inhibitory synapse.

diagram of the retina-tectum network is shown in Fig. 5.2

5.2.2 Model development

Assuming the linear-nonlinear (LNL) model for the retinal neurons and following the standard notations used in the literature [Ama77, Erm98, Tay99] the average membrane potential of a neuron population of type α near position $\vec{x} = (x_1, x_2)$ in the two-dimensional space at time t will be denoted by $u_\alpha(\vec{x}, t)$. The dynamics of $u_\alpha(\vec{x}, t)$ is described as,

$$u_\alpha(\vec{x},t) = \int_{\Omega\subset\mathbb{R}^2} \int_0^t \sum_\beta \Phi_{\alpha\beta}(\vec{x},\vec{y},t-t') F_\beta(u_\beta(\vec{y}',t'))dt'd\vec{y}, \tag{5.5}$$

where $\Phi_{\alpha\beta}(\vec{x},\vec{y},t)$ represents the temporal filtering effects of synaptic processing from the pre-synaptic neuron population β positioned at $\vec{y}$ to the post-synaptic neuron population α positioned at $\vec{x}$. We assume that $\Phi_{\alpha\beta}$ is in the form $\Phi_{\alpha\beta}(\vec{x},\vec{y},t) = \omega_{\alpha\beta}(\vec{x},\vec{y})\phi_{\alpha\beta}(t)$, where $\omega_{\alpha\beta}(\vec{x},\vec{y})$ is the average intensity of connection from neurons of type β at position $\vec{y}$ to neurons of type α at position $\vec{x}$. Function $F_\beta(u_\beta(\vec{y},t))$ is called the output function and denotes the average activity (represented typically as the mean firing rate) of a local homogeneous population of the pre-synaptic neuron of type β near position $\vec{y}$ at time t. Thus, the right-hand side of Eq. 5.5 represents the total amount of influence received by neurons of type α at $\vec{x}$ from neurons of different types summed over the relevant domain $\Omega \subset \mathbb{R}^2$.

5.2.3 Novelty detecting ganglion cells

Schwartz *et al.* [SHS07] have found ganglion cells that showed the omitted stimulus response (OSR), in which neurons show a response to the omission of a stimulus from a periodic sequence. Such omission detecting ganglion cells will be considered as the "circuit element", or a basic "building block", of the retina-tectum network model. We first consider a building block of the full network consisting of six groups of cells—photoreceptor cells (P), ON-bipolar cells (N), OFF-bipolar cells (F), ganglion cells (G), and amacrine cells (A)—on an isolated point in space at $\vec{x} = (x, y)$. The spatial interactions among photoreceptor cells mediated by horizontal cells (Fig. 5.3) will not be included explicitly in the current study. In other words, we set $\Phi_{\alpha\beta}(\vec{x},\vec{y},t) = \omega_{\alpha\beta}(\vec{x},\vec{y})\phi_{\alpha\beta}(t) = \delta(\vec{x})\phi_{\alpha\beta}(t)$, where $\delta(\vec{x})$ is the two-dimensional Dirac delta function. Such form of connectivity function will effectively remove the integration over the space domain in the general form (Eq. 5.5).

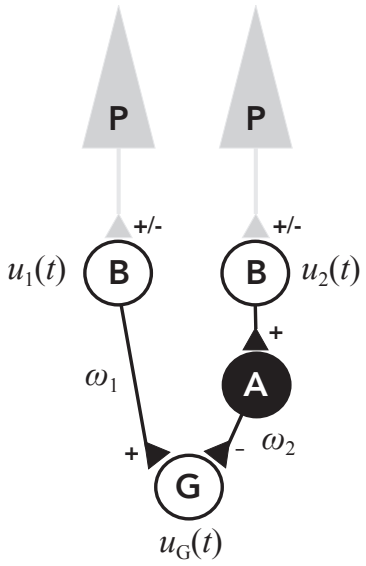

Figure 5.3: **A schematic diagram of the building block.** The building block of the retina-tectum network consists of the two signaling pathways that converge at the ganglion cell layer. A direct input coming from ON- or OFF- bipolar cell layer and an indirect input via the amacrine cell layer coming from ON - or OFF bipolar cell layer. We only consider the case in which the two signaling pathways are from the same type of bipolar cells (*i.e.,* u_1 and u_2 are both ON- or both OFF- bipolar cells).

First, the activity of photoreceptors, denoted by $u_P(\vec{x}, t)$, is described as,

$$u_P(t) = \int_0^t \phi_P(t - t')S(t')dt' \qquad P : \text{photoreceptor cells}, \tag{5.6}$$

$$\phi_P(t) = -\lambda_P e^{-\lambda_P t},$$

$$F_P(u_P) = u_P, \tag{5.7}$$

where $S(t)$ represents the incoming light stimulus. Without loss of generality, we will set the steady state of u_P during dark at 0. The temporal filtering effect of the phototransduction $\phi_P(t)$ is negative, since the light causes hyperpolarization of the photoreceptors. The output function of photoreceptor cells is approximated as a linear function of u_P, based on the measurements in [BM02] For the repeated light stimulus used in the experiment we set,

$$S(t) = \Sigma_k \Pi_d(t - kT), \tag{5.8}$$

where T is the period of the repeated stimulus and $\Pi_d(t)$ is the simple rectangular pulse function of duration d.

Hyperpolarization induced by phototransduction in photoreceptor cells results in a decrease in intracellular calcium level and consequently a decrease in the amount of glutamate release to both ON- and OFF-type bipolar cells [PBC08]. These two types of bipolar cells are distinguished by the type of glutamate receptor they express. ON-bipolar cells (N) express metabotropic receptors (mGlu6) that result in negative current when activated. In contrast, OFF-bipolar cells (F) express ionotropic receptors (AMPA) that result in positive current [MS86]. Thus, the two types of bipolar cells respond in an opposite manner to light; ON-bipolar cells depolarize with positive synaptic current flowing in, while OFF-bipolar cells hyperpolarize with negative synaptic current flowing out during a light stimulus. The activity of ON- and OFF-bipolar cells can be described as,

$$u_N(t) = \int_0^t \phi_{NP}(t-t')F_P(u_P(t'))dt', \qquad N : \text{ON-bipolar} \tag{5.9}$$

$$\phi_{NP}(t) = -k_N t e^{-\lambda_N t}$$

$$u_F(t) = \int_0^t \phi_{FP}(t-t')F_P(u_P(t'))dt', \qquad F : \text{OFF-bipolar} \tag{5.10}$$

$$\phi_{FP}(t) = k_\alpha t e^{-\lambda_F t},$$

$$F_\alpha(u_\alpha) = u_\alpha, \qquad \alpha \in \{N, F\}$$

where $\phi_{NP}(t)$ and $\phi_{FP}(t)$ are temporal filtering functions of ON- and OFF-bipolar cells for inputs from photoreceptors (P) with normalizing constants k_N and k_F. The functional forms are chosen based on measurements in [CAS83]. The negative sign of $\phi_{NP}(t)$ represents the inhibitory nature of the synapse between ON-bipolar cells and photoreceptors. Moreover, the two types of bipolar cells have different characteristic time constants for the temporal filtering effect, since ionotropic receptors usually operate in faster time scale than metabotropic receptors [CAS83]. We assume accordingly that $\lambda_F > \lambda_N$.

Both types of bipolar cells make excitatory synapses onto ganglion cells of the same type

or amacrine cells. Bipolar cells also communicate through graded potential, and we assume that the output functions of ON- and OFF-bipolar cells, $F_{\mathrm{N}}(u)$ and $F_{\mathrm{F}}(u)$, are simply linear functions based on the study in [BM02]. The membrane potential of amacrine cells can be described as,

$$\begin{aligned} u_A(t) &= \int_0^t \phi_A(t-t')u_\alpha(t')dt' && A : \text{Amacrine cell} \\ \phi_A(t) &= \lambda_A e^{-\lambda_A t} && \\ F_A(u_A) &= -u_A && \alpha \in N, F \end{aligned} \tag{5.11}$$

where $\phi_A(t)$ is the temporal filtering function of amacrine cells. Again, the output function of amacrine cells is approximated as a linear function of u_A based on the previous study in [BM02]. The negative sign represents the inhibitory synaptic output of amacrine cells to its post-synaptic neurons.

Finally, we assume that synaptic inputs from amacrine cells and bipolar cells are integrated into the ganglion cell layer as a weighted sum. Under such assumption, the membrane potential of ganglion cells can be described as,

$$\begin{aligned} u_G(t) &= \omega_{G\alpha} \int_0^t \phi_{G\alpha}(t-t')F_\alpha(u_\alpha(t'))dt' && G : \text{Ganglion cell} \\ &\quad + \omega_{GA} \int_0^t \phi_{GA}(t-t')F_A(u_A)(t')dt', && \alpha \in \{N, F\} \\ \phi_{G\beta}(t) &= \lambda_{G\beta} e^{-\lambda_{G\beta} t} && \beta \in \{N, F, A\} \end{aligned} \tag{5.12}$$

where the afferent connection strength of ganglion cells from bipolar cells (of type α) and amacrine cells are denoted by $\omega_{G\alpha}$ and ω_{GA}, respectively. The temporal filtering function $\phi_{G\beta}(t)$ was approximated as an exponentially decreasing function for simplicity. Substituting the output functions of the bipolar and amacrine cells, $F_\alpha(u_\alpha) = u_\alpha$ and $F_A(u_A) = u_A$ in the expression, we can rewrite Eq. 5.12 as

$$u_G(t) = \omega_{G\alpha} \int_0^t \phi_{G\alpha}(t-t')u_\alpha(t')dt' - \omega_{GA} \int_0^t \phi_{GA}(t-t')u_A(t')dt'. \tag{5.13}$$

The ganglion cell layer receives the direct synaptic input from only one type of bipolar cell (α is either N or F, but not both), as noted earlier.

For simplicity, we assume that the membrane potential dynamics of the photoreceptors, ON- and OFF-ganglion cells, and amacrine cells are sufficiently fast and consider the limiting case of $\lambda_P, \lambda_{GN}, \lambda_{GF}, \lambda_{GA}, \lambda_A \to \infty$. Note that the convolution of a function $u(t)$ with an exponentially decaying function, $\lambda e^{-\lambda t}$ becomes

$$\lambda \int_0^t e^{-\lambda(t-t')}u(t')dt' \to u(t), \tag{5.14}$$

as $\lambda \to \infty$ and Eqs. 5.6-5.12 can be approximated under the limit as

$$u_P = -S(t), \tag{5.15}$$

$$u_\alpha(t) = -\int_0^t \phi_\alpha(t-t')S(t')dt', \tag{5.16}$$

$$u_A(t) = u_\beta(t), \tag{5.17}$$

$$u_G(t) = \omega_{G\alpha}u_\alpha(t) - \omega_{GA}u_\beta(t). \qquad \alpha, \beta \in \{N, F\} \tag{5.18}$$

Here we assumed that the inhibitory input from the amacrine cell layer is also driven by either ON- or OFF-bipolar cells, but not both (*i.e.,* β is N or F).

Before presenting the analysis of the main model, we present a toy model with some simplifying assumptions that are mathematically more tractable to illustrate the key mechanisms of our model of the OSR. Readers who wish to proceed directly to discussions on the main model may skip the following subsection.

5.2.4 A toy model

For mathematical tractability, we consider a toy model for novelty detecting ganglion cell as follows:

$$\begin{aligned} u_i(t) &= -\int_0^t \phi_i(t-t')S(t')dt', \\ \phi_i(t) &= \pm\lambda_i e^{-\lambda_i t}, \\ u_G(t) &= \omega_1 u_1(t) - \omega_2 u_2(t), \end{aligned} \tag{5.19}$$

which has the identical form to the model developed in the previous section (Eqs. 5.15-5.18) except for the temporal filtering function of the bipolar cell i is denoted by $\phi_i(t)$ and assumed to be a decreasing exponential function with the corresponding decay rate λ_i. The activities of two bipolar cells is integrated as a weighted sum at the ganglion cell (u_G), with their corresponding synaptic weights denoted as ω_i. The sign of $\phi_i(t)$ and subsequently the sign of u_i depends on the type of bipolar cell it represents. If the i^{th} bipolar cell associated with $u_i(t)$ is an ON-bipolar (OFF-bipolar) cell then the sign of $\phi_i(t)$ is negative (positive) and the sign of u_i is positive (negative). The negative sign of the second term on the right-hand side of Eq. 5.19 indicates that the synaptic weight ω_2 represents the connection with the amacrine cell layer (Eq. 5.11, 5.17 and 5.18). The two synaptic inputs $u_1(t)$ and $u_2(t)$ from the bipolar cells layer are driven by the same kind and we will not consider the cross-talk between the ON- and OFF-channels in this work. Without loss of generality, we will assume that u_1 and u_2 are both associated with ON-bipolar cells.

We consider a pulsed light stimulus represented given at time $t = t_k$ by the Dirac-delta function $\delta(t-t_k)$. The activity of the bipolar cell after a single light stimulus, $S(t) = \delta(t-t_k)$, becomes $u_i(t) = \lambda_i e^{-\lambda_i(t-t_k)}$, which decays exponentially over time. Repeated pulse inputs with a fixed interval of T beginning at $t = 0$ can be written as,

$$S(t) = \sum_{k=0} \delta(t - kT), \tag{5.20}$$

which leads to

$$u_i(t) = \int_0^t \lambda_i e^{\lambda_i(t-t')} \sum_{k=0} \delta(t' - kT)dt' = \lambda_i \sum_{t-kT>0} e^{-\lambda_i(t-kT)}$$
$$= \lambda_i \sum_{t-kT>0} e^{-\lambda_i t'} e^{-\lambda_i kT} = \lambda_i e^{-\lambda_i t'} \sum_{t>kT} (e^{-\lambda_i T})^k, \tag{5.21}$$

where t' denotes the time passed since the last pulse (*i.e.*, $t' = t \mod T$). The expression for $u_i(t)$'s can be cast as a simple geometric series with the common ratio, $r_i = \exp(-\lambda_i T)$ and $u_G(t)$ can be expressed as:

$$u_i(t) = \lambda_i e^{-\lambda_i t'} \sum_{kT<t} r_i^k, \tag{5.22}$$

$$u_G(t) = \omega_1 \lambda_1 e^{-\lambda_1 t'} \sum_{kT<t} r_1^k - \omega_2 \lambda_2 e^{-\lambda_2 t'} \sum_{kT<t} r_2^k. \tag{5.23}$$

The first term ($k = 0$) in the series represents the influence of the most recent input and the second term ($k = 1$) represents the influence of the second most recent input, and so on. The last term in the series, the term with the largest k such that $kT < t$, represents the influence of the oldest stimulus and decreases exponentially over time as expected, since the largest k increases as t increases. At each pulse ($t = kT,\ k \in \mathbb{Z}$), a neuron's activity jumps by λ_i, and the increase caused by each jump decays exponentially at the rate of λ_i until the arrival of the next stimulus. After the first couple of pulses, each of the geometric series converges quickly to its limit (since $r_i < 1$) and the peak of the bipolar cell activity can be approximated as the geometric series $u_i \approx \frac{\lambda_i}{1-r_i}$. As the two geometric sum converge, u_G also converges towards the weighted sum of the limits. Once the peak of u_G is near its limit, the sum fluctuates between $u_G = \omega_1 \frac{\lambda_1}{1-r_1} - \omega_2 \frac{\lambda_2}{1-r_2}$ ($t' = 0$, at the beginning of each cycle) and $u_G = \omega_1 \frac{\lambda_1}{1-r_1} e^{-\lambda_1 T} - \omega_2 \frac{\lambda_2}{1-r_2} e^{-\lambda_2 T}$ ($t' = T$, at the end of each cycle). Finally, we can approximate $u_G(t)$ as,

$$u_G(t) \approx c_1 e^{-\lambda_1 t'} - c_2 e^{-\lambda_2 t'}, \tag{5.24}$$
$$c_i = \omega_i \frac{\lambda_i}{1 - e^{-\lambda_i T}}. \qquad t' \equiv t \mod T$$

For concreteness, we consider a stimulus with period $T = 1$ and a ganglion cell receiving inputs from bipolar cells with $\lambda_1 = 0.4$ and $\lambda_2 = 0.2$, where the positive input comes from a bipolar cell with faster kinetics (greater λ_i) and the negative input from a bipolar cell with slower kinetics (smaller λ_i). For example, $u_1(t)$ may represent the synaptic input coming directly from the ON-bipolar cell layer (positive when the light stimulus is "ON", $n_1 = 0$) and $u_2(t)$ may represent the synaptic input also coming from the ON-bipolar cell layer indirectly through the amacrine cell layer ($n_2 = 1$). We only consider the case of $n_1 \neq n_2$. Clearly, other cases give ganglion cells that are always active (positive) or always inactive (negative) at each stimulus.

Initially at small t, Eqn. 5.23 is governed by the difference in the convergence rates of the two geometric series. If $\omega_1\lambda_1 > \omega_2\lambda_2$ and $c_1 > c_2$, the difference between the peaks of two inputs u_1 and u_2 (Fig. 5.4B) is initially positive and increasing since the geometric series of $u_1(t)$ converges to its limit, c_1, more quickly than that of $u_2(t)$ converging to its limit, c_2. Once $u_1(t)$ is sufficiently near its limit, the difference between the peaks of two inputs decreases since the peak of $u_1(t)$ remains nearly constant; while $u_2(t)$ continues to increase towards its limit (Fig. 5.4B). Overall, the activity of $u_G(t)$ stays positive and reaches its peak response shortly after the beginning of the repeated stimulus, thereafter decreasing to its limit, $c_1 - c_2$. The response of the ganglion cell subdues after the initial response and stays inactive, once the slower (lower λ_2) bipolar cell input, $u_2(t)$ catches up and balances the input from the faster (greater λ_1) bipolar cell input, $u_1(t)$. Such balanced state that follows the initial active phase characterizes the establishment of the "expectation of regularity".

We consider the model's response to two types of violations of the expected stimuli pattern: (i) an extra stimulus between the periodic stimulus (ii) an omission, or a delay, of the expected stimulus. Fig. 5.4C illustrates how the toy model responds to an extra

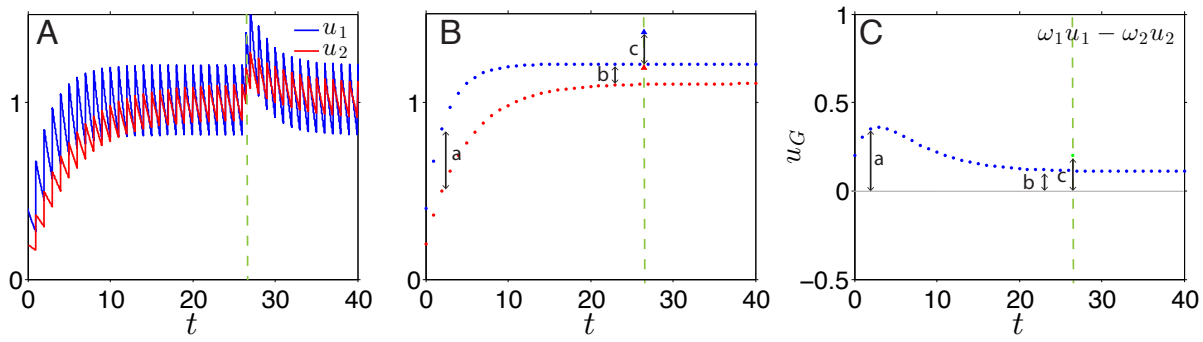

Figure 5.4: **Establshing the expectation of regularity and the effect of an extra stimulus.** (A) Plots of u_1 (blue) and u_2 (red) are overlayed for the comparison. u_1 converges faster to its limiting state. An extra stimulus is given at $t = 26.5$ (green dashed line). (B) Peaks of u_1 and u_2 are plotted for better visualization. Due to the faster convergence rate of u_1, the difference between u_1 and u_2 (labeled **a**) is large at the beginning of the repeated stimulus. As u_1 reaches near its limit and u_2 catches up, the difference between u_1 and u_2 (labeled **b**) becomes smaller and approaches its limit. When there is an extra pulse introduced after u_1 and u_2 reaching their limits, u_1 and u_2 increase by $\omega_1\lambda_1$ and $\omega_2\lambda_2$, respectively (blue and red triangles). The overall difference (labeled **c**) increases if $\omega_1\lambda_1 - \omega_2\lambda_2 > 0$. The difference decreases back to its limit soon after the extra stimulus. (C) The evolution of the difference between the peaks of u_1 and u_2. The weights were set $\omega_1 = \omega_2 = 1$ for concreteness but may be adjusted to maximize the response to an extra stimulus.

stimulus by increasing its activity level. At the time of the extra pulse, $u_G(t)$ increases instantaneously by $\omega_1\lambda_1 - \omega_2\lambda_2 > 0$, showing a positive response. The activity due to the extra pulse decays exponentially as the contribution of each pulse in each bipolar cell output decreases exponentially, as discussed above. The magnitude of the response to the extra stimulus clearly depends on ω_i's and λ_i's. Without loss of generality, we let $\omega_1 = 1$ and consider the relative synaptic strength ω_2, normalized by the synaptic strength of the bipolar cell input from u_1. Fig. 5.5A shows that $u_G(t)$ with smaller $\omega_2 = 0.7$ stays active throughout the repeated stimulus. The contribution of the inhibitory input from u_2 is not sufficient to balance the excitatory input from u_1, and $u_G(t)$ does not become inactive after the initial response. Consequently, the ganglion cell always stays active throughout the repeated stimulus, failing to distinguish the violation of the repeated pattern by an extra stimulus. On the other hand, if ω_2 is sufficiently large (*e.g.*, $\omega_2 \geq \frac{1-e^{-\lambda_1 T}}{1-e^{-\lambda_2 T}}$), c_2 can be

greater than c_1, even if $\omega_1\lambda_1 - \omega_2\lambda_2 > 0$ remains true. In such case, say $\omega_2 = 1.5$, $u_G(t)$ stays inactive after the initial response to the beginning of the stimulus; since the inhibitory input dominates and keeps the activity of $u_G(t)$ low. Fig. 5.5C verifies such prediction, also showing that the increase by $\omega_1\lambda_1 - \omega_2\lambda_2$ at the time of the extra stimulus is not sufficient to overcome the dominating inhibitory input. Thus if ω_2 is too big, the ganglion cell also fails to respond to the extra pulse and detect the violation in the repeated pulse.

The toy model of the ganglion cell implies that there exists a range of the ratio between the strengths of the two synaptic inputs that allows the ganglion cells to (i) respond to the beginning of the stimulus, (ii) stay inactive during repetition, and (iii) respond to a violation of the repeated pattern by an extra stimulus. When the inhibitory synaptic strength is too low compared to the excitatory input ($\omega_1 \gg \omega_2$), the ganglion cell stays active throughout the stimuli, and the response to an extra pulse cannot be distinguished. On the other hand, when the inhibitory synaptic strength is too high, the ganglion cell stays inactive during the repetition and to an extra stimulus. Fig. 5.5D illustrates different qualitative behaviors of the ganglion cell over a range of ω_2, with $\omega_1 = 1$.

The range of ω_2, or the relative synaptic strength of the inhibitory input, that allows detection of an extra stimulus by ganglion cell model depends on the period of the stimulus, T. A repeated stimulus of $T = 4$ does not induce the same qualitative behavior of the same ganglion cell described above. The relative synaptic strength of $\omega_2 = 1.1$ that allowed the extra stimulus detecting ganglion cell for the repeated stimulus of $T = 1$ stays active throughout the repeated stimulus of $T = 4$ and fails to respond to an extra stimulus (Fig. 5.5). As the ratio of the geometric series, $r_i = \frac{\lambda_i}{1-e^{-\lambda_i T}}$, decreases in T, the convergence rate of the geometric series depends on T; subsequently the initial and the limiting behavior of the ganglion cell to a repeated stimulus depend on T. Without discussing the details of exactly how the qualitative behavior of the ganglion cell model depends on T, we confirm the dependency by comparing plots in Fig. 5.6 ($T = 4$) to that of Fig. 5.5 ($T = 1$), in which repeated stimuli of different periods are given to an identical ganglion cell model.

The toy model also responds to an omitted stimulus. With the same values of $\lambda_1 = 0.4$ and $\lambda_2 = 0.2$ as above, the initial response to the initiation of the stimuli remains the same.

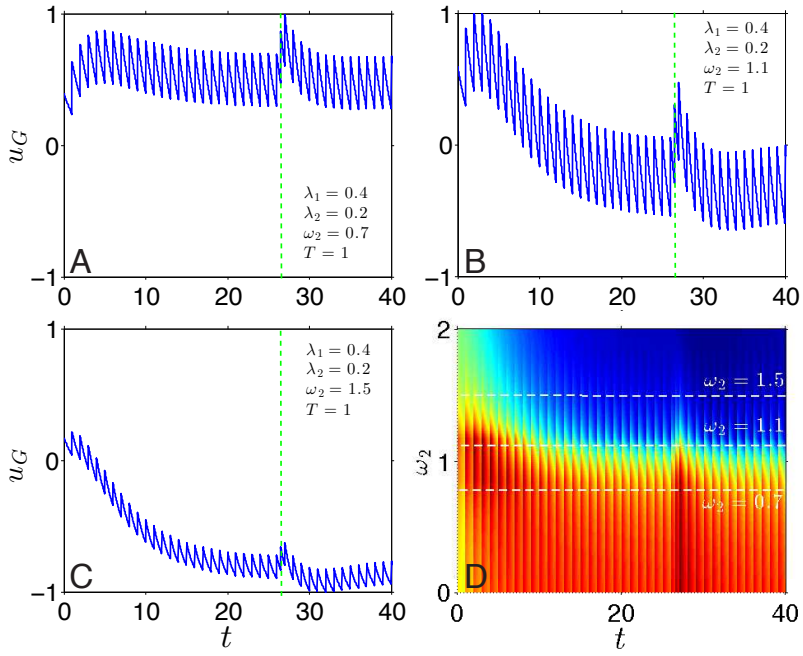

Figure 5.5: **Extra stimulus detection of the toy model.** (A) When the negative synaptic input is sufficiently weaker than the positive one, $\omega_2 < \omega_1$, the ganglion cell stays active (above zero) throughout the repeated stimulus and fails to respond differently to an extra stimulus (given at the time marked by the green dashed line). (B) For an intermediate ratio of the two synaptic weights, the ganglion cell responds positively to the beginning of the stimuli and an extra stimulus. (C) When the negative synaptic input is sufficiently stronger than the positive one, the ganglion cell stays inactive (below zero) after the initial response and fails to change its behavior in response to an extra stimulus. (D) The time course of the activity level of the ganglion cell is plotted horizontally across relative weight of negative input ranging from 0 to 2, spanned vertically. Red colors indicate high activity levels and blue colors indicate low activity levels.

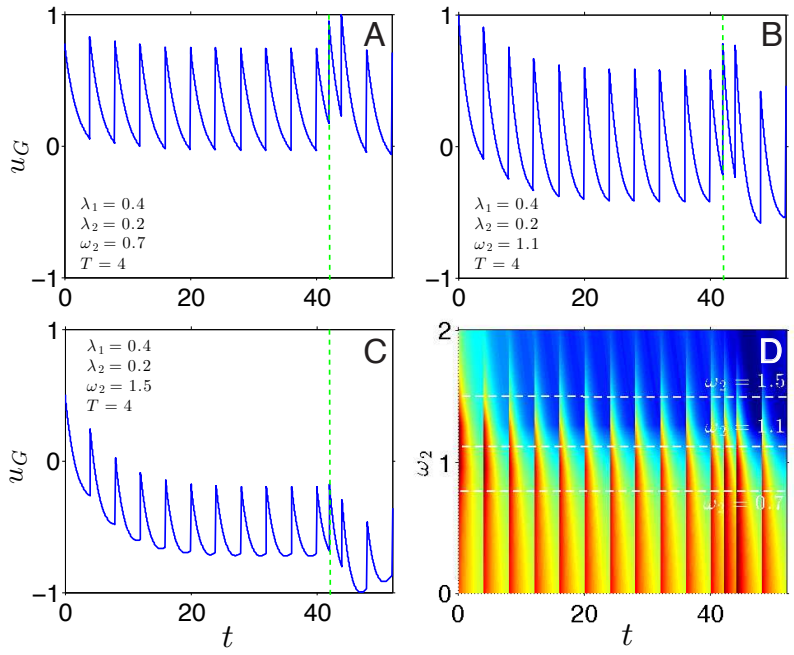

Figure 5.6: **Stimulus frequency and extra stimulus detection.** (A)-(D) are analogous plots of Fig. 5.5A-D and generated using the same toy model used in those figures, but with the repeated stimulus with a period $T = 4$. The same ganglion cell model cannot detect an extra stimulus for any values of $\omega_2 \in [0, 2]$.

After the expectation of regularity has been established, one of the stimuli is omitted at $t = 30$ in Fig. 5.7. For time t between the time of the omitted stimulus and the first stimulus after the omission, $30 < t < 31$, $u_G(t)$ can be written as:

$$u_G(t) = \omega_1 \lambda_1 e^{-\lambda_1 t'} \sum_{0<kT<t} r_1^k - \omega_2 \lambda_2 e^{-\lambda_2 t'} \sum_{0<kT<t} r_2^k, \tag{5.25}$$

since the most recent stimulus ($k = 0$) is omitted in the series. The series can be re-written by shifting the index:

$$u_G(t) = \omega_1 \lambda_1 e^{-\lambda_1(T+t')} \sum_{kT<t-T} r_1^k - \omega_2 \lambda_2 e^{-\lambda_2(T+t')} \sum_{kT<t-T} r_2^k, \tag{5.26}$$

$$u_G(t) \approx c_1 e^{-\lambda_1(t'+T)} - c_2 e^{-\lambda_2(t'+T)}. \tag{5.27}$$

Since $\lambda_1 > \lambda_2$, the first term decays faster than the second and u_G decreases (Fig. 5.7B and C) until the next stimulus arrives and reaches the minimum at $u_G = c_1 e^{-2\lambda_1 T} - c_2 e^{-2\lambda_2 T}$. Depending on the ω_i's, u_G may become negative between the regular stimulus (Fig. 5.7B and C). Moreover, u_G decreases even further during the extended time between the last stimulus before and the first stimulus after the omitted stimulus. The influence of the omitted stimulus decays away quickly once the repeated stimulus resumes and $u_G(t)$ converges back to its limiting behavior.

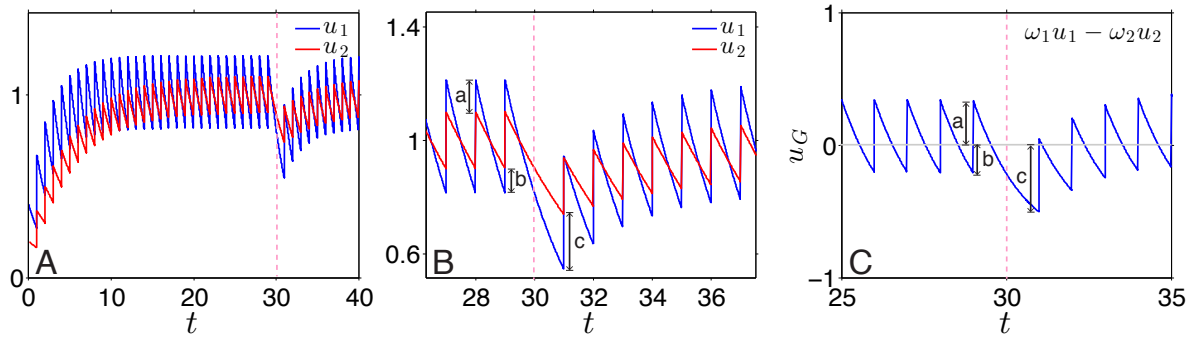

Figure 5.7: **Extended decay over an omitted stimulus induces negative response.** (A) Plots of u_1 (blue) and u_2 (red) are overlayed for the comparison. The time of the omitted stimulus is marked by the red dashed line. (B) A closer look at the plot (A) near the time of the omitted stimulus. u_1 decays more rapidly between the repeated stimilus and may decrease from above (labeled by **a**) to below (labeled by **b**) u_2 for a range of ω_2. The extended period between the last stimulus before and the first stimulus after the omitted stimulus allows u_1 to decrease further and widens the gap (labeled by **c**). (C) Plot of u_G near the time of the omission. The synaptic weights are set $\omega_1 = \omega_2 = 1$ for concreteness. u_G continues to decrease over the extended time interval over the omitted stimulus.

The example shown in Fig. 5.7 with $\omega_{1,2} = 1$ illustrates how an omission of stimulus decreases the activity of the ganglion cell, u_G. The decrease in u_G between two stimuli is due to the faster decay of the effect of the excitatory input, $u_1(t)$. The decrease during inter-

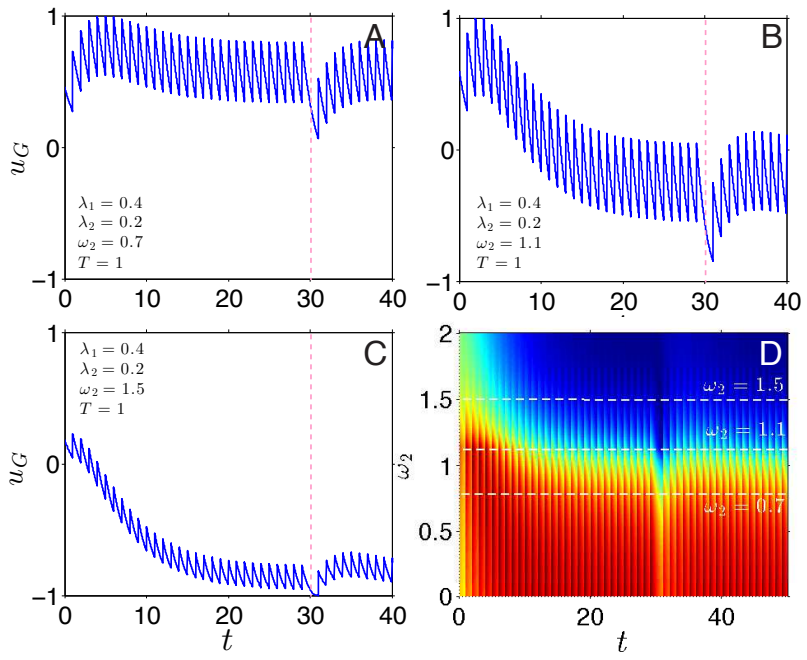

Figure 5.8: **Negative response of the toy model to an omitted stimulus.** (A) When the negative synaptic input is sufficiently weaker than the positive one, $\omega_2 < \omega_1$, the ganglion cell stays active (above zero) throughout the repeated stimulus and fails to respond differently to an omitted stimulus (given at the time marked by the red dashed line). (B) For an intermediate ratio of the two synaptic weights, the ganglion cell responds negatively to an omitted stimulus. (C) When the negative synaptic input is sufficiently stronger than the positive one, the ganglion cell stays inactive (below zero) throughout the repeated stimulus and fails to change its behavior in response to an omitted stimulus. (D) The time course of the activity level of the ganglion cell is plotted horizontally across relative weight of negative input ranging from 0 to 2, spanned vertically. Red colors indicate high activity levels and blue colors indicate low activity levels.

stimulus period occurs for a wide range of ω_2, as verified in Fig. 5.8. Thus, the ganglion cell does not respond positively to an omitted stimulus if the bipolar cell with the positive synaptic input has faster kinetics than the negative one (*i.e.*, $\lambda_1 > \lambda_2$).

The decrease induced by an omitted stimulus suggests that the negative of u_G would *increase* its activity in response to an omission. The negative of the model $-u_G = -\omega_1 u_1 + \omega_2 u_2$ has the same form as the original with its λ_i's switched. The negative form of the toy model suggests that a ganglion cell receiving a positive input from a bipolar cell with a relatively slower kinetics than that of the bipolar cell that projects a negative input (*e.g.*,

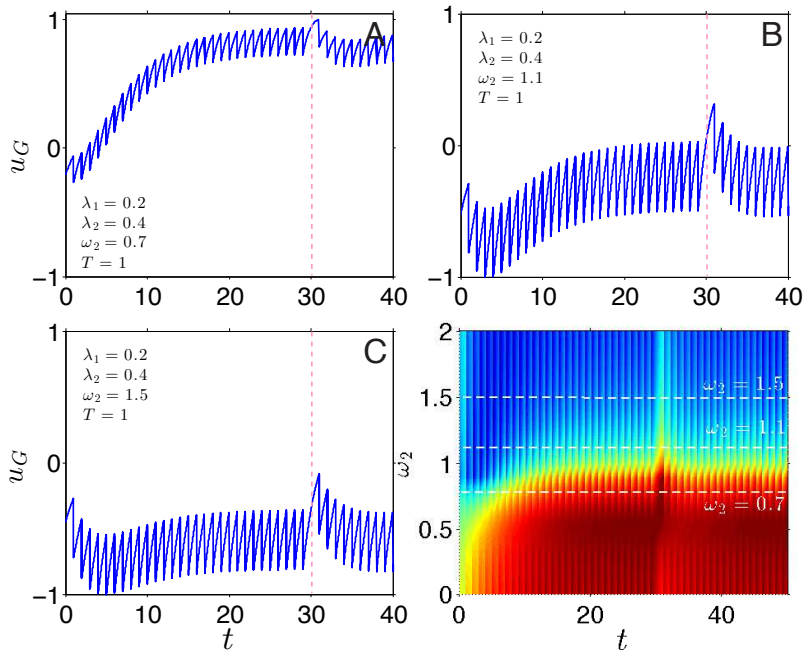

Figure 5.9: **Positive response of the toy model to an omitted stimulus.**(A)-(D) are analogous plots of Fig. 5.8A-D and generated using the same toy model used in Fig. 5.8, except with λ_1 and λ_2 switched. The positive input has slower kinetics compared to that of the negative input ($\lambda_1 < \lambda_2$). As expected from the negative response to an omitted stimulus shown in the other case ($\lambda_2 < \lambda_1$), the toy model responds positively to an omitted stimulus for intermediate values of ω_2.

$\lambda_1 = 0.2$ and $\lambda_2 = 0.4$) would increase its activity in response to an omitted stimulus. Fig. 5.9 confirms that such ganglion cell does show a positive response to an omitted stimulus for a range of ω_2. Note that the ganglion cells with ω_2 that allows detection of the omitted stimulus stay inactive throughout the stimulus, only reacting to an omission (Fig. 5.9B). Others ganglion cell models with ω_2's outside of the range either stay always active (ω_2 is too low, Fig. 5.9A) or always inactive (ω_2 is too high, Fig. 5.9C).

For completeness, we consider the response to an extra stimulus of the ganglion cell with the switched λ_i's, which behaves the same as $-u_G(t)$. One can easily see from Fig. 5.5 (by reflecting the plots over the horizontal axis) that such ganglion cell *cannot* detect an extra stimulus for range of ω_2's considered since an extra pulse will always induce a downward jump in $u_G(t)$.

We conclude the section with a summary of the key features of the toy model:

(i) The initial response to the stimulus is governed by the difference in the convergence rates of the two input sources.

(ii) There exists a range of ω_2's alloing the model to detect an extra (omitted) stimulus if the positive and direct input bipolar cell has relatively faster (slower) kinetics than the negative and indirect input through amacrine cell.

(iii) The range of ω_2's allowing the detection of each type of novelty depends on the period of the stimulus, T.

5.2.5 The building block model

The general form for the building block model was as following

$$u_\alpha(t) = -\int_0^t \phi_\alpha(t-t')S(t')dt', \tag{5.28}$$

$$\phi_\alpha = k_\alpha t e^{-\lambda_\alpha t}$$

$$u_G(t) = \omega_{G\alpha} u_\alpha(t) - \omega_{GA} u_\alpha, \qquad \alpha \in \{N, F\} \tag{5.29}$$

where the temporal filtering function $\phi_\alpha(t)$ for ON- ($\alpha = N$) and OFF-bipolar ($\alpha = F$) cells were assumed to be a decreasing exponential function in the toy model. For a more realistic description, we refer to the experiment by [CAS83] that approximated $\phi_\alpha(t)$ from the intracellular microelectrode recordings made in the bipolar cells of the snapping turtles. The measurements suggested a filtering function of the form $\phi_\alpha(t) = k_\alpha t e^{-\lambda_\alpha t}$, where λ_α denotes the kinetic parameter of the temporal processing of synaptic input from photoreceptors to bipolar cell of the type $\alpha \in \{N, F\}$. The amplitude k_α is adjusted to set the peak of the function at one. The kinetic parameters vary over intensity of the light stimulus [CAS83] and also adapt to the changing temporal contrast [BM02]. ON-bipolar cells are observed to have a slower kinetics than OFF-bipolar cells and we assume that $\lambda_F > \lambda_N$ in general. For concreteness, we will let $\lambda_F \approx 0.05$ and $\lambda_N \approx 0.02$ based on the approximations in [CAS83]

and [BM02] for the rest of the discussion. Note that all the inputs of u_G are of the same type as we do not consider any cross-talk between the ON- and OFF-channels.

Based on the study by [Rie01], bipolar cells adapt to changes in temporal contrast by changing their kinetics: The measurements indicated that the time-to-peak (λ_α^{-1}) and the amplitude (k_α) of the temporal filtering function was decreased by about 10% and 25%, respectively, in OFF-bipolar cells when the temporal contrast was increased from 10% to 30%. In the ON-bipolar cells, the same change in temporal contrast induced about 20% decrease in the amplitude; but little or no change in the time-to-peak. Thus, if the input from the photoreceptor is spatially inhomogeneous, λ_α will vary over space.

The space-time patterns of activity across arrays of retinal neurons measured in [RNO00] have shown that the region of bipolar cells that receive direct synaptic input from photoreceptors contracts over time, due to feedback activity of horizontal cells in the photoreceptor layer. Such contraction indicates that temporal profile of the synaptic input received by bipolar cells varies over space. Consequently, the temporal contrast in synaptic input received by bipolar cells will also vary over space when repeated light stimuli are given. The space-varying temporal contrast observed in [RNO00] and the adaptation of bipolar cells shown in [Rie01] together suggest that the bipolar cell layer will be inhomogeneous in the kinetic variables, and λ_F's will be vary over space. The details of the underlying mechanism of the contraction fall beyond the scope of this work and have been left as future work. For the rest of the section, we incorporate the varying λ_F's into our building block model and study their implications on the response of ganglion cells to violations in the repeated pattern in the stimuli.

First, we consider a building block in which a direct input from OFF-bipolar cell layer, denoted as $u_F(t)$, and an indirect input coming in through amacrine cell layer also from OFF-bipolar cell layer, denoted as $u_{F'}(t)$ are summed at the ganglion cell layer. Here, $u_{F'}$ is analogous to u_1 and u_F is analogous to u_2 of the toy model from the previous section. We consider two distinct values of the kinetic parameters, $\lambda_F, \lambda_{F'} \in \{0.05, 0.055\}$, assuming that the time-to-peak of one of the bipolar cell layers that connects directly or indirectly with the ganglion cell layer is about 9% shorter than that of the other bipolar cell layer. Such

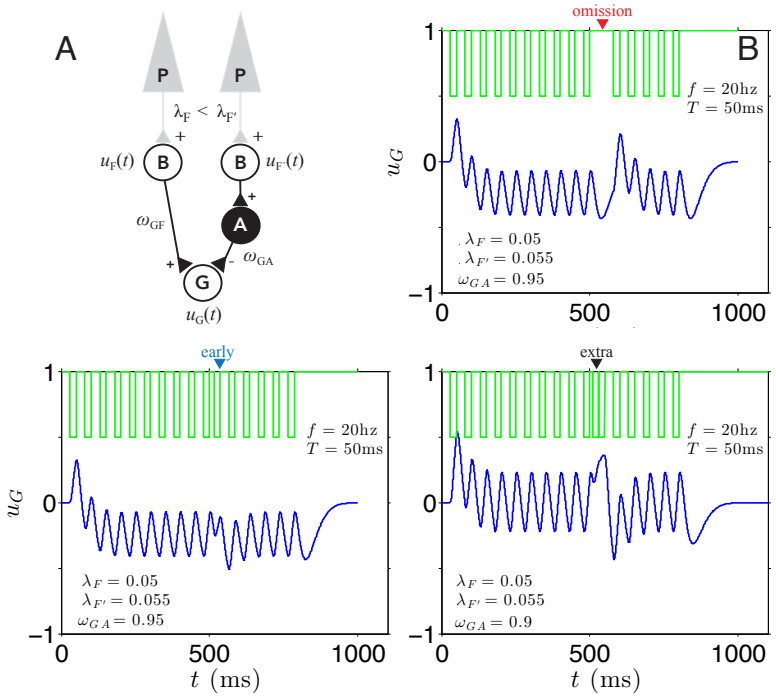

Figure 5.10: **A building block with a slow direct and a fast indirect OFF-bipolar cells.** (A) A schematic diagram of the building block consits of a direct input from ON-bipolar cell and an indirect input from another ON-bipolar cell. Relative synaptic weights are denoted as ω_{GF} and $\omega_{GF'}$. Without loss of generality, we assume $\omega_{GF} = 1$ and only consider ω_{GA} to represent the relative strength of the two inputs. (B)-(D) The weights are chosen to give the most distinctive response to a novelty introduced in the stimuli. (B) The building block model responds at the beginning of the repeated stimulus and becomes inactive (below zero) from the third stimulus. The model does not respond to an omission, but responds to the first stimulus after the omission. (C) The building block model cannot detect an early arrival of a stimulus. (D) The building block model exhibits a slightly positive response to an extra stimulus, which could elicit an output response if the thershold of the output is set appropriately.

assumption is based on the observed adaptation of the bipolar cells due to the inhomogeneity in the temporal contrast discussed above. In Fig. 5.10, the response of the ganglion cell to different types of novelty introduced to a repeated stimulus. Each repeated stimulus lasted for 20ms and was repeated with the period of 50ms ($f = 20$Hz, $T = 50$ms). The relative synaptic weights are selected in each type of novelty so that the responses to changes in stimulus pattern are most apparent. When the bipolar cell layer with direct synapse has the slower synaptic filtering process, $\lambda_{F'} > \lambda_F$, the ganglion cell responds to the beginning of the stimulus and the first stimulus after the omitted stimulus (u_G peaks near such points in Fig. 5.10B). On the other hand, the ganglion cell cannot detect an early stimulus that arrives 15ms earlier (Fig. 5.10C).

Analogous to the toy model with $\lambda_1 > \lambda_2$, the initial activation results from the faster convergence of $u_{F'}$ to its limiting state. However, the convergence to the limiting state is very similar for the two pathways in such case; since λ_F and $\lambda_{F'}$ only differ by 10% (Figs. 5.11B, C, and D). The rate of convergence is very rapid for both pathways for the frequencies considered ($f = 20$Hz, $T = 50$ms), since the contribution of stimuli as few as three cycles ago becomes negligible in the convolution of Eq. 5.28; the contribution of each stimulus is weighted by the filtering function at the position determined by the amount of time passed since the arrival of the stimulus. In Fig. 5.11A, one can see that the filtering function begins to decay rapidly after the time-to-peak and stimuli of three cycles ago are already far away from the peak and their contribution becomes negligible. This implies that $u_G(t)$ converges to its limiting behavior within two or three cycles of stimulus when the interval between stimuli is large compared to the time-to-peak of the temporal filtering function (Fig. 5.10A). Consequently, the contribution of a stimulus arriving early becomes negligible too quickly and fails to increase u_G sufficiently above the limiting state (Fig. 5.10C). Finally, we consider the case in which an extra stimulus is presented between two regular stimuli. This case can be viewed as having two consecutive stimuli arriving early. The latter of the two early stimuli arrives before the effect of the first early stimulus decays and the effects of the two accumulate. The difference of the two weighted inputs from the bipolar cell layer grows and u_G increases above the limiting state (Fig. 5.10D).

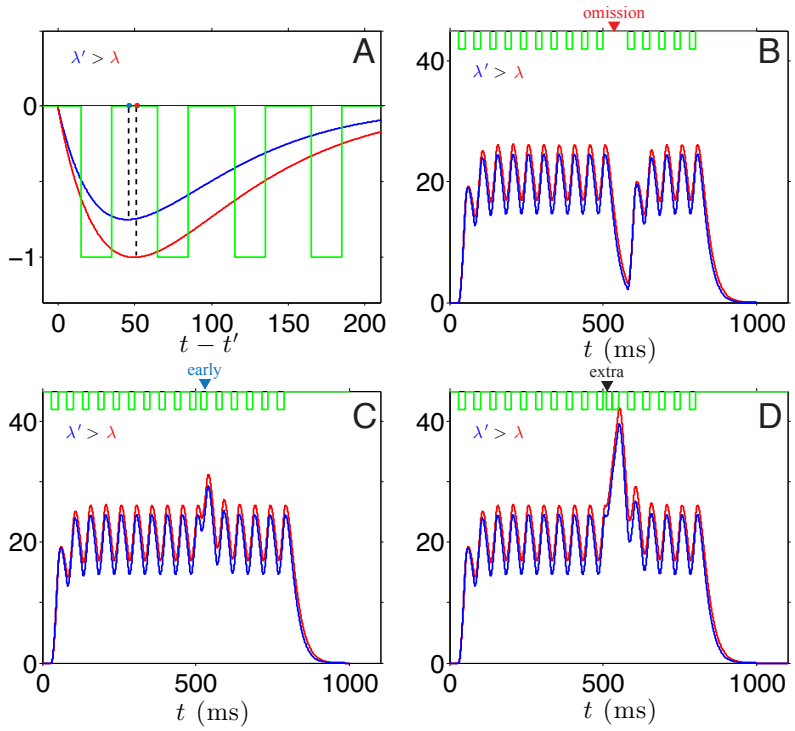

Figure 5.11: **Linear filtering process of a periodic stimulus in bipolar cells.** (A) The temporal filtering functions (ON-bipolar cells are chosen for better visualization) with a greater (blue) and smaller (red) λ's are plotted with regular stimuli (green) with the period of $T = 50$ms and duration of 20ms. The time-to-peak of the bipolar cell with the larger λ (blue dot) is shorter than that of the bipolar cell with the smaller λ (red dot). The amplitudes of the filtering functions are adjusted arbitrarily for better visualization. (B) The filtering of the repeated stimuli converges quickly to the limiting state by the arrival of the second stimulus. The overall behaviors of the bipolar cells with slightly different λ's are almost identical as expected. (C) The contribution of an early stimulus on the convolution decays quickly and becomes negligible after two cycles. The effect of the early stimulus decays away by the time when the next stimulus arrives and the difference between the two inputs cannot grow large enough. (D) An extra stimulus is followed by another stimulus with a shorter time interval between them, which allows the difference between the two weighted inputs to grow, effectively *accumulating* the contributions of the two early stimuli on the convolution.

Following the analysis of the toy model, we consider the case in which the direct synapse has the slower synaptic filtering process, $\lambda_{F'} < \lambda_F$ (Fig. 5.12A). The ganglion cell responds to the omission and termination of the stimulus (Fig. 5.12B) as expected from the analysis of the toy mode with $\lambda_1 < \lambda_2$. Surprisingly, the building block model also responds to an early and an extra stimulus (Figs. 5.12C and D). The response is more apparent with the extra stimulus, as its effect can be thought of as an accumulation of two early stimuli presented consecutively. We suspect that such discrepancy between the toy model and the current model is due to the increasing regime of the new filtering function that was not present in the filtering function used in the toy model. We will leave further analysis of such phenomenon for future work.

5.2.6 Conclusion

In this preliminary work, we have developed a simple and mathematically tractable model for the activity in the ganglion cell layer of the retina-tectum network. The qualitative features of the model can be characterized by four parameters: the kinetic parameter of the temporal filtering function of the two pathways, λ_α and $\lambda_{\alpha'}$, converging at the ganglion cell layer and the synaptic weights of the two inputs, $\omega_{G\alpha}$ and $\omega_{G\alpha'}$ coming from the two pathways. The two kinetic parameters can be reduced to one by rescaling the time variable with one of the kinetic parameters and the ratio between the two weights $\omega = \frac{\omega_{G\alpha'}}{\omega_{G\alpha}}$ determines the qualitative behavior of the model. Here, α and α' are either both ON-bipolar cells or both OFF-bipolar cells. The model represents a component, or a region, in the ganglion cell layer that detects and responds to different types of novelties introduced in a repeated stimuli. The type of novelty a component is sensitive to is determined by the four parameters associated with the component. We believe that such phenomenological model can be used as a "building block" of the network that–as a whole–can generate spatiotemporal patterns, which encode the information of the type of novelty observed in a regularly repeated stimulus.

The current model relies on some simplifying assumptions. The adaptation in the kinetic parameter due to variable temporal contrast will change over time, and λ_α's may be viewed

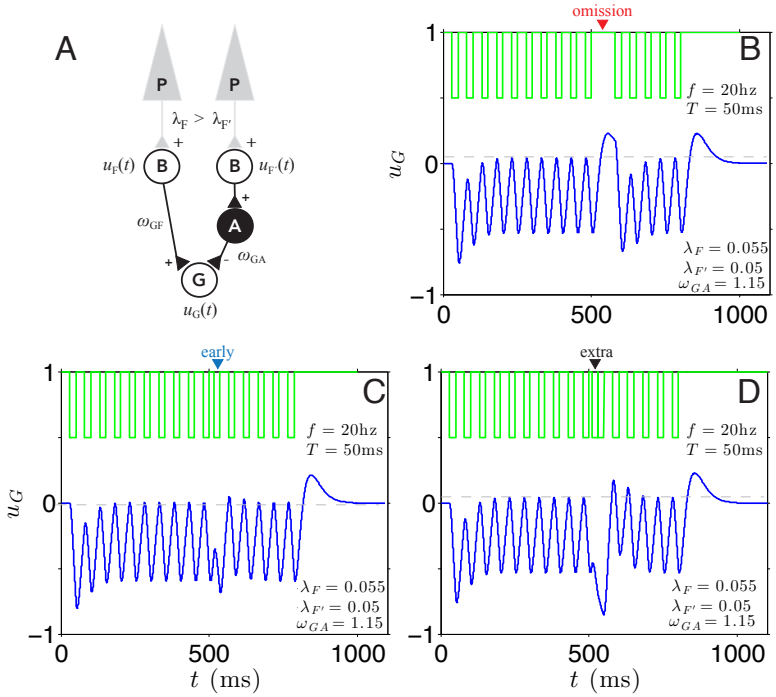

Figure 5.12: **A building block with fast direct and slow indirect OFF-bipolar cells.** (A) A schematic diagram of the building block consisting of a direct input from OFF-bipolar cell with faster kinetics and an indirect input from another OFF-bipolar cell with slower kinetics. Relative synaptic weights are denoted as ω_{GF} and ω_{GA}. Without loss of generality, we assume $\omega_{GF} = 1$ and only consider ω_{GA} to represent the relative strength of the two inputs. (B)-(D) The weights are chosen to give the most distinctive response to a novelty introduced in the stimuli. (B) The building block model responds to an omitted stimulus and the end of the repeated stimulus. (C) The building block model exhibits a very slight activation in response to an early stimulus. (D) The building block model exhibits a clear response to an extra stimulus.

as a time-dependent parameter in future models. The distribution of synaptic strength over space and between layers will be investigated in the future to put together the building block models developed here and complete the model of the retina-tectum network. Moreover, the output function of ganglion cells will be approximated to connect the ganglion cell layer and the tectum cell layer. With various activity patterns that are potentially available from the building blocks, we suspect that the complete model can produce spatiotemporal patterns that are physiologically relevant in novelty detection.

REFERENCES

[AB00] P. Averill and J. Beck. "Posttraumatic stress disorder in older adults: a conceptual review." *Journal of Anxiety Disorders*, **14**(2):133–156, 2000.

[AKG79] K. Abe, J. Kroning, M. A. Greer, and V. Critchlow. "Effects of destruction of the suprachiasmatic nuclei on the circadian rhythms in plasma corticosterone, body temperature, feeding and plasma thyrotropin." *Neuroendocrinology*, **29**(2):119–131, 1979.

[Ama77] S. Amari. "Dynamics of pattern formation in lateral-inhibition type neural fields." *Biological Cybernetics*, **27**(2):77–87, 1977.

[AVO13a] M. Andersen, F. Vinther, and J. Ottesen. "Mathematical modeling of the hypothalamic–pituitary–adrenal gland (HPA) axis, including hippocampal mechanisms." *Mathematical Biosciences*, **246**(1):122–138, 2013.

[AVO13b] M. Andersen, F. Vinther, and J. Ottesen. "Mathematical modeling of the hypothalamic–pituitary–adrenal gland (HPA) axis, including hippocampal mechanisms." *Mathematical Biosciences*, **246**(1):122–138, 2013.

[Bau93] A. Baum. "Implications of psychological research on stress and technological accidents." *American Psychologist*, **48**(6):665, 1993.

[BCC08] N. Bairagi, S. Chatterjee, and J. Chattopadhyay. "Variability in the secretion of corticotropin-releasing hormone, adrenocorticotropic hormone and cortisol and understandability of the hypothalamic-pituitary-adrenal axis dynamics — a mathematical study based on clinical evidence." *Mathematical Medicine and Biology*, 2008.

[Ber15] R. Bertram. "Mathematical Modeling in Neuroendocrinology." *Comprehensive Physiology*, 2015.

[BM02] S. A. Baccus and M. Meister. "Fast and slow contrast adaptation in retinal circuitry." *Neuron*, **36**(5):909–919, 2002.

[BO17] E. O. Bangsgaard and J. T. Ottesen. "Patient specific modeling of the HPA axis related to clinical diagnosis of depression." *Mathematical Biosciences*, **287**:24–35, 2017.

[BVB09] A. Ben-Zvi, S. D. Vernon, and G. Broderick. "Model-based therapeutic correction of hypothalamic-pituitary-adrenal axis dysfunction." *PLoS Computational Biology*, **5**(1):e1000273, 2009.

[BVK07] D. Bremner, E. Vermetten, and M. E. Kelley. "Cortisol, dehydroepiandrosterone, and estradiol measured over 24 hours in women with childhood sexual abuse-related posttraumatic stress disorder." *The Journal of Nervous and Mental Disease*, **195**(11):919–927, 2007.

[CAS83] D. Copenhagen, J. Ashmore, and J. Schnapf. "Kinetics of synaptic transmission from photoreceptors to horizontal and bipolar cells in turtle retina." *Vision Research*, **23**(4):363–369, 1983.

[CHF09] M. Conrad, C. Hubold, B. Fischer, and A. Peters. "Modeling the hypothalamus–pituitary–adrenal system: homeostasis by interacting positive and negative feedback." *Journal of Biological Physics*, **35**(2):149–162, 2009.

[Chr98] G. Chrousos. "Editorial: ultradian, circadian, and stress-related hypothalamic-pituitary-adrenal axis activity — a dynamic digital-to-analog modulation." *Endocrinology*, **139**(2):437–440, 1998.

[CHW91] Y. Chen, S. Hua, C. Wang, L. Wu, Q. Gu, and B. Xing. "An electrophysiological study on the membrane receptor-mediated action of glucocorticoids in mammalian neurons." *Neuroendocrinology*, **53**(Suppl. 1):25–30, 1991.

[CKK00] M. A. Cole, P. J. Kim, B. A. Kalman, and R. L. Spencer. "Dexamethasone suppression of corticosteroid secretion: evaluation of the site of action by receptor measures and functional studies." *Psychoneuroendocrinology*, **25**(2):151–167, 2000.

[CSM10] B. Conway-Campbell, R. Sarabdjitsingh, M. McKenna, J. Pooley, Y. Kershaw, O. Meijer, E. De Kloet, and S. Lightman. "Glucocorticoid ultradian rhythmicity directs cyclical gene pulsing of the clock gene period 1 in rat hippocampus." *Journal of Neuroendocrinology*, **22**(10):1093–1100, 2010.

[CYC04] L. Crofford, E. Young, N. Engleberg K. Cary, A. Korszun, C. Brucksch, L. McClure, M. Brown, and M. Demitrack. "Basal circadian and pulsatile ACTH and cortisol secretion in patients with fibromyalgia and/or chronic fatigue syndrome." *Brain, Behavior, and Immunity*, **18**(4):314–325, 2004.

[Den09] R. Denver. "Structural and Functional Evolution of Vertebrate Neuroendocrine Stress Systems." *Annals of the New York Academy of Sciences*, **1163**(1):1–16, 2009.

[DRM14a] S. M. Dince, R. D. Rome, B. S. McEwen, and A. C. Tang. "Enhancing offspring hypothalamic-pituitary-adrenal (HPA) regulation via systematic novelty exposure: the influence of maternal HPA function." *Frontiers in Behavioral Neuroscience*, **8**, 2014.

[DRM14b] S. M. Dinces, R. D. Romeo, B. S. McEwen, and A. C. Tang. "Enhancing offspring hypothalamic-pituitary-adrenal (HPA) regulation via systematic novelty exposure: the influence of maternal HPA function." *Frontiers in Behavioral Neuroscience*, **8**, 2014.

[EPL90] D. Engler, T. Pham, J. Liu, M. Fullerton, I. Clarke, and J. Funder. "Studies of the Regulation of the Hypothalamic-Pituitary-Adrenal Axis in Sheep with

Hypothalamic-Pituitary Disconnection. II. Evidence for in Vivo Ultradian Hypersecretion of Proopiomelanocortin Peptides by the Isolated Anterior and Intermediate Pituitary." *Endocrinology*, **127**(4):1956–1966, 1990.

[Erm98] B. Ermentrout. "Neural networks as spatio-temporal pattern-forming systems." *Reports on Progress in Physics*, **61**(4):353, 1998.

[ETH10] N. K. Evanson, J. G. Tasker, M. N. Hill, C. J. Hillard, and J. P. Herman. "Fast feedback inhibition of the HPA axis by glucocorticoids is mediated by endocannabinoid signaling." *Endocrinology*, 2010.

[FCS90] S. Feldman, N. Conforti, and D. Saphier. "The preoptic area and bed nucleus of the stria terminalis are involved in the effects of the amygdala on adrenocortical secretion." *Neuroscience*, **37**(3):775–779, 1990.

[FK76] E. Famiglietti and H. Kolb. "Structural basis for ON-and OFF-center responses in retinal ganglion cells." *Science*, **194**(4261):193–195, 1976.

[FKF08] E. Foa, T. Keane, M. Friedman, and J. Cohen. "Effective treatments for PTSD: practice guidelines from the International Society for Traumatic Stress Studies." 2008.

[GAG07] S. Gupta, E. Aslakson, B. M. Gurbaxani, and S. D. Vernon. "Inclusion of the glucocorticoid receptor in a hypothalamic pituitary adrenal axis model reveals bistability." *Theoretical Biology and Medical Modelling*, **4**:8, 2007.

[GAT01] B. Gréco, E. Allegretto, M. Tetel, and J. Blaustein. "Coexpression of ERβ with ERα and progestin receptor proteins in the female rat forebrain: effects of estradiol treatment." *Endocrinology*, **142**(12):5172–5181, 2001.

[GC98] F. P. Giraldi and F. Cavagnini. "Corticotropin-releasing hormone is produced by rat corticotropes and modulates ACTH secretion in a paracrine/autocrine fashion." *Journal of Clinical Investigation*, **101**(11):2478, 1998.

[GC02] P. Gold and G. Chrousos. "Organization of the stress system and its dysregulation in melancholic and atypical depression: high vs low CRH/NE states." *Molecular Psychiatry*, **7**(3):254–275, 2002.

[GCD03] A. Ginsberg, S. Campeau, H. Day, and R. Spencer. "Acute Glucocorticoid Pretreatment Suppresses Stress-Induced Hypothalamic-Pituitary-Adrenal Axis Hormone Secretion and Expression of Corticotropin-Releasing Hormone hnRNA but Does Not Affect c-fos mRNA or Fos Protein Expression in the Paraventricular Nucleus of the Hypothalamus." *Journal of Neuroendocrinology*, **15**(11):1075–1083, 2003.

[GG02] P. W. Gold and GP G. P. Chrousos. "Organization of the stress system and its dysregulation in melancholic and atypical depression: high vs low CRH/NE states." *Molecular Psychiatry*, **7**(3):254, 2002.

[GHJ05] A. Di Giorgio, M. Hudson, W. Jerjes, and A. Cleare. "24-hour pituitary and adrenal hormone profiles in chronic fatigue syndrome." *Psychosomatic Medicine*, **67**(3):433–440, 2005.

[GM14] D. Gupta and J. E. Morley. "Hypothalamic-Pituitary-Adrenal (HPA) Axis and Aging." *Comprehensive Physiology*, **4**(4):1495–1510, 2014.

[GTO14] J. Gudmand-Hoeyer, S. Timmermann, and J. T. Ottesen. "Patient-specific modeling of the neuroendocrine HPA-axis and its relation to depression: Ultradian and circadian oscillations." *Mathematical Biosciences*, **257**:23–32, 2014.

[HC97] J. Herman and W. Cullinan. "Neurocircuitry of stress: central control of the hypothalamo–pituitary–adrenocortical axis." *Trends in Neurosciences*, **20**(2):78–84, 1997.

[HFM03] J. P. Herman, H. Figueiredo, N. K. Mueller, Y. Ulrich-Lai, M. Ostrander, D.. Choi, and W. Cullinan. "Central mechanisms of stress integration: hierarchical circuitry controlling hypothalamo–pituitary–adrenocortical responsiveness." *Frontiers in Neuroendocrinology*, **24**(3):151 – 180, 2003.

[HRW15] N. Hosseinichimeh, H. Rahmandad, and A. K. Wittenborn. "Modeling the hypothalamus–pituitary–adrenal axis: a review and extension." *Mathematical Biosciences*, **268**:52–65, 2015.

[HT12] M. N. Hill and J.G. Tasker. "Endocannabinoid signaling, glucocorticoid-mediated negative feedback, and regulation of the hypothalamic-pituitary-adrenal axis." *Neuroscience*, **204**:5–16, 2012.

[HTP94] R. L. Hauger, K. V. Thrivikraman, and P. M. Plotsky. "Age-related alterations of hypothalamic-pituitary-adrenal axis function in male Fischer 344 rats." *Endocrinology*, **134**(3):1528–1536, 1994.

[IXS95] T. Imaki, W. Xiao-Quan, T. Shibasaki, K. Yamada, S. Harada, N. Chikada, M. Naruse, and H. Demura. "Stress-induced activation of neuronal activity and corticotropin-releasing factor gene expression in the paraventricular nucleus is modulated by glucocorticoids in rats." *Journal of Clinical Investigation*, **96**(1):231, 1995.

[JCP04] M. Juruena, A. Cleare, and C. Pariante. "The hypothalamic pituitary adrenal axis, glucocorticoid receptor function and relevance to depression." *Revista Brasileira de Psiquiatria*, **26**(3):189–201, 2004.

[JE97] M. S. Jasper and W. C. Engeland. "Splanchnicotomy increases adrenal sensitivity to ACTH in nonstressed rats." *American Journal of Physiology-Endocrinology And Metabolism*, **273**(2):E363–E368, 1997.

[JHB77] M. Jones, E. Hillhouse, and J. Burden. "Dynamics and mechanics of corticosteroid feedback at the hypothalamus and anterior pituitary gland." *Journal of Endocrinology*, **73**(3):405–417, 1977.

[JPT06] W. Jerjesnd, T. Peters, N. Taylor, P. Wood, S. Wessely, and A. Cleare. "Diurnal excretion of urinary cortisol, cortisone, and cortisol metabolites in chronic fatigue syndrome." *Journal of Psychosomatic Research*, **60**(2):145–153, 2006.

[JSC05] S. Jelic, V. Smiljana, Cupic, and L. Kolar-Anic. "Mathematical modeling of the hypothalamic–pituitary–adrenal system activity." *Mathematical Biosciences*, **197**(2):173–187, 2005.

[KDC16] L. Kim, M. R. D'Orsogna, and T. Chou. "Onset, timing, and exposure therapy of stress disorders: mechanistic insight from a mathematical model of oscillating neuroendocrine dynamics." *Biology Direct*, **11**(13), 2016.

[KKS81] M. Kaneko, K. Kaneko, J. Shinsako, and M. F. Dallman. "Adrenal sensitivity to adrenocorticotropin varies diurnally." *Endocrinology*, **109**(1):70–75, 1981.

[KSJ00] E. Kandel, J. Schwartz, T. Jessell, et al. *Principles of neural science*, volume 4. McGraw-Hill New York, 2000.

[KSV05] V. Kyrylov, L. Severyanova, and A. Vieira. "Modeling robust oscillatory behavior of the hypothalamic-pituitary-adrenal axis." *IEEE Transactions on Biomedical Engineering*, **52**(12):1977–1983, 2005.

[KY88a] M. Kasai and H. Yamashita. "Cortisol suppresses noradrenaline-induced excitatory responses of neurons in the paraventricular nucleus; an in vitro study." *Neuroscience letters*, **91**(1):65–70, 1988.

[KY88b] M. Kasai and H. Yamashita. "Inhibition by cortisol of neurons in the paraventricular nucleus of the hypothalamus in adrenalectomized rats; an in vitro study." *Neuroscience Letters*, **91**(1):59–64, 1988.

[LC95] A. Lemieux and C. Coe. "Abuse-related posttraumatic stress disorder: evidence for chronic neuroendocrine activation in women." *Psychosomatic Medicine*, **57**(2):105–115, 1995.

[LWA08] S. L. Lightman, C. C. Wiles, H. C. Atkinson, D. E. Henley, G. M. Russell, J. A. Leendertz, M. A. McKenna, F. Spiga, S. A. Wood, and B. L. Conway-Campbell. "The significance of glucocorticoid pulsatility." *European Journal of Pharmacology*, **583**(2):255–262, 2008.

[MA99] X. Ma and G. Aguilera. "Differential regulation of corticotropin-releasing hormone and vasopressin transcription by glucocorticoids." *Endocrinology*, **140**(12):5642–5650, 1999.

[Mas68] J. Mason. "Organization of psychoendocrine mechanisms." *Psychosomatic Medicine*, **30**, 1968.

[McE98] B. S. McEwen. "Stress, adaptation, and disease: Allostasis and allostatic load." *Annals of the New York Academy of Sciences*, **840**(1):33–44, 1998.

[MEI76] A. H. MEIER. "Daily variation in concentration of plasma corticosteroid in hypophysectomized rats." *Endocrinology*, **98**(6):1475–1479, 1976.

[MHG02] S. Makino, K. Hashimoto, and P. Gold. "Multiple feedback mechanisms activating corticotropin-releasing hormone system in the brain during stress." *Pharmacology Biochemistry and Behavior*, **73**(1):147–158, 2002.

[MPB16] M. Morena, S. Patel, J. S. Bains, and M. N. Hill. "Neurobiological interactions between stress and the endocannabinoid system." *Neuropsychopharmacology*, **41**(1):80–102, 2016.

[MRJ72] H. Matsuyama, A. Ruhmann-Wennhold, L. R. Johnson, and D. H. Nelson. "Disappearance rates of exogenous and endogenous ACTH from rat plasma measured by bioassay and radioimmunoassay." *Metabolism*, **21**(1):30–35, 1972.

[MRV07] M. Meewisse, J. B. Reitsma, G. De Vries, B. P. Gersons, and M. Olff. "Cortisol and post-traumatic stress disorder in adults." *The British Journal of Psychiatry*, **191**(5):387–392, 2007.

[MS86] R. Miller and M. Slaughter. "Excitatory amino acid receptors of the retina: diversity of subtypes and conductance mechanisms." *Trends in Neurosciences*, **9**:211–218, 1986.

[MS93] B. S. McEwen and E. Stellar. "Stress and the individual: mechanisms leading to disease." *Arch. Intern. Med.*, **153**:2093–2101, 1993.

[MSS02] D.L. McCullers, P. G. Sullivan, S. W. Scheff, and J. P. Herman. "Traumatic brain injury regulates adrenocorticosteroid receptor mRNA levels in rat hippocampus." *Brain Research*, **947**(1):41–49, 2002.

[OCM85] N. Ono, J. De Castro, and S. McCann. "Ultrashort-loop positive feedback of corticotropin (ACTH)-releasing factor to enhance ACTH release in stress." *Proceedings of the National Academy of Sciences*, **82**(10):3528–3531, 1985.

[OVG07] M. Olff, G. de Vries, Y. Güzelcan, J. Assies, and B. Gersons. "Changes in cortisol and DHEA plasma levels after psychotherapy for PTSD." *Psychoneuroendocrinology*, **32**(6):619–626, 2007.

[Pap77] E. Papaikonomou. "Rat adrenocortical dynamics." *The Journal of Physiology*, **265**(1):119–131, 1977.

[PBC08] D. Purves, E. Brannon, R. Cabeza, S. Huettel, K. LaBar, M. Platt, and M. Woldorff. *Principles of Cognitive Neuroscience*, volume 83. Sinauer Associates Sunderland, MA, 2008.

[PP09] A. Papadimitriou and K. Priftis. "Regulation of the hypothalamic-pituitary-adrenal axis." *Neuroimmunomodulation*, **16**(5):265, 2009.

[PRS98] Eduardo M Perez, Lynnette K Rogers, Charles V Smith, and Leonard E Weisman. "Pharmacokinetics of Dexamethasone in Rats 346." *Pediatric Research*, **43**:61–61, 1998.

[RBB88] D. Regier, J. Boyd, J. Burke, D. Rae, J. Myers, M. Kramer, L. Robins, L. George, M. Karno, and B. Locke. "One-month prevalence of mental disorders in the United States: based on five Epidemiologic Catchment Area sites." *Archives of General Psychiatry*, **45**(11):977–986, 1988.

[RDP09] A. D. Radant, D. J. Dobie, E. R. Peskind, M. M. Murburg, E. C. Petrie, E. D. Kanter, M. A. Raskind, and C. W. Wilkinson. "Adrenocortical responsiveness to infusions of physiological doses of ACTH is not altered in posttraumatic stress disorder." *Frontiers in Behavioral Neuroscience*, **3**:40, 2009.

[RER12] S. Rauch, A. Eftekhari, and J. Ruzek. "Review of exposure therapy: a gold standard for PTSD treatment." *The Journal of Rehabilitation Research and Development*, (49):679–88, 2012.

[RFD90] M. R. Ralph, R. G. Foster, F. C. Davis, and M. Menaker. "Transplanted suprachiasmatic nucleus determines circadian period." *Science*, **247**(4945):975, 1990.

[Rie01] F. Rieke. "Temporal contrast adaptation in salamander bipolar cells." *Journal of Neuroscience*, **21**(23):9445–9454, 2001.

[RJW04] N. Rohleder, L. Joksimovic, J. Wolf, and C. Kirschbaum. "Hypocortisolism and increased glucocorticoid sensitivity of pro-Inflammatory cytokine production in Bosnian war refugees with posttraumatic stress disorder." *Biological Psychiatry*, **55**(7):745–751, 2004.

[RLW01] A. M. Rasmusson, D. S. Lipschitz, S. Wang, S. Hu, D. Vojvoda, J. D. Bremner, S. M. Southwick, and D. S. Charney. "Increased pituitary and adrenal reactivity in premenopausal women with posttraumatic stress disorder." *Biological Psychiatry*, **50**(12):965–977, 2001.

[RNO00] B. Roska, E. Nemeth, L. Orzo, and F. S. Werblin. "Three levels of lateral inhibition: A space–time study of the retina of the tiger salamander." *Journal of Neuroscience*, **20**(5):1941–1951, 2000.

[RWW12] J. Rankin, J. Walker, R. Windle, S. Lightman, and J. Terry. "Characterizing dynamic interactions between ultradian glucocorticoid rhythmicity and acute stress using the phase response curve." *PloS One*, **7**(2):e30978, 2012.

[SAG84] T. H. Schürmeyer, P. C. Avgerinos, P. W. Gold, W. T. Gallucci, T. P. Tomai, G. B. Cutler Jr, D. L. Loriaux, and G. P. Chrousos. "Human corticotropin-releasing factor in man: pharmacokinetic properties and dose-response of plasma adrenocorticotropin and cortisol secretion." *The Journal of Clinical Endocrinology & Metabolism*, **59**(6):1103–1108, 1984.

[SHS07] G. Schwartz, R. Harris, D. Shrom, M. J. Berry, et al. "Detection and prediction of periodic patterns by the retina." *Nature Neuroscience*, **10**(5):552, 2007.

[SJB06] D. Savic, S. Jelic, and N. Buric. "Stability of a general delay differential model of the hypothalamo-pituitary-adrenocortical system." *International Journal of Bifurcation and Chaos*, **16**(10):3079–3085, 2006.

[SKO00] D. Savic, G. Knezevic, and G. Opacic. "A mathematical model of stress reaction: Individual differences in threshold and duration." *Psychobiology*, **28**(4):581–592, 2000.

[SKR05] T. Steckle, N. H. Kalin, J. M. Reul, and M. Hans. *Handbook of Stress and the Brain Part 1: The Neurobiology of Stress: The Neurobiology of Stress*, volume 15. Elsevier, 1 edition, 2005.

[SRD12] K. Sriram, M. Rodriguez-Fernandez, and F. J. Doyle III. "Modeling cortisol dynamics in the neuro-endocrine axis distinguishes normal, depression, and post-traumatic stress disorder (PTSD) in humans." *PLoS Computational Biology*, **8**:e1002379, 2012.

[SS02] U. Schibler and P. Sassone-Corsi. "A web of circadian pacemakers." *Cell*, **111**(7):919–922, 2002.

[SS06] M. Stratmann and U. Schibler. "Properties, entrainment, and physiological functions of mammalian peripheral oscillators." *Journal of biological rhythms*, **21**(6):494–506, 2006.

[SSC90] R. B. Simerly, L. W. Swanson, C. Chang, and M. Muramatsu. "Distribution of androgen and estrogen receptor mRNA-containing cells in the rat brain: An in situ hybridization study." *Journal of Comparative Neurology*, **294**(1):76–95, 1990.

[SSH08] K. Simunkova, L. Starka, M. Hill, L. Kriz, R. Hampl, and K. Vondra. "Comparison of total and salivary cortisol in a low-dose ACTH (Synacthen) test: influence of three-month oral contraceptives administration to healthy women." *Physiological Research*, **57**:193, 2008.

[SSL14] D. J. Sharp, G. Scott, and R. Leech. "Network dysfunction after traumatic brain injury." *Nature Reviews Neurology*, **10**(3):156–166, 2014.

[SSW01] T. E. Seeman, B. Singer, C. W. Wilkinson, and B. McEwen. "Gender differences in age-related changes in HPA axis reactivity." *Psychoneuroendocrinology*, **26**(3):225–240, 2001.

[Ste97] K. H. Steven. *Drug facts and comparisons.* Facts & Comparisons, Saint Louis, Missouri, 51 edition, 1997.

[SYK97] M. B. Stein, R. Yehuda, C. Koverola, and C. Hanna. "Enhanced dexamethasone suppression of plasma cortisol in adult women traumatized by childhood sexual abuse." *Biological Psychiatry*, **42**(8):680–686, 1997.

[SZ72] F. K. Stephan and I. Zucker. "Circadian rhythms in drinking behavior and locomotor activity of rats are eliminated by hypothalamic lesions." *Proceedings of the National Academy of Sciences*, **69**(6):1583–1586, 1972.

[Tay99] J. G. Taylor. "Neural 'bubble'dynamics in two dimensions: foundations." *Biological Cybernetics*, **80**(6):393–409, 1999.

[TCW88] S. Y. Tsai, J. Carlstedt-Duke, N. L. Weigel, K. Dahlman, J. Gustafsson, M.Tsai, and B. W. O'Malley. "Molecular interactions of steroid hormone receptor with its enhancer element: evidence for receptor dimer formation." *Cell*, **55**(2):361–369, 1988.

[TDD14] K. Thomaes, E. Dorrepaal, N. Draijer, E. P. Jansma, D. J. Veltman, and A. J. van Balkom. "Can pharmacological and psychological treatment change brain structure and function in PTSD? A systematic review." *Journal of Psychiatric Research*, **50**:1–15, 2014.

[TDM06] J. Tasker, S. Di, and R. Malcher-Lopes. "Rapid glucocorticoid signaling via membrane-associated receptors." *Endocrinology*, **147**(12):5549–5556, 2006.

[TST13] S. Trouche, J. Sasaki, T. Tu, and L. Reijmers. "Fear extinction causes target-specific remodeling of perisomatic inhibitory synapses." *Neuron*, **80**(4):1054–1065, 2013.

[UAE06] Y. M. Ulrich-Lai, M. M. Arnhold, and W. C. Engeland. "Adrenal splanchnic innervation contributes to the diurnal rhythm of plasma corticosterone in rats by modulating adrenal sensitivity to ACTH." *American Journal of Physiology-Regulatory, Integrative and Comparative Physiology*, **290**(4):R1128–R1135, 2006.

[UCO06] M. Uhart, R. Y. Chong, L. Oswald, P. Lin, and G. S. Wand. "Gender differences in hypothalamic–pituitary–adrenal (HPA) axis reactivity." *Psychoneuroendocrinology*, **31**(5):642–652, 2006.

[VAO11] F. Vinther, M. Andersen, and J. T. Ottesen. "The minimal model of the hypothalamic-pituitary-adrenal axis." *Journal of Mathematical Biology*, **63**:663–690, 2011.

[Wat05] A. Watts. "Glucocorticoid regulation of peptide genes in neuroendocrine CRH neurons: a complexity beyond negative feedback." *Frontiers in Neuroendocrinology*, **26**(3):109–130, 2005.

[WBB16] I. P. Watson, M. Brüne, and A. J. Bradley. "The evolution of the molecular response to stress and its relevance to trauma and stressor-related disorders." *Neuroscience & Biobehavioral Reviews*, **68**:134–147, 2016.

[WOS11] M. Weiser, C. Osterlund, and R. Spencer. "Inhibitory Effects of Corticosterone in the Hypothalamic Paraventricular Nucleus (PVN) on Stress-Induced Adrenocorticotrophic Hormone Secretion and Gene Expression in the PVN and Anterior Pituitary." *Journal of Neuroendocrinology*, **23**(12):1231–1240, 2011.

[WS95] A. Watts and G. Sanchez-Watts. "Region-specific regulation of neuropeptide mRNAs in rat limbic forebrain neurones by aldosterone and corticosterone." *The Journal of Physiology*, **484**(3):721–736, 1995.

[WTL10] J. J. Walker, J. R. Terry, and S. L. Lightman. "Origin of ultradian pulsatility in the hypothalamic–pituitary–adrenal axis." *Proceedings of the Royal Society of London B: Biological Sciences*, **277**(1688):1627–1633, 2010.

[WWL98] R. Windle, S. Wood, S. Lightman, and C. Ingram. "The Pulsatile Characteristics of Hypothalamo-Pituitary-Adrenal Activity in Female Lewis and Fischer 344 Rats and Its Relationship to Differential Stress Responses." *Endocrinology*, **139**(10):4044–4052, 1998.

[WWS98] R. Windle, S. Wood, N. Shanks, S. Lightman, and C. Ingram. "Ultradian Rhythm of Basal Corticosterone Release in the Female Rat: Dynamic Interaction with the Response to Acute Stress." *Endocrinology*, **139**(2):443–450, 1998.

[Yau94] King-Wai Yau. "Phototransduction mechanism in retinal rods and cones." *Investigative Ophthalmology and Visual Science*, **35**:9–32, 1994.

[Yeh02] R. Yehuda. "Post-traumatic stress disorder." *New England Journal of Medicine*, **346**(2):108–114, 2002.

[YGG04] R. Yehuda, S. L. Halliganand J. A. Golier, R. Grossman, and L. M. Bierer. "Effects of trauma exposure on the cortisol response to dexamethasone administration in PTSD and major depressive disorder." *Psychoneuroendocrinology*, **29**(3):389–404, 2004.

[YGY04a] R. Yehuda, J. A. Golier, R. Yang, and L. Tischler. "Enhanced sensitivity to glucocorticoids in peripheral mononuclear leukocytes in posttraumatic stress disorder." *Biological Psychiatry*, **55**(11):1110–1116, 2004.

[YGY04b] R. Yehuda, J. A. Golier, R. Yang, and L. Tischler. "Enhanced sensitivity to glucocorticoids in peripheral mononuclear leukocytes in posttraumatic stress disorder." *Biological Psychiatry*, **55**(11):1110–1116, 2004.

[YKB95] R. Yehuda, B. Kahana, K. Binder-Brynes, S. M. Southwick, et al. "Low urinary cortisol excretion in Holocaust survivors with posttraumatic stress disorder." *The American Journal of Psychiatry*, **152**(7):982, 1995.

[YL07] R. Yehuda and J. LeDoux. "Response variation following trauma: a translational neuroscience approach to understanding PTSD." *Neuron*, **56**:19–32, 2007.

[YSN90] R. Yehuda, S. M. Southwick, G. Nussbaum, V. Wahby, E. L. Giller Jr., and John J. W. Mason. "Low urinary cortisol excretion in patients with posttraumatic stress disorder." *The Journal of Nervous and Mental Disease*, **178**(6):366–369, 1990.

[YTL94] R. Yehuda, M. Teicher, R. Levengood, R. Trestman, and L. Siever. "Circadian regulation of basal cortisol levels in posttraumatic stress disorder." *Annals of the New York Academy of Sciences*, **746**(1):378–380, 1994.

[YTL96] R. Yehuda, M. Teicher, R. Levengood, R. Trestman, R. Levengood, and L. Siever. "Cortisol regulation in posttraumatic stress disorder and major depression: a chronobiological analysis." *Biological Psychiatry*, **40**(2):79–88, 1996.